R. & M. No. 3223

R. & M. No. 3223

MINISTRY OF AVIATION

AERONAUTICAL RESEARCH COUNCIL
REPORTS AND MEMORANDA

Part I

The Longitudinal Stability and Control of the Tandem-Rotor Helicopter

Part II

The Lateral Stability and Control of the Tandem-Rotor Helicopter

By A. R. S. Bramwell

LONDON: HER MAJESTY'S STATIONERY OFFICE
1961
PRICE £2 0s. 0d. NET

Part I

The Longitudinal Stability and Control of the Tandem-Rotor Helicopter

By A. R. S. Bramwell

Communicated by the Deputy Controller Aircraft (Research and Development), Ministry of Aviation

*Reports and Memoranda No. 3223**

January, 1960

Summary. A simple method of calculating downwash interference is presented and comparison of theoretical and flight test trim curves indicates that the method is reasonably accurate.

Since the stability of the tandem-rotor helicopter depends largely on small differences between the thrusts of the front and rear rotors it is necessary to calculate the rotor thrust derivatives far more accurately than for the single-rotor helicopter. More accurate expressions than those given in Ref. 8 have therefore been calculated.

The downwash interference causes a reversal of stick position with speed for part of the speed range with an associated divergence in the dynamic stability. This may be eliminated by choosing a suitable value of swash-plate dihedral angle. If, in addition, a suitable differential delta-three hinge angle is applied the tandem-rotor helicopter appears to be stable over the whole speed range except at hovering and very low speeds.

If the swash-plate dihedral is too small the normal acceleration curve, following a step input of control, flattens out and then increases again. Thus the tandem-rotor helicopter may satisfy the N.A.C.A. manoeuvrability criterion yet possess unsatisfactory response characteristics. It is suggested that the N.A.C.A. criterion is unnecessary if stability of the short and long period modes is ensured. Again, a proper choice of swash-plate dihedral and differential delta-three hinge enables satisfactory control response characteristics to be obtained.

1. *Introduction.* The longitudinal stability of the tandem-rotor helicopter presents an easier problem to the helicopter designer than that of the single-rotor helicopter. It is well known that the single-rotor helicopter without tailplane or automatic means is inherently dynamically unstable. But when the lift of the aircraft is shared by more than one lifting surface, as in most fixed-wing aircraft or the multi-rotor helicopter, it is possible to arrange that the configuration is stable by suitably choosing the rates of change of pitching moment of the lifting surfaces, *i.e.* of the wing and tail combination of the fixed wing aircraft and front and rear rotor combination of the tandem-rotor helicopter. In the fixed-wing aircraft this is achieved by correct choice of the C.G. position. In the tandem-rotor helicopter not only is C.G. movement available to control stability but there are also the powerful effects of varying the angle between the rotor-hub axes (called swash-plate dihedral) and applying differential δ_3-hinges to front and rear rotors to control their lift-slopes.

* Previously issued as R.A.E. Report Naval 3 (A.R.C. 21,943).

This report examines in detail the effects of varying these parameters on the control to trim, dynamic stability and control response of a tandem-rotor helicopter having a configuration similar to the Bristol 173.

2. *Estimation of Downwash Effect.* The longitudinal stability and control of the tandem-rotor helicopter depends almost entirely on small differences in the thrusts of the front and rear rotors. Since thrust depends greatly on the rotor inflow it is evident that a reasonably accurate estimate of the effect of the downwash of the front rotor on the rear rotor must be made before attempting the estimation of the stability derivatives. Various forms of the downwash pattern in forward flight have been considered in the past, the most usual being a uniform cylindrical jet of air, *e.g.* Ref. 1, and the distribution due to a cylindrical vortex sheet, *e.g.* Ref. 2, but neither of these two patterns represents a precise physical description of the flow.

The idea of a cylindrical wake probably arose from Glauert's proposal[3], that the induced velocity, assumed constant, at the rotor disc is the same as that of a wing of span $2R$ carrying the same lift distributed elliptically across its span, *i.e.* as given by

$$T = 2\pi R^2 \rho V v_{i0} \tag{1}$$

This expression is the same as would have been calculated if the thrust had been supposed due to the increase of momentum of a cylindrical stream of air whose cross-sectional area on passing through the rotor is the same as the rotor area and whose velocity is increased from $\mathbf{V}$ before reaching the rotor to $\mathbf{V} + 2\mathbf{v}_{i0}$ in the final wake, where $\mathbf{v}_{i0}$ is a vector velocity in the opposite direction to the thrust. Such a physical picture is convenient as it is identical with that of the slipstream of a hovering rotor or propeller and provides an easy way of calculating the induced velocity for a given thrust and forward speed for $V \gg v_{i0}$ (strictly speaking, for the momentum considerations, we should take the flow velocity through the rotor disc at all speeds as $(V^2 + v_{i0}^2)^{1/2}$ which reverts to V at high speed, as in equation (1), and v_{i0} at hovering).

An extensive series of wind tunnel tests[4] have shown, however, that the flow behind a lifting rotor at forward speed is very similar to that of a wing of the same span and aspect ratio, *i.e.* the well known horse-shoe vortex system, and indeed measurement of the induced velocity behind a rotor shows very good agreement with the calculated values behind such a wing.

As shown in Ref. 4, and as predicted for a circular wing in Ref. 5, the vortex sheet in the vicinity of the rotor rolls up very rapidly and is almost completed at the rear edge of the rotor. Thus it can be said that in forward flight, the rear rotor of a tandem helicopter is completely immersed in the flow of a horse-shoe vortex system for values of μ at least as low as $0{\cdot}095$ which was the lowest value of μ in the tests of Ref. 4. Obviously, between $\mu = 0$ and $\mu = 0{\cdot}095$ there is transition from the propeller type slipstream at hovering to the line-vortex flow of forward flight but it is not known exactly in what manner the change takes place. It is likely that the flow due to the cylindrical vortex sheet of Ref. 2 would give satisfactory results for very low μ, say up to about $0{\cdot}04$, although, unfortunately, the lateral variation is given only for the plane through the centre of the (front) rotor and judgment must be used to estimate the induced velocity at other positions behind the rotor, the longitudinal distributions being used as a guide. The line-vortex flow should be satisfactory for values of μ of $0{\cdot}1$ and above but the gap between $\mu = 0{\cdot}04$ and $\mu = 0{\cdot}1$ will have to be 'faired in' graphically. Ref. 7 gives expressions for the induced velocity behind a rotor based on the idea of the horse-shoe vortex system and is intended for use at all speeds by using an artificial expression for the circulation which reduces to zero in hovering and to a value which corresponds to the lifting

wing at high speeds. However, a good deal of computation is necessary to find the induced velocity at enough positions to give a good idea of the flow in the whole region of the rear rotor. What we require is a suitable mean value of the induced velocity in this region so that it can be included as part of the inflow ratio λ and used in the familiar expression for thrust coefficient

$$t_c = c_1\theta_0 + c_2\lambda \tag{2}$$

where

$$c_1 = \frac{a}{4}\left\{\frac{\frac{2}{3}B\,(B^4 - B^2\mu^2 + \frac{9}{4}\mu^4)}{B^2 + \frac{3}{2}\mu^2}\right\}$$

and

$$c_2 = \frac{aB^2}{4} \cdot \frac{B^2 - \frac{1}{2}\mu^2}{B^2 + \frac{3}{2}\mu^2}.$$

This mean value can be obtained from the measurements of Ref. 4 where it is seen that, except in the region near the vortex cores, the induced velocity is fairly uniform laterally across the disc for given longitudinal and vertical positions. Thus the lateral variation of induced velocity could well be replaced by its arithmetic mean value. Now one would expect that the distribution of non-dimensional induced velocity $v_i/v_{i\,0}$ relative to the axes of the vortices would be constant at all speeds and the mean values of the lateral variation have been plotted relative to axes fixed, following Ref. 2, so that the origin is at the centre of the rear rotor and the ξ-axis lying parallel to a line making an angle $v_{i\,0}/V$ (downwards) relative to the direction of flight, as shown in Fig. 3. This is different from the orientation of the axes of Ref. 4 where the X/R-axis (corresponding to the ξ-axis) lies in the plane of the front rotor disc, that direction, of course, being arbitrary.

The values thus obtained are shown in Fig. 4 for the three longitudinal positions $\xi = 1{\cdot}07$, $2{\cdot}07$ and $3{\cdot}14$ corresponding roughly to the front edge, centre and rear edge of a rear rotor. The ξ-axis is not exactly parallel to the axis of the trailing vortices since in general the latter are curved slightly and it is for this reason that the curves shown in Fig. 4 are not symmetrical about the $\zeta = 0$ axis. Thus for any given value of ζ, which measures the distance of the particular part of the rear rotor above the trailing vortices, the value of $v_i/v_{i\,0}$ can be read off for the three values of ξ and the mean of these three values gives the mean interference velocity due to the front rotor.

The mean induced interference velocity at the rear rotor can now be expressed as

$$v_i = kv_{i\,0} \tag{3}$$

$$= \frac{kst_{c\,F}\,\Omega R}{2(\mu^2 + \lambda^2)^{1/2}} \tag{4}$$

or if $\hat{v}_i = v_i/\Omega R$

$$\hat{v}_i = \frac{kst_{c\,F}}{2(\mu^2 + \lambda^2)^{1/2}} \tag{5}$$

where $t_{c\,F}$ is the thrust coefficient of the front rotor.

The effective downwash angle is taken as

$$\epsilon = \frac{kv_{i\,0}}{V} = \frac{kst_{c\,F}}{2\hat{V}(\mu^2 + \lambda^2)^{1/2}}. \tag{6}$$

The derivatives of ϵ with respect to $\hat{u}$, $\hat{w}$ and θ_0 are

$$\frac{d\epsilon}{d\hat{u}} = \frac{k}{\hat{V}}\frac{d\hat{v}_i}{d\hat{u}} - \frac{k\hat{v}_i}{\hat{V}^2}$$

$$= \frac{k}{\hat{V}}\left\{\frac{s\dfrac{\partial t_{cF}}{\partial \hat{u}}}{2(\mu^2+\lambda^2)^{1/2}} - \frac{st_{cF}}{2(\mu^2+\lambda^2)^{3/2}}\left(\mu\frac{d\mu}{d\hat{u}} + \lambda\frac{d\lambda}{d\hat{u}}\right) - \frac{st_{cF}}{2\hat{V}(\mu^2+\lambda^2)^{1/2}}\right\} \tag{7}$$

$$\frac{d\epsilon}{d\hat{w}} = \frac{k}{\hat{V}}\left\{\frac{s\dfrac{\partial t_{cF}}{\partial \hat{w}}}{2(\mu^2+\lambda^2)^{1/2}} - \frac{st_{cF}}{2(\mu^2+\lambda^2)^{3/2}}\left(\mu\frac{d\mu}{d\hat{w}} + \lambda\frac{d\lambda}{d\hat{w}}\right)\right\} \tag{8}$$

$$\frac{d\epsilon}{d\theta_0} = \frac{k}{\hat{V}}\left\{\frac{\dfrac{\partial t_{cF}}{\partial \theta_0}}{2(\mu^2+\lambda^2)^{1/2}} - \frac{st_{cF}}{2(\mu^2+\lambda^2)^{3/2}}\left(\mu\frac{d\mu}{d\theta_0} + \lambda\frac{d\lambda}{d\theta_0}\right)\right\}. \tag{9}$$

In order to check the above method of estimating the downwash effect wind tunnel tests are needed of the loss of rear rotor thrust due to the downwash of the front rotor. Unfortunately, no reliable tests are available but the pitching moment of the helicopter, in the lower half of the speed range at least, depends almost entirely on differential thrust changes (since pitching moments due to the flapping will be comparatively small) so that comparisons of theoretical and measured trim curves should be a good test of the method. These comparisons are made in the following section on the stick position to trim.

3. *Control Angle to Trim.* 3.1. *Derivation of Equation for Control Angle.* The general layout of the tandem rotor helicopter is shown in Fig. 1 and the force and moment diagram in Fig. 2. The reference line of the tandem-rotor helicopter is taken as the line which passes through the C.G. and meets the rotor hub axes at equal angles $\pi/2 - \phi$, where 2ϕ is the angle between the rotor hub axes (positive when the axes meet above the C.G.). The angle 2ϕ will be referred to as 'swash-plate dihedral'.

It is assumed that the movement of the stick applies the same amount of cyclic pitch to both rotors, *i.e.*

$$B_1 = k_1\eta \tag{10}$$

where k_1 is the gearing between stick and rotor-hub tilts. We also assume that a forward movement of the stick, η, reduces the collective pitch of the front rotor by $k_2\eta$ and increases the collective pitch of the rear rotor by $k_2\eta$ so that

$$\theta_F = \theta_0 - k_2\eta \tag{11}$$

and

$$\theta_R = \theta_0 + k_2\eta \tag{12}$$

where k_2 is the gearing between the changes of stick angle and changes of collective pitch angle.

The relative values of k_1 and k_2 define what is known as the 'control mixture' in tandem-rotor helicopters.

Finally a trimmer will be added such that a trimmer movement of ξ increases the collective pitch on the front rotor by $k_2\xi$ and decreases the collective pitch on the rear rotor by $k_2\xi$. We will then have

$$\theta_F = \theta_0 + k^2\xi - k_2\eta \tag{13}$$

and

$$\theta_R = \theta_0 - k_2\xi + k_2\eta\,. \tag{14}$$

Resolving forces horizontally

$$T_F \sin(B_1 - a_{1F} - \theta - \phi) + T_R \sin(B_1 - a_{1R} - \theta + \phi) - H_F \cos(B_1 - a_{1F} - \theta - \phi) - H_R \cos(B_1 - a_{1R} - \theta + \phi) - D_f \cos\gamma_e = 0. \quad (15)$$

Resolving vertically

$$T_F \cos(B_1 - a_{1F} - \theta - \phi) + T_R \cos(B_1 - a_{1R} - \theta + \phi) + H_F \sin(B_1 - a_{1F} - \theta - \phi) + H_R \sin(B_1 - a_{1R} - \theta + \phi) - D_f \sin\gamma_e - W = 0. \quad (16)$$

and taking moments about the C.G.,

$$T_F \cos(B_1 - a_{1F} - \phi)(l_F - h_F \tan\phi) R - T_R \cos(B_1 - a_{1R} + \phi)(l_R - h_R \tan\phi) R - T_F \sin(B_1 - a_{1F} - \phi) h_F R - T_R \sin(B_1 - a_{1R} - \phi) h_R R + H_F \sin(B_1 - a_{1F} - \phi)(l_F - h_F \tan\phi) R - H_R \sin(B_1 - a_{1R} + \phi)(l_R - h_R \tan\phi) R + H_F \cos(B_1 - a_{1F} - \phi) h_F R + H_R \cos(B_1 - a_{1R} + \phi) h_R R + M_f = 0. \quad (17)$$

This report assumes that the tandem-rotor helicopter has rotors of the same diameter, so that after dividing by $\rho s A(\Omega R)^2$ and approximating for small angles equation (17) becomes

$$t_{cF} l_F - t_{cR} l_R - (t_{cF} h_F - t_{cR} h_R)\phi - t_{cF} h_F (B_1 - a_{1F} - \phi) - t_{cR} h_R (B_1 - a_{1R} + \phi) + h_{cF}(B_1 - a_{1F} - \phi)(l_F - h_F\phi) - h_{cR}(B_1 - a_{1R} + \phi)(l_R - h_R\phi) + h_{cF} h_F + h_{cR} h_R + 2C_{mf} = 0. \quad (18)$$

We will now write

$$t_c = c_1\theta_0 + c_2\lambda \quad (2)$$

and

$$a_1 = c_3\theta_0 + c_4\lambda \quad (19)$$

for each rotor, where

$$c_3 = \frac{8}{3}\frac{B\mu}{B^2 + \frac{3}{2}\mu^2}$$

and

$$c_4 = \frac{2\mu}{B^2 + \frac{3}{2}\mu^2}.$$

The functions c_1, c_2, c_3 and c_4 are shown in Fig. 48, plotted for a range of μ and with $B = 0{\cdot}97$. It will also be assumed that $h_c = \frac{1}{4}\mu\delta$ since the contribution of the in-plane rotor forces to the total pitching moment should be very small in the tandem-rotor helicopter. Substituting in equations (18) for t_c and a_1 and using equations (1), (13) and (14) we obtain

$$\begin{aligned}
&[c_1\{\theta_0 - k_2(\eta - \xi)\}] l_F + l_F c_2\lambda_F - [c_1\{\theta_0 - k_2(\eta - \xi\}] h_F\phi - h_F c_2\lambda_F\phi \\
&- [c_1\{\theta_0 + k_2(\eta - \xi)\}] l_R - l_R c_2\lambda_R + [c_1\{\theta_0 + k_2(\eta - \xi)\}] h_R\phi + h_R c_2\lambda_R\phi \\
&- h_F [c_1\{\theta_0 - k_2(\eta - \xi)\} + c_2\lambda_F] [k_1\eta - c_3\{\theta_0 - k_2(\eta - \xi)\} - c_4\lambda_F - \phi] \\
&- h_R [c_1\{\theta_0 + k_2(\eta - \xi)\} + c_2\lambda_R] [k_1\eta - c_3\{\theta_0 + k_2(\eta - \xi)\} - c_4\lambda_R + \phi] \\
&+ h_{cF} [k_1\eta - c_3\{\theta_0 - k_2(\eta - \xi)\} - c_4\lambda_F - \phi](l_F - h_F\phi) \\
&- h_{cR} [k_1\eta - c_3\{\theta_0 + k_2(\eta - \xi)\} - c_4\lambda_R + \phi](l_R - h_R\phi) \\
&+ h_{cF} h_F + h_{cR} h_R + 2C_{mf} = 0. \quad (20)
\end{aligned}$$

Equation (20) is a quadratic in η but it has been found from numerical calculations that most of the terms in the coefficients are very small, so that retaining only the important terms equation (20) can be written

$$A\eta^2 + B\eta + C = 0 \tag{21}$$

where $A = c_1k_1k_2\,(h_F - h_R) + c_1c_3k_2^2\,(h_F + h_R)$

$$B = -\,c_2k_1\,(h_F\lambda_F + h_R\lambda_R) - c_1k_2\,(l_F + l_R) - c_1k_1\theta_0\,(h_F + h_R)$$
$$-\,2c_1c_3k_2\theta_0\,(h_F - h_R) - 2c_1c_3k_2^2\,(h_F + h_R)\,\xi$$

$$C = c_1\theta_0\,(l_F - l_R) + c_2\,(l_F\lambda_F - l_R\lambda_R) + c_1c_3\theta_0^2\,(h_F + h_R)$$
$$+\,(c_1c_4 + c_2c_3)\,(h_F\lambda_F + h_R\lambda_R)\,\theta_0 + c_1k_2\,(l_F + l_R)\,\xi$$
$$+\,c_1c_3k_2\theta_0\,(h_F - h_R)\,\xi + 2C_{mf}\,.$$

A typical solution of (21) gives a very large root, which has no practical significance, and a small root which gives us the control angle we are seeking.

To a good approximation this latter root is given by

$$\eta = -\,C/B$$

3.2. *Calculation of Parameters for use in Trim Equation and Stability Derivatives.* The solution of the trim equations for the single-rotor helicopter corresponding to equations (15), (16) and (17) of this report is comparatively simple since the horizontal force equation is independent of the other two. Equations (15), (16) and (17) however are interdependent and require further equations relating λ, α_D and t_c and to solve them simultaneously would result in great complication. It is much simpler to represent t_c and a_1 in terms of θ_0 and λ and calculate the latter by approximate means.

Now for small angles and taking the level flight case we can write equation (15) as

$$D_f + H_F + H_R = -\,\{T_F\,(\alpha_D)_F + T_R\,(\alpha_D)_R\}\,.$$

If we assume $H_F = H_R$, this equation in non-dimensional form is

$$\mu^2 d_0 + h_c = -\,\tfrac{1}{2}\,\{t_{cF}\,(\alpha_D)_F + t_{cR}\,(\alpha_D)_R\}\,. \tag{22}$$

The relation between the front and rear thrust coefficients can be expressed approximately as

$$t_{cF}l_F = t_{cR}l_R \tag{23}$$

and since

$$t_{cF} + t_{cR} = 2t_c' \tag{24}$$

$$\mu^2 d_0 + h_c = \frac{t_c'}{l_F + l_R}\,\{l_R\,(\alpha_D)_F + l_F\,(\alpha_D)_R\}\,. \tag{25}$$

Now

$$\lambda_F = \hat{V}\,(\alpha_D)_F - (\hat{v}_i)_F \tag{26}$$

and

$$\lambda_R = \hat{V}\,(\alpha_D)_R - (\hat{v}_i)_R - k\,(\hat{v}_i)_F\,. \tag{27}$$

The values of $(\hat{v}_i)_F$ and $(\hat{v}_i)_R$ in equations (26) and (27) can be obtained from Fig. 50 using the approximate values of t_{cF} and t_{cR} from

$$t_{cF} = \frac{2t_c' \, l_R}{l_F + l_R}$$

and

$$t_{cR} = \frac{2t_c' \, l_F}{l_F + l_R}.$$

Also

$$(\alpha_{nf})_F = (\alpha_{nf})_R + 2\phi$$

and

$$\alpha_{nf} = \alpha_D - a_1$$

therefore

$$(\alpha_D)_F = (\alpha_D)_R - (a_1)_R + (a_1)_F + 2\phi \,. \tag{28}$$

Writing

$$(a_1)_F = c_3\theta_F + c_4\lambda_F$$

and

$$(a_1)_R = c_3\theta_R + c_4\lambda_R$$

and assuming the collective pitch is the same on both rotors

$$(a_1)_F - (a_1)_R = c_4 \, (\lambda_F - \lambda_R)$$

i.e.

$$(a_1)_F - (a_1)_R = \hat{V} \, c_4 \, \{(\alpha_D)_F - (\alpha_D)_R\} - c_4 \, \{(\hat{v}_i)_F - (\hat{v}_i)_R - k \, (\hat{v}_i)\} \,.$$

But k is very close to unity so that approximately

$$(a_1)_F - (a_1)_R = \hat{V} \, c_4 \, \{(\alpha_D)_F - (\alpha_D)_R\} + c_4 \, (\hat{v}_i)_R$$

therefore from equation (28) we obtain

$$(\alpha_D)_R = (\alpha_D)_F - \frac{2\phi + c_4 \, (\hat{v}_i)_R}{1 - \hat{V} \, c_4} \tag{29}$$

and substituting in equation (25) gives

$$(\alpha_D)_F = - \frac{\mu^2 d_0 + h_c}{t_c'} + \frac{l_F \, \{2\phi + c_4 \, (\hat{v}_i)_R\}}{(l_F + l_R) \, (1 - \hat{V} \, c_4)} \,. \tag{30}$$

$(\alpha_D)_R$ can now be obtained by using equation (29) and then λ_F and λ_R from equations (26) and (27). Finally the mean collective pitch angle θ_0 can be obtained from

$$\theta_0 = \frac{2t_c' - c_2 \, (\lambda_F + \lambda_R)}{c_1} \,.$$

3.3. *Comparison of Theoretical Trim Calculations with Flight Tests Results.* Figs. 5(a) and 5(b) show the comparison between the theoretical level flight trim curves and some flight test measurements for two different helicopters. In Fig. 5(a) the theoretical curve would show much better agreement if it could be displaced downwards by about $\frac{1}{2}$ deg. This may mean that the nominal trimmer setting in the flight tests was not in fact being achieved since there is no such disagreement in Fig. 5(b). Also, a fuselage pitching moment to account for this disagreement would have to be extremely large and beyond any reasonable value. Apart from this the agreement in both cases is quite good although the theoretical curves have, perhaps, too sharp a peak in the neighbourhood of

$\mu = 0{\cdot}1$. For this case the interference factor k $(= v_i/v_{i\,0})$ was taken, from Fig. 4, as $1{\cdot}5$ and it may be that at such a low value of μ, the values of k given by Fig. 4 are a little too large. For lower values of μ, k was estimated from the results of Ref. 2.

Since, as mentioned in Section 2, the trim curves depend very largely on the rotor downwash effect, especially at the lower values of μ, the above comparisons indicate that the present method of calculating the downwash is reasonably accurate.

3.4. *The Theoretical Trim Curves for the Bristol 173 Configuration.* Figs. 6 to 9 show the effects of C.G. position and swash-plate dihedral on the trim curves of a helicopter similar to the Bristol 173. When $\phi = 0$ deg there is a marked reversal of stick position with speed in the range $\mu = 0{\cdot}1$ to $\mu = 0{\cdot}25$ due to the powerful downwash effect. Also, in this range, there is a rapid divergence in the dynamic stability. Increasing the swash-plate dihedral reduces the severity of the stick reversal until at $\phi = 3$ deg the reversal is almost absent. Again, this is reflected in a marked improvement of the dynamic stability.

Movement of the centre of gravity seems to have little effect other than that of displacing the trim curves vertically.

4. *Equations of Motion and Stability Derivatives.* 4.1. *The Equations of Motion.* As in Ref. 8 wind axes are chosen for the stability axes and the assumption of no coupling between lateral and longitudinal motions is also made but we must now include the downwash lag terms $M_{\dot{u}}$ and $M_{\dot{w}}$ which, for the tandem-rotor helicopter, are considerable, as will be shown in later sections. The derivatives $X_{\dot{u}}$, $X_{\dot{w}}$, $Z_{\dot{u}}$ and $Z_{\dot{w}}$ have been found to be extremely small and are omitted.

In order to render the equations of motion non-dimensional we use the same scheme as in Ref. 8 but divide the equations by a factor which includes the total disc area, *i.e.* if A is the area of one rotor we divide the force equations by $2\rho sA(\Omega R)^2$ and the moment equation by $2\rho sA(\Omega R)^2 R$ and the non-dimensional form of the equations of motion is

$$\frac{d\hat{u}}{d\tau} - x_u\hat{u} - x_w\hat{w} + t_c'\theta\cos\gamma_e - \frac{x_q}{\mu_2}\frac{d\theta}{d\tau} = x_\eta\eta + x_{\theta\,0}\theta_0 \tag{31}$$

$$-z_u\hat{u} + \frac{d\hat{w}}{d\tau} - z_w\hat{w} + t_c'\theta\sin\gamma_e - \left(\hat{V} + \frac{z_q}{\mu_2}\right)\frac{d\theta}{d\tau} = z_\eta\eta + z_{\theta\,0}\theta_0 \tag{32}$$

$$\beta\frac{d\hat{u}}{d\tau} + \mathscr{H}\hat{u} + \chi\frac{d\hat{w}}{d\tau} + \omega\hat{w} + \frac{d^2\theta}{d\tau^2} + \nu\frac{d\theta}{d\tau} = \frac{\mu_2 m_\eta}{i_B} + \frac{\mu_2 m_{\theta\,0}}{i_B} \tag{33}$$

where

$$\beta = -\frac{m_{\dot{u}}}{i_B}, \qquad \mathscr{H} = -\frac{\mu_2 m_u}{i_B}, \qquad \chi = -\frac{m_{\dot{w}}}{i_B}$$

$$\omega = -\frac{\mu_2 m_w}{i_B} \quad \text{and} \quad \nu = -\frac{m_q}{i_B}.$$

Solving the above equations by the usual substitution $\hat{u} = u_0 e^{\lambda\tau}$, etc. and putting

$$x_\eta = x_{\theta\,0} = z_\eta = z_{\theta\,0} = m_\eta = m_{\theta\,0} = 0$$

gives the frequency equation for disturbed motion

$$A\lambda^4 + B\lambda^3 + C\lambda^2 + D\lambda + E = 0$$

where

$$B = N + \nu + \chi\left(\hat{V} + \frac{x_q}{\mu_2}\right) \tag{34}$$

$$C = P + N\nu + Q\chi + \omega\left(\hat{V} + \frac{x_q}{\mu_2}\right) S\beta \tag{35}$$

$$D = P\nu + R\chi + Q\omega - S\mathscr{H} - \beta T \tag{36}$$

$$E = R\omega - T\mathscr{H} \tag{37}$$

and

$$N = -x_w - z_w \tag{38}$$

$$P = x_u z_w - x_w z_u \tag{39}$$

$$Q = -\left(\hat{V} + \frac{z_q}{\mu_2}\right) x_u - t_c' \sin\gamma_e + z_u \frac{x_q}{\mu_2} \tag{40}$$

$$R = -t_c'(z_u \cos\gamma_e - x_u \sin\gamma_e) \tag{41}$$

$$S = t_c' \cos\gamma_e - x_w\left(\hat{V} + \frac{z_q}{\mu_2}\right) + z_w \frac{x_q}{\mu_2} \tag{42}$$

$$T = -t_c'(z_w \cos\gamma_e - x_w \sin\gamma_e). \tag{43}$$

Usually the terms z_q/μ_2 and x_q/μ_2 and products involving them are negligibly small.

4.2. *Calculation of Rotor Derivatives.* 4.2.1. *Derivatives of t_c and a_1 with respect to $\hat{u}$, $\hat{w}$ and θ_0.* Since the pitching moment of the tandem-rotor helicopter depends mainly on the difference in thrust between front and rear rotor it is necessary to calculate very accurately (*e.g.* to at least four significant figures) the thrust derivatives of each rotor. The approximate expressions and values given in the graphs of Ref. 8 for the thrust derivatives are not accurate enough for tandem rotor work. The derivatives of the basic relations between t_c, a_1 and α_D have therefore been recalculated without making approximations except, perhaps, in the final form when known to be satisfactory for the tandem rotor work. These calculations are made in Appendix 1 and the approximate results given again below. They are

$$\frac{\partial t_c}{\partial \hat{u}} = \frac{c_2\left\{\alpha_D + \dfrac{\mu s t_c}{2(\mu^2+\lambda^2)^{3/2}}\right\} + \mu\left\{c_2\left(c_3'\theta_0 + c_4'\lambda\right) - c_4\left(c_1'\theta_0 + c_2'\lambda\right)\right\} + \left(c_1'\theta_0 + c_2'\lambda\right)\left\{1 - \dfrac{\lambda s t_c}{2(\mu^2+\lambda^2)^{3/2}}\right\}}{\Delta} \tag{44}$$

$$\frac{\partial a_1}{\partial \hat{u}} = \frac{c_4\left\{\alpha_D + \dfrac{\mu s t_c}{2(\mu^2+\lambda^2)^{3/2}}\right\} + \left(c_3'\theta_0 + c_4'\lambda\right)\left\{1 - \dfrac{\lambda s t_c}{2(\mu^2+\lambda^2)^{3/2}} + \dfrac{c_2 s}{2(\mu^2+\lambda^2)^{1/2}}\right\}}{\Delta} \tag{45}$$

$$\frac{\partial t_c}{\partial \hat{w}} = \frac{c_2}{\Delta} \tag{46}$$

$$\frac{\partial a_1}{\partial \hat{w}} = \frac{c_4}{\Delta} \tag{47}$$

$$\frac{\partial t_c}{\partial \theta_0} = \frac{c_1\left\{1 - \dfrac{\lambda s t_c}{2(\mu^2+\lambda^2)^{3/2}}\right\} - \mu\left(c_1 c_4 - c_2 c_3\right)}{\Delta} \tag{48}$$

$$\frac{\partial a_1}{\partial \theta_0} = \frac{c_3\left\{1 - \dfrac{\lambda s t_c}{2(\mu^2 + \lambda^2)^{3/2}}\right\} + \dfrac{s}{2(\mu^2 + \lambda^2)^{1/2}}\left(c_1 c_4 - c_2 c_3\right)}{\Delta} \tag{49}$$

where

$$\Delta = 1 - \frac{\lambda s t_c}{2(\mu^2 + \lambda^2)^{3/2}} + \frac{c_2 s}{2(\mu^2 + \lambda^2/^{1/2}} - c_4 \mu \,. \tag{50}$$

Equations (44), (46) and (48) should be used as they stand for the front rotor only. Expressions for the rear rotor thrust derivatives must include corrections for the downwash interference which appears as a change of rotor incidence.

If the suffices $_F$ and $_R$ denote the values of the derivatives of front and rear rotors as calculated from equations (44), (46) and (48) and if the suffix $_{RD}$ denotes the value of the rear-rotor derivative corrected for downwash interference, we have

$$\left(\frac{\partial t_c}{\partial \hat{u}}\right)_{RD} = \left(\frac{\partial t_c}{\partial \hat{u}}\right)_R - \hat{V}\left(\frac{\partial t_c}{\partial \hat{w}}\right)_F \frac{d\epsilon}{d\hat{u}} \tag{51}$$

$$\left(\frac{\partial t_c}{\partial \hat{w}}\right)_{RD} = \left(\frac{\partial t_c}{\partial \hat{w}}\right)_R - \hat{V}\left(\frac{\partial t_c}{\partial \hat{w}}\right)_F \frac{d\epsilon}{d\hat{w}}$$

$$= \left(\frac{\partial t_c}{\partial \hat{w}}\right)_R \left\{1 - \hat{V}\frac{d\epsilon}{d\hat{w}}\right\} \tag{52}$$

since in this case the values of $\left(\dfrac{\partial t_c}{\partial \hat{w}}\right)_R$ and $\left(\dfrac{\partial t_c}{\partial \hat{w}}\right)_F$ are almost exactly the same.

$$\left(\frac{\partial t_c}{\partial \theta_0}\right)_{RD} = \left(\frac{\partial t_c}{\partial \theta_0}\right)_R - \hat{V}\left(\frac{\partial t_c}{\partial \hat{w}}\right)\frac{d\epsilon}{d\theta_0} \tag{53}$$

4.2.2. *Rotor derivatives with respect to q.* The usual method of calculating the rate of pitch derivatives in previous stability work, *e.g.* Ref. 8, has been to use the results of Ref. 9. It is claimed in Ref. 10, however, that these results do not compare well with flight tests and a more detailed analysis is given there which gives better agreement. A similar analysis, but using the notation and system of axes of this report and giving also the roll derivatives, is presented in Appendix 2. The result for m_q is

$$(m_q)_r = -\frac{4ah}{\gamma(B^2 - \frac{1}{2}\mu^2)}\left\{\tfrac{2}{3}B\theta_0 + \tfrac{3}{2}\lambda - \tfrac{1}{2}\mu a_1\right\}. \tag{54}$$

The x_q derivative is usually negligibly small and $z_q = 0$.

4.2.3. *Effect of δ_3-hinge on rotor thrust derivatives.* It will be seen in a later section that the front rotor downwash causes severe instability with incidence, i.e. m_w becomes large and positive. A method of achieving a negative m_w on the tandem-rotor helicopter is to provide differential δ_3-hinges for the rotor blades—negative on the front rotor and positive on the rear, where a negative δ_3-hinge is one in which the blade angle decreases with increase in flapping angle. This has the effect of decreasing the lift slope of the front rotor and increasing that of the rear, thereby providing a powerful nose-down pitching moment with incidence. The calculation of $\partial t_c/\partial \hat{w}$ for a rotor

with a δ_3-hinge is given in Appendix 3 and shows that if $\partial t_0/\partial\hat{w}$ is the value of the lift slope of a rotor without a δ_3-hinge, then the corresponding value with the δ_3-hinge $(\partial t_c/\partial\hat{w})_{\delta 3}$ is

$$\left(\frac{\partial t_c}{\partial\hat{w}}\right)_{\delta 3} = \frac{\partial t_c}{\partial\hat{w}}\left\{1 \pm \frac{cc_1\gamma}{6c_2\left(1 - \frac{\gamma c}{8}\right)}\right\} \tag{55}$$

where the positive sign refers to a positive δ_3-hinge and *vice-versa.*

4.3. *Complete Helicopter Derivatives.* The expressions for the force derivatives are

$$\begin{aligned} x_u &= (x_u)_F + (x_u)_R + (x_u)_f \\ &= -\tfrac{1}{2}\left[\left\{\left(\frac{\partial t_c}{\partial\hat{u}}\alpha_D\right)_F + \left(t_c\frac{\partial a_1}{\partial\hat{u}}\right)_F + \left(\frac{\partial h_c}{\partial\hat{u}}\right)_F\right\} + \left\{\left(\frac{\partial t_c}{\partial\hat{u}}\alpha_D\right)_{RD}\right. \right. \\ &\qquad \left.\left. + \left(t_c\frac{\partial a_1}{\partial\hat{u}}\right)_R + \left(\frac{\partial h_c}{\partial\hat{u}}\right)_R\right\}\right] - 2\mu d_0 \end{aligned} \tag{56}$$

where

$$d_0 = \frac{D_0}{10^4\rho s 2A} \text{ and } \left(\frac{\partial h_c}{\partial\hat{u}}\right)_F = \left(\frac{\partial h_c}{\partial\hat{u}}\right)_R = \frac{\delta}{4} \text{ approximately.}$$

$$\begin{aligned} x_w &= (x_w)_F + (x_w)_R \\ &= -\tfrac{1}{2}\left[\left\{\left(\frac{\partial t_c}{\partial\hat{w}}\alpha_D\right)_F + \left(t_c\frac{\partial a_1}{\partial\hat{w}}\right)_F\right\} + \left\{\left(\frac{\partial t_c}{\partial\hat{w}}\alpha_D\right)_{RD} + \left(t_c\frac{\partial a_1}{\partial\hat{w}}\right)_R\right\}\right] \end{aligned} \tag{57}$$

the h_c terms being very small

$$z_u = -\tfrac{1}{2}\left\{\left(\frac{\partial t_c}{\partial\hat{u}}\right)_F + \left(\frac{\partial t_c}{\partial\hat{u}}\right)_{RD}\right\} \tag{58}$$

$$z_w = -\tfrac{1}{2}\left\{\left(\frac{\partial t_c}{\partial\hat{w}}\right)_F + \left(\frac{\partial t_c}{\partial\hat{w}}\right)_{RD}\right\}. \tag{59}$$

The total derivatives of rotor force with respect to rate of pitch are very small and are not worth including but the separate components must be found in order to calculate the moment derivatives.

Thus

$$x_q = (x_q)_F + (x_q)_R = \{(x_u h_1)_F - (x_w l_1)_F\} + \{(x_w l_1)_R - (x_u h_1)_R\} \tag{60}$$

and

$$z_q = (z_q)_F + (z_q)_R = \{(z_u h_1)_F - (z_w l_1)_F\} + \{(z_w l_1)_R - (z_u h_1)_R\}. \tag{61}$$

The moment derivatives are then

$$m_u = -(z_u l_1)_F - (x_u h_1)_F + (z_u l_1)_R - (x_u h_1)_R \tag{62}$$

$$m_w = -(z_w l_1)_F - (x_w h_1)_F + (z_w l_1)_R - (x_w h_1)_R \tag{63}$$

$$m_q = -(z_q l_1)_F - (x_q h_1)_F + (z_q l_1)_R - (x_q h_1)_R + (m_q)_r \tag{64}$$

where $(m_q)_r$ is the moment due to rotor tilt given by equation (54) and

$$h_{1F} = h_F\cos(\alpha_s + \phi) + l_F\sin\alpha_s \simeq h_F + l_F\alpha_s \tag{65}$$

$$h_{1R} = h_R\cos(\alpha_s - \phi) - l_R\sin\alpha_s \simeq h_R - l_R\alpha_s \tag{66}$$

$$l_{1F} = l_F\cos\alpha_s - h_F\sin(\alpha_s + \phi) \simeq l_F - h_F(\alpha_s + \phi) \tag{67}$$

$$l_{1R} = l_R\cos\alpha_s + h_R\sin(\alpha_s - \phi) \simeq l_R - h_R(\alpha_s - \phi). \tag{68}$$

4.4. *Derivatives due to Downwash Lag.* 4.4.1. *Lag in change of incidence.* Let ϵ be the mean downwash angle at the rear rotor and α the change of helicopter incidence. The distance between the rotor centres is $(l_F + l_R)R$ and we will treat this as the significant distance between the rotors although the downwash pattern in this region is by no means well defined. The time taken to traverse this distance is $(l_F + l_R)R/V$ and the downwash angle at the rear rotor is therefore

$$\epsilon = \frac{d\epsilon}{d\alpha}\left[\alpha - \frac{d\alpha}{dt}\frac{(l_F + l_R)R}{V}\right]. \tag{69}$$

The incidence α' at the rear rotor is

$$\begin{aligned}\alpha' &= \alpha - \epsilon = \alpha - \frac{d\epsilon}{d\alpha}\left[\alpha - \frac{d\alpha}{dt}\frac{(l_F + l_R)R}{V}\right] \\ &= \alpha\left(1 - \frac{d\epsilon}{d\alpha}\right) + \frac{d\epsilon}{d\alpha}\frac{d\alpha}{dt}\frac{(l_F + l_R)R}{V}\end{aligned} \tag{70}$$

Now $$\frac{d\alpha}{dt} = \frac{\dot{w}}{V}$$

therefore

$$\alpha' = \alpha\left(1 - \frac{d\epsilon}{d\alpha}\right) + \frac{d\epsilon}{d\alpha}\frac{\dot{w}}{V}\frac{(l_F + l_R)R}{V}$$

or

$$w' = V\alpha\left(1 - \frac{d\epsilon}{d\alpha}\right) + \frac{d\epsilon}{d\alpha}\cdot\frac{\dot{w}}{V}(l_F + l_R)R$$

and

$$dM = (Z_w)_R\, w' l_R R = Z_w\left\{V\alpha\left(1 - \frac{d\epsilon}{d\alpha}\right) + \frac{d\epsilon}{d\alpha}\frac{\dot{w}}{V}(l_F + l_R)\right\} l_R R$$

so that

$$M_{\dot{w}} = (Z_w)_R\frac{\partial w'}{\partial \dot{w}} = (Z_w)_R\frac{d\epsilon}{d\alpha}\frac{(l_F + l_R)l_R R^2}{V}$$

i.e.

$$m_{\dot{w}} = (z_w)_R\,(l_F + l_R)l_R\frac{d\epsilon}{d\hat{w}} \tag{71}$$

The derivatives $x_{\dot{w}}$ and $z_{\dot{w}}$ can, of course, be calculated but they are negligibly small.

4.4.2. *Lag due to change of forward speed.* The change of downwash due to change of forward speed is

$$\epsilon = \frac{d\epsilon}{du}\left[u - \frac{du}{dt}\frac{(l_F + l_R)R}{V}\right] \tag{72}$$

and

$$w' = -V\frac{d\epsilon}{du}\left[u - \frac{du}{dt}\frac{(l_F + l_R)R}{V}\right].$$

Thus, in a similar manner to that of 4.4.1

$$m_{\dot{u}} = (z_w)_R(l_F + l_R)l_R\frac{d\epsilon}{d\hat{u}}. \tag{73}$$

Again the force derivatives with respect to $\dot{u}$ are negligible. It is interesting to note that derivative $m_{\dot{u}}$ does not appear in fixed-wing aircraft calculations as $d\epsilon/d\hat{u}$ is zero.

5. *Discussion of Derivatives.* 5.1. *Force Derivatives.* The force derivatives are shown in Figs. 12 to 15. The variations of the total derivatives due to changes of ϕ and C.G. position are negligible since the changes of front rotor derivatives are cancelled by opposite changes on the rear rotor. The variations of the derivatives with tip-speed ratio μ are thus very similar to those of the single-rotor helicopter. These variations have been fully discussed in Ref. 8 and so will not be repeated here.

5.2. *Moment Derivatives.*

5.2.1. $\nu \left(\equiv - \frac{m_q}{i_B} \right)$

The variation of ν with μ is shown in Fig. 16. The contribution due to precession of the rotor discs (which is the only source of rotor damping in the single rotor helicopter) is also shown and is seen to be small and, except in hovering, may even be considered negligible. The large damping in pitch of the tandem-rotor helicopter is due, of course, to the fact that a steady rate of pitch increases the rear rotor incidence and decreases the front rotor incidence thus providing a large nose-down pitching moment.

5.2.2. $\mathscr{H} \left(\equiv - \frac{\mu_2 m_u}{i_B} \right)$

The variation of $\mathscr{H}$ with μ is shown in Fig. 17. It will be seen that there are three effects:

(a) large variations with μ due to downwash changes

(b) large variations with ϕ

(c) mainly small variations with C.G. position.

In considering (a), we assume that the downwash effect is zero at hovering and rises to a maximum at about $\mu = 0{\cdot}1$. The downwash effect with forward speed above $\mu = 0{\cdot}1$ is determined from equation (7) of Section 2. The three terms of equation (7) can be recognised as (i) the change of induced velocity due to change of thrust and (ii) and (iii) as the change in downwash angle due to change of induced velocity at constant forward speed and change of forward speed with constant induced velocity. The first term (i) is usually small. The last two terms can be shown to be of equal sign and magnitude for $\mu \gg \lambda$ and represent a decrease of downwash angle with forward speed. Thus when $\mu \ll \lambda$ the downwash always causes a nose-down pitching moment with increase of forward speed, the effect being most severe at about $\mu = 0{\cdot}1$.

In (b), variations of ϕ alter the incidences of front and rear rotors and it can be seen from equation (44) of Section 4.2.1 that in general the derivatives of thrust with respect to forward speed of front and rear rotors will be different. If ϕ is positive the front rotor will have a larger thrust derivative than the rear one and this will provide a nose-up pitching moment with speed. A given value of ϕ will provide a contribution to $\mathscr{H}$ which is roughly constant over the lower part of the speed range (*see* Fig. 17), whereas the destabilizing effect of the downwash varies considerably in this range. The value of ϕ required to eliminate the downwash effect is probably about 5 deg for the type chosen and with central C.G. position. However, this value may then be too large for the hovering case, where the downwash effect is absent, and would lead to a rapidly divergent oscillation similar to that of the single-rotor helicopter. The same effect may also appear at high speeds where the downwash effect is small.

It would be desirable, therefore, to have means of varying ϕ in flight in order to have the optimum, or at least a suitable, value of $\mathscr{H}$ at any given speed. This could be achieved, for example, by a trimmer which moves the front and rear swash-plates in opposite directions. The trimmer could be calibrated in terms of forward speed so that the pilot could select the appropriate value of $\mathscr{H}$ for the speed at which he wished to cruise.

Whether or not it is worth providing such a trimmer depends on the designer's opinions as to the seriousness of the instability and the complexity of the other flying controls.

5.2.3. $\omega \left(\equiv - \frac{\mu_2 m_w}{i_B} \right)$

Fig. 18 shows the variation of ω with μ for zero δ_3-hinge for different values of ϕ and C.G. position. It will be seen that the effect of ϕ on ω is smaller. For the tandem-rotor helicopter the longitudinal cyclic pitch B_1 does not cancel the backward flapping a_1, in fact at high speeds a_1 may be several times larger than B_1, and the rotor force vectors are then tilted backwards in trimmed flight and cause a destabilizing nose-up pitching moment when the incidence is increased. This effect gets worse with increase of speed as shown in the case of $\phi = 0$. Increasing ϕ changes the moment arms of the force vectors in the stabilizing sense as shown by the case $\phi = 3$ deg.

The effect of C.G. position on ω is very marked. The downwash effect reduces the thrust derivative on the rear rotor tending to result in a destabilizing nose-up moment with incidence. This destabilizing moment can be reduced, of course, by setting the C.G. forward, the moment being directly proportional to C.G. position. The downwash effect can be seen in the peaks of the curves in the region of $\mu = 0{\cdot}1$.

Fig. 19 shows how a δ_3-hinge affects the case $\phi = 0$ and C.G. position central. It is seen that ω, even for this 'worst case' ,can be completely shifted into the stable region for a reasonable value of C.

5.2.4. $\beta \left(\equiv - \frac{m_{\dot{u}}}{i_B} \right)$ and $\chi \left(\equiv - \frac{m_{\dot{w}}}{i_B} \right)$

The variations with μ of the downwash lag derivatives β and χ are shown in Figs. 20 and 21. The curves were calculated from equations (7), (8), (71) and (73) for $\mu = 0{\cdot}1$ to $\mu = 0{\cdot}4$ and faired in for the region $\mu = 0$ to $\mu = 0{\cdot}1$ on the assumption that the derivatives are zero at $\mu = 0$. The slight variations with C.G. position are due to the variations in length of moment arm and strength of downwash from the front rotor.

6. *Discussion of Stick-Fixed Dynamic Stability.* 6.1. *Effect of C.G. Position and Swash-Plate Dihedral.* 6.1.1. *Stability in hovering.*

The dynamic stability in hovering of the tandem-rotor helicopter, as can be seen from Figs. 22(b) and 22(c), is independent of C.G. position and varies only with the 'dihedral' angle of the rotor-hub axes, 2ϕ. In fact, as with the single-rotor helicopter, stability of the tandem helicopter in hovering depends almost entirely on m_u and m_q; both m_u and m_q are unaffected in hovering by C.G. position but m_u is directly proportional to ϕ. If m_u is positive there is a divergent oscillation, which becomes more divergent and whose period becomes shorter as m_u is increased.

On the tandem helicopter it is possible to reduce m_u to zero by tilting the rotor-hub axes outwards (i.e. ϕ becomes negative) so that the positive contribution to m_u from the rotor tilt derivatives is

balanced by a negative contribution from the thrust derivatives. This can be expressed by

$$t_{cF}h_F\left(\frac{\partial a_1}{\partial \hat{u}}\right)_F + t_{cR}h_R\left(\frac{\partial a_1}{\partial \hat{u}}\right)_R + l_F\left(\frac{\partial t_c}{\partial \hat{u}}\right)_F - l_R\left(\frac{\partial t_c}{\partial \hat{u}}\right)_R = 0\,. \tag{74}$$

In hovering

$$\left(\frac{\partial t_c}{\partial \hat{u}}\right)_F = \frac{c_2(\alpha_s + \phi)}{\Delta}\,;\left(\frac{\partial t_c}{\partial \hat{u}}\right)_R = \frac{c_2(\alpha_s - \phi)}{\Delta}\,.$$

Inserting typical values for the Bristol 173 into equation (74) gives $\phi = -1{\cdot}3$ deg, *i.e.* when the rotor-hub axes are tilted outwards and make an angle of $2{\cdot}6$ deg to one another m_u is zero and the helicopter is neutrally stable. If m_u is negative there is a pure divergence and, as with the single-rotor helicopter, it is impossible to obtain dynamic stability with m_u and m_q alone.

6.1.2. *Stability at* $\mu = 0{\cdot}1$. It will be seen from Figs. 23(a) and 23(b) that at about $\mu = 0{\cdot}1$ the stick-fixed motion of the tandem helicopter is rapidly divergent for all the cases considered, the motion doubling its amplitude in about $2\frac{1}{2}$ seconds. In these cases the constant term E, which is proportional to $m_w z_u - m_u z_w$, is negative since the m_u term is positive because of the powerful downwash effect, as explained in Section 5.2.2. The rotor-hub dihedral necessary to make the m_u term negative would be about 16 deg ($\phi = 8$ deg) and this may be an excessive value in practice. The m_w term, which is much smaller, also acts in the destabilizing sense due to the downwash effect and it can be seen from Fig. 23(b) that the variations in m_w due to C.G. movement are too small to have much effect.

It appears, then, that at speeds in the region of $\mu = 0{\cdot}1$ the tandem-rotor helicopter, except perhaps with δ_3-hinges, will suffer from a purely divergent instability.

6.1.3. *Stability above* $\mu = 0{\cdot}1$. As the trimmed speed increases above $\mu = 0{\cdot}1$ the downwash effect on the stability diminishes rapidly and it can be seen from Figs. 24(b), 25(b) and 26(b) that the purely divergent motion occurs only for $\phi < 2$ deg at $\mu = 0{\cdot}2$ and for $\phi < 1$ deg for $\mu = 0{\cdot}3$ and $0{\cdot}4$. Forward movement of the C.G. also becomes more effective in improving the stability and it can be seen that with the correct combination of ϕ and C.G. position it is possible to make the helicopter dynamically stable.

6.2. *Effect of* δ_3*-hinge.* It will be recalled from Section 4.1.3 that the fitting of δ_3-hinges enables the derivative m_w to be varied over a wide range and the effect on the dynamic stability of varying the δ_3-hinge angle is shown in Figs. 27 to 30. In hovering there is no coupling between the vertical motion and the fore-and-aft and pitching motion so that the δ_3-hinge has no effect on the stability.

At $\mu = 0{\cdot}1$, as can be seen from Fig. 27, the δ_3-hinge effect alleviates the strong divergence although increasing the value of C beyond $0{\cdot}15$ has no further effect. However, it appears that a much smaller value of ϕ—about 4 deg instead of 8 deg without δ_3-hinges—can now be used to obtain positive stability and this value may be acceptable.

For $\mu = 0{\cdot}2$ and above Figs. 28 to 30 (C.G. back) show that the δ_3-hinge greatly improves the stability but again there is little further improvement when C exceeds $0{\cdot}15$.

The problem, which occurs with the single-rotor helicopter, of introducing a pure divergence by having too great a value of m_w at the higher speeds (where z_u is positive) need not arise with the tandem-rotor helicopter since the static stability can always be made positive by choosing a suitable value of m_u by varying ϕ.

6.3. *Effect of Downwash Lag on the Stability.* The effect of downwash lag on the stability has been calculated for two cases at $\mu = 0{\cdot}1$ (where the derivatives are largest) and the results given below.

	$\phi = 0°$ C.G. Central	$\phi = 3°$ C.G. Forward
χ and β included	$r = 0{\cdot}332$ sec^{-1}	$r = 0{\cdot}233$ sec^{-1}
χ omitted	$r = 0{\cdot}343$ sec^{-1}	$r = 0{\cdot}252$ sec^{-1}
β omitted	$r = 0{\cdot}418$ sec^{-1}	$r = 0{\cdot}311$ sec^{-1}
χ and β omitted	$r = 0{\cdot}431$ sec^{-1}	$r = 0{\cdot}342$ sec^{-1}

It will be seen that both derivatives improve the stability, the lag due to forward acceleration having the greater effect.

7. *Discussion of Control Response.* Figs. 31 to 46 show the time histories of the response of the tandem-rotor helicopter to a sudden 1 deg backward displacement of the stick. A peculiarity of tandem-rotor helicopter response can be seen in many of the normal acceleration-time curves. In Fig. 31, for example, the slope of the curve increases up to about $t = 1$ sec, then decreases slightly up to about $t = 3$ secs and then increases again. This cannot be regarded as a satisfactory response because the normal acceleration never 'settles down'; nevertheless the curve satisfies the N.A.C.A. manoeuvrability criterion[8], since $d^2n/dt^2 < 0$ before $t = 2$ secs. The reason for this shape of curve is that there is large damping in pitch (large m_q) which damps the motion in its early stages, but as speed increases the divergent m_u effect predominates and causes the acceleration to 'run away'. Thus, satisfaction of the N.A.C.A. criterion does not necessarily indicate acceptable manoeuvrability for the tandem-rotor helicopter. The N.A.C.A. criterion was devised from measurements of the normal acceleration of the single-rotor helicopter where m_u usually has a small positive value and where there is no purely divergent mode. In this case (and also for the subsonic fixed-wing aircraft case) the condition $d^2n/dt^2 < 0$ is all that is required to ensure that the normal acceleration curve is satisfactory. A typical curve for the latter case is shown in Fig. 47 together with the desirable response curve and a typical curve for the tandem-rotor helicopter. It is clear that the N.A.C.A. criterion, which is intended to describe an acceptable response curve, is not detailed enough to cater for the case of the tandem-rotor helicopter. It is difficult to express a satisfactory response curve in words but since the response is determined by the dynamic stability satisfactory response will certainly occur if there is good damping of the short period mode and if the long period mode is no worse than slowly divergent. Thus for the single-rotor helicopter a tailplane strongly damps the short period mode and improves the long period mode so that even if the latter is still unstable the manoeuvre will have been completed before its amplitude begins to increase rapidly. The tandem-rotor helicopter has adequate damping in pitch but if the swash-plate dihedral is too small the latter part of the manoeuvre will be divergent. To ensure satisfactory response requires that the stability associated with speed changes must not be rapidly divergent. A slow divergence or slowly divergent oscillation is permissible since the effect of the speed changes will not be felt much before the manoeuvre is over.

Another peculiarity of helicopter control response, described in Ref. 13, is the sudden change of normal acceleration with sudden stick movements. On the single-rotor helicopter this is followed by an unpleasant pause in the increase of acceleration in a pull-out and its severity is determined by the ratio of rotor thrust change to rotor pitching moment with stick movement. In this case, the ratio can be varied only between narrow limits but on the tandem-rotor helicopter it can be varied arbitrarily through the control 'mixture' (Section 3.1) since differential collective pitch supplies a moment without a change of total thrust. For typical control mixtures the force-moment ratio is much smaller than values for the single-rotor helicopter and the pause in normal acceleration, although clearly seen in Figs. 31 to 46, should barely be noticeable in practice.

Forward movement of the C.G. improves the response but is more effective when associated with values of $\phi > 0$.

The effect on the control response of fitting δ_3-hinges is shown in Figs. 39 to 46. It can be seen that although the response is considerably improved for the case $\phi = 0$ deg it is seldom satisfactory at any speed even for the largest δ_3-hinge angles. However, when $\phi = 3$ deg the response is well damped in nearly every case.

8. *Conclusions.* 8.1. Reasonably accurate estimates of the front rotor's downwash effect can be made from the wind-tunnel measurements of Ref. 4 for $\mu > 0{\cdot}1$ and from Ref. 2 for $\mu < 0{\cdot}05$. The relevant measurements from Ref. 4 are represented in Fig. 4 of this report. These estimates can be checked by comparing theoretical trim curves with those measured in flight. Agreement is quite good.

8.2. The trim curves show a stick reversal with speed between $\mu = 0{\cdot}1$ and $\mu = 0{\cdot}25$ for $\phi = 0$ deg. Increasing ϕ reduces the stick reversal and eliminates it when ϕ is about 5 deg.

8.3. In hovering the tandem-rotor helicopter has a divergent long period oscillation whose rate of divergence and frequency of oscillation increases with ϕ. When ϕ is about $-1{\cdot}3$ deg (for a helicopter similar to the Bristol 173) m_u is zero and the motion is neutrally stable but it is impossible to make the helicopter positively stable.

8.4. At about $\mu = 0{\cdot}1$ and for a certain range above this value (depending on ϕ) there is a rapidly divergent stability mode associated with the stick reversal of $8{\cdot}2$, *i.e.* negative m_u. Increasing ϕ improves the stability and when $\phi = 5$ deg m_u is positive at all speeds but there may then be a divergent oscillation if the C.G. is not fully forward $\{(l_R - l_F)/(l_R + l_F) = 0{\cdot}1\}$.

8.5. Differential δ_3-hinges greatly improve the stability and by a correct choice of swash-plate dihedral and δ_3-hinge angle the helicopter may be made positively stable at all speeds except hovering. It appears that there is little further improvement when C exceeds about $0{\cdot}15$.

8.6. The control response is unsatisfactory if there is a pure divergence, unless it is fairly slow, since although there is large damping in pitch the normal acceleration 'runs away' before the manoeuvre is over. In fact it is possible for the helicopter to satisfy the N.A.C.A. divergence requirement yet still possess unsatisfactory response. Again, a suitable choice of δ_3-hinge angle and swash-plate dihedral can be made to provide satisfactory control response.

a — Lift slope of blade section. (Taken in this report as 5·6)

a_0 — Coning angle of rotor blades

a_1 — Angle between tip-path plane and plane perpendicular to no-feathering axis. Positive for backward tilt of disc

a_{1s} — Angle between tip-path plane and plane perpendicular to rotor hub axis. Positive for backward tilt of disc

A — Area of one rotor disc

A — Coefficient of η^2 in trim quadratic

$\mathbf{A}$ — Angular velocity vector of blade

A_1 — Lateral cyclic pitch application

b — Number of blades

b_1 — Lateral tilt of rotor disc relative to no-feathering axis. Positive when disc tilts towards advancing blade

b_{1s} — Lateral tilt of rotor disc relative to rotor hub axis. Positive when disc tilts towards advancing blade

B — Tip-loss factor. (Taken in this report as 0·97)

B — Coefficient of λ^3 in stability quartic

B — Moment of inertia of helicopter about lateral axis, slugs ft^2

B — Coefficient of η in trim equation

B_1 — Longitudinal cyclic pitch application

c — Blade chord ft

C — Rate of change of blade pitch with flapping (*see* equation (131) of Appendix 3 on δ_3-hinge)

C_1, C_2 — *See* equation (2)

C_3, C_4 — *See* equation (19)

$C_1' \ldots C_4' = \dfrac{dC_1}{d\mu} \ldots \dfrac{dC_4}{d\mu}$

C — Constant term in trim quadratic

C — Coefficient of λ^2 in stability quartic

$C_l = \dfrac{L}{2\rho s A(\Omega R)^2}$ rolling-moment coefficient

$C_y = \dfrac{Y}{2\rho s A(\Omega R)^2}$ side-force coefficient

$C_{mf} = \dfrac{M_f}{2\rho s A(\Omega R)^2 R}$

D Coefficient of λ in stability quartic

D_f Drag of fuselage lb

D_0 Drag of fuselage at 100 ft/sec

$d_0 = \dfrac{D_0}{10^4 \rho s 2A}$

E Constant term in stability quartic

hR *See* Fig. 1

$h_1 R$ *See* Fig. 2

H Component of rotor force parallel to tip-path plane lb

$h_c = \dfrac{H}{\rho s A(\Omega R)^2}$

$\mathbf{H}$ Angular momentum vector of blade

$\mathbf{i}, \mathbf{j}, \mathbf{k}$ Set of perpendicular unit vectors; $\mathbf{i}$ lies in the plane of blade flapping and $\mathbf{k}$ is parallel to the rotor hub axis

$i_B = \dfrac{B}{WR^2/g}$ dimensionless form of pitching moment of inertia

I_1 Moment of inertia of blade about flapping hinge, slugs ft^2

$k = v_i/v_{i0}$, ratio of induced velocity at a point in the induced velocity field to the momentum velocity

k_1 Ratio of longitudinal cyclic pitch angle to stick angle, *see* equation (10)

k_2 Ratio of differential collective pitch angle to stick angle. *See* equations (11) and (12)

L Lift of a blade, lb

L Rolling moment, lb ft. Positive when it tends to roll helicopter to starboard

M Pitching moment, lb ft. Positive in nose up sense

M_u, M_w etc. Moment derivatives $\partial M/\partial u$, $\partial M/\partial w$ etc.

m_u, m_w etc. Dimensionless moment derivatives

M_f Fuselage pitching moment lb ft

n Increment of normal acceleration in g-units

p Rate of roll, angular velocity about longitudinal axis, positive when to starboard

q Rate of pitch, angular velocity about lateral axis, positive in nose-up sense

r		Distance of blade element from axis of rotation, ft
r		Real part of root of stability quartic
R		Rotor radius, ft
s		$\frac{bc}{\pi R}$ solidity of rotor
T		Rotor-force component perpendicular to tip-path plane
t_c	$=$	$\frac{T}{\rho s A(\Omega R)^2}$
t_c'	$=$	$\frac{W}{2\rho s A(\Omega R)^2}$
u		Increment of velocity along flight path, ft/sec
$\hat{u}$	$=$	$\frac{u}{\Omega R}$, dimensionless form of u
U_P		Component of relative wind perpendicular to blade, ft/sec
U_T		Component of relative wind parallel to blade chord, ft/sec
V		Trimmed speed of helicopter, ft/sec
$\hat{V}$	$=$	$\frac{V}{\Omega R}$, dimensionless form of V
v_i		Induced velocity, ft/sec
$v_{i\,0}$		Induced velocity at rotor disc as calculated from momentum theory, ft/sec
$\hat{v}_i$	$=$	$\frac{v_i}{\Omega R}$, dimensionless form of v_i
w		Increment of velocity perpendicular to flight path, ft/sec, positive downwards
$\hat{w}$	$=$	$\frac{w}{\Omega R}$, dimensionless form of w
x	$=$	r/R, fraction of blade radius
X		Component of force parallel to x-axis (wind axes)
X_u, X_w etc.		Force derivatives $\partial X/\partial u$, $\partial X/\partial w$ etc.
x_u, x_w etc.		Dimensionless form of X_u, X_w etc.
Y		Component of force parallel to y-axis (wind axes)
Z		Component of force parallel to z-axis (wind axes)
Z_u, Z_w		Force derivatives $\partial Z/\partial u$, $\partial Z/\partial w$ etc.
z_u, z_w etc.		Dimensionless form of Z_u, Z_w etc.

α_D Incidence of rotor disc, angle between relative wind and tip-path plane, positive for backward tilt of disc

α_{nf} Incidence of no-feathering axis, angle between plane perpendicular to no-feathering axis and relative wind. Positive for backward tilt

α_s Incidence of helicopter, angle between flight path and reference line of helicopter. Reference line defined in Section 3.1. Positive when nose up

α Incremental change of α_s

α' Change of incidence of rear rotor

β Blade flapping angle relative to plane perpendicular to no-feathering axis

β_s Blade flapping angle relative to plane perpendicular to rotor-hub axis

γ Lock's inertia number, $\dfrac{\rho a c R^4}{I_1}$

γ_e Angle between horizon and trimmed flight path. Positive when aircraft climbing

δ Blade profile drag coefficient. (Taken in this report as $0{\cdot}016$)

Δ Defined in equation (50)

ϵ Downwash angle

ξ, η, ζ System of perpendicular axes used for describing induced velocity distribution. The ξ-axis passes through the centre of the rotor and lies in the plane of symmetry at an angle ϵ_0 ($= \tan^{-1} v_{i\,0}/V$) pointing downwards. The η-axis is positive to starboard and ζ positive upwards

ξ Differential application of collective pitch due to trimmer movement. Positive when collective pitch of front rotor is increased

η Angular displacement of stick. Positive when forward

θ Angle of displacement in pitch of helicopter from flight path. Positive when nose up

θ_0 Collective pitch angle at $0{\cdot}75R$

$\lambda = \dfrac{V \sin \alpha_D - v_i}{\Omega R}$, coefficient of airflow perpendicular to tip-path plane. Positive for upward flow through disc

$\lambda_{nf} = \dfrac{V \sin \alpha_{nf} - v_i}{\Omega R}$, coefficient of airflow parallel to no-feathering axis. Positive for upward flow through disc

$\mu = \dfrac{V \cos \alpha_D}{\Omega R}$ coefficient of airflow parallel to tip-path plane

$\mu_2 = \dfrac{W}{2g\rho sAR}$ relative density parameter

ρ Air density, slugs ft^{-3}

τ Non-dimensional measure of time

ϕ Half swash-plate dihedral. Semi-angle between rotor-hub axes. Positive when axes meet above helicopter

ϕ Angle between relative velocity at blade and tip-path plane

ψ Azimuth angle of blade, angle between blade and rearward longitudinal axis

Ω Angular velocity of rotor-hub axis rad/sec

Suffices

$( )_f$ Fuselage

$( )_F$ Front rotor

$( )_r$ Rotor contribution (to be distinguished from fuselage contribution)

$( )_R$ Rear rotor

$( )_{RD}$ Rear rotor corrected for downwash

REFERENCES

Ref. No.	*Author*	*Title, etc.*
1	W. Z. Stepniewski	A simplified approach to the aerodynamic rotor interference of tandem helicopters. Paper presented to the West Coast American Helicopter Society, September 21st and 22nd, 1955.
2	W. Castles Jnr. and J. H. de Leeuw ..	The normal component of the induced velocity in the vicinity of a lifting rotor and some examples of its application. N.A.C.A. Report 1184.
3	H. Glauert	A general theory of the Autogyro. R. & M. 1111.
4	H. Heyson and S. Katzoff	Induced velocities near a lifting rotor with non-uniform disc loading. N.A.C.A. Report 1319.
5	J. R. Spreiter and H. A. Sacks ..	The rolling up of the trailing vortex sheet and its effect on the downwash behind wings. *Jour. Aero. Sci.*, Vol. 18, No. 1, January, 1951.
6	W. Castles Jnr. and H. L. Durham Jnr.	Distribution of normal component in induced velocity in lateral plane of a lifting rotor. N.A.C.A. T.N. 3841.
7	I. C. Cheeseman	A method of calculating the effect of one helicopter rotor upon another. A.R.C. 20,165. C.P. 406.
8	A. R. S. Bramwell	Longitudinal stability and control of the single-rotor helicopter. R. & M. No. 3104.
9	K. B. Amer	Theory of helicopter damping in pitch or roll and a comparison with flight measurements. N.A.C.A. T.N. 2136.
10	D. F. Gebhard and L. Goland ..	On the damping in pitch of a helicopter rotor in forward flight. *Jour. Aero. Sci.*, Vol. 23, No. 11, November, 1956. (Readers' Forum.)
11	Princeton University	Stability and control of tandem helicopters. Phases I and II Static and dynamic longitudinal stability and control. Aeronautical Engineering Department, Report No. 362. September, 1956.
12	Bristol Aircraft Ltd.	Handling and performance assessment during initial forward flight tests up to flight No. 50. Type 192—XG. 447. Report FRD/192/5330 C.
13	A. R. S. Bramwell	Control response measurements on a single-rotor helicopter. (Westland *Dragonfly*.) A.R.C. 19,966.

APPENDIX I

Calculation of Rotor Derivatives

The equations for t_c, a_1, μ and λ are

$$t_c = c_1\theta_0 + c_2\lambda \tag{75}$$

$$a_1 = c_3\theta_0 + c_4\lambda \tag{76}$$

$$\mu = \hat{V}\cos\alpha_D \tag{77}$$

$$\lambda = \hat{V}\sin\alpha_D - \frac{st_c}{2(\mu^2 + \lambda^2)^{1/2}}. \tag{78}$$

Differentiating with respect to $\hat{u}$ (*i.e.* with respect to $\hat{V}$ also)

$$\frac{\partial t_c}{\partial \hat{u}} = (c_1'\theta_0 + c_2'\lambda)\frac{\partial \mu}{\partial \hat{u}} + c_2\frac{\partial \lambda}{\partial \hat{u}} \tag{79}$$

$$\frac{\partial a_1}{\partial \hat{u}} = (c_3'\theta_0 + c_4'\lambda)\frac{\partial \mu}{\partial \hat{u}} + c_4\frac{\partial \lambda}{\partial \hat{u}} \tag{80}$$

$$\frac{\partial \mu}{\partial \hat{u}} = \cos\alpha_D - \hat{u}\sin\alpha_D\frac{\partial a_1}{\partial \hat{u}} \tag{81}$$

$$\frac{\partial \lambda}{\partial \hat{u}} = \sin\alpha_D + \hat{u}\cos\alpha_D\frac{\partial a_1}{\partial \hat{u}} - \frac{s\dfrac{\partial t_c}{\partial \hat{u}}}{2(\mu^2 + \lambda^2)^{1/2}} + \frac{st_c}{2(\mu^2 + \lambda^2)^{3/2}}\left(\mu\frac{\partial \mu}{\partial \hat{u}} + \lambda\frac{\partial \lambda}{\partial \hat{u}}\right). \tag{82}$$

The results of solving these four simultaneous equations are

$$\frac{\partial t_c}{\partial \hat{u}} = \frac{\begin{array}{l} c_2\left\{\sin\alpha_D + \dfrac{\mu\cos\alpha_D st_c}{2(\mu^2 + \lambda^2)^{3/2}}\right\} + \cos\alpha_D(c_1'\theta_0 + c_2'\lambda)\left\{1 - \dfrac{\lambda st_c}{2(\mu^2 + \lambda^2)^{3/2}}\right\} \\ + \hat{V}\{c_2(c_3'\theta_0 + c_4'\lambda) - c_4(c_1'\theta_0 + c_2'\lambda)\} \end{array}}{\Delta} \tag{83}$$

$$\frac{\partial a_1}{\partial \hat{u}} = \frac{\begin{array}{l} c_4\left\{\sin\alpha_D + \dfrac{\mu\cos\alpha_D st_c}{2(\mu^2 + \lambda^2)^{3/2}}\right\} + \cos\alpha_D(c_3'\theta_0 + c_4'\lambda)\left\{1 - \dfrac{\lambda st_c}{2(\mu^2 + \lambda^2)^{3/2}}\right\} \\ + \dfrac{s}{2(\mu^2 + \lambda^2)^{1/2}}\{c_2(c_3'\theta_0 + c_4'\lambda) - c_4(c_1'\theta_0 + c_2'\lambda)\} \end{array}}{\Delta} \tag{84}$$

where

$$\Delta = \left\{1 - \frac{\lambda st_c}{2(\mu^2 + \lambda^2)^{3/2}} + \frac{c_2 s}{2(\mu^2 + \lambda^2)^{1/2}}\right\}\{1 + \mu\tan\alpha_D(c_3'\theta_0 + c_4'\lambda)\} - \mu c_4\left\{1 - \frac{s\tan\alpha_D}{2(\mu^2 + \lambda^2)^{1/2}}\left[\frac{\mu t_c}{\mu^2 + \lambda^2} - (c_1'\theta_0 + c_2'\lambda)\right]\right\}. \tag{85}$$

Differentiating equations (75) and (78) with respect to $\hat{w}$ gives

$$\frac{\partial t_c}{\partial \hat{w}} = (c_1'\theta_0 + c_2'\lambda)\frac{\partial \mu}{\partial \hat{w}} + c_2\frac{\partial \lambda}{\partial \hat{w}} \tag{86}$$

$$\frac{\partial a_1}{\partial \hat{w}} = (c_3'\theta_0 + c_4'\lambda)\frac{\partial \mu}{\partial \hat{w}} + c_4\frac{\partial \lambda}{\partial \hat{w}} \tag{87}$$

$$\frac{\partial \mu}{\partial \hat{w}} = \frac{\partial}{\partial \hat{w}}\{\hat{V}\cos(\alpha_s + a_1)\} = -\sin\alpha_D - \hat{V}\sin\alpha_D\frac{\partial a_1}{\partial \hat{w}} \tag{88}$$

$$\frac{\partial \lambda}{\partial \hat{w}} = \cos\alpha_D + \hat{V}\sin\alpha_D\frac{\partial a_1}{\partial \hat{w}} - \frac{s\dfrac{\partial t_c}{\partial \hat{w}}}{2(\mu^2+\lambda^2)^{1/2}} + \frac{st_c}{2(\mu^2+\lambda^2)^{3/2}}\left(\mu\frac{\partial \mu}{\partial \hat{w}} + \lambda\frac{\partial \lambda}{\partial \hat{w}}\right). \tag{89}$$

These equations give

$$\frac{\partial t_c}{\partial \hat{w}} = \frac{c_2\cos\alpha_D - \sin\alpha_D\left\{\dfrac{c_2\mu st_c}{2(\mu^2+\lambda^2)^{3/2}} + (c_1'\theta_0 + c_2'\lambda)\left[1 - \dfrac{\lambda st_c}{2(\mu^2+\lambda^2)^{3/2}}\right]\right\}}{\Delta} \tag{90}$$

$$c_4\left\{\cos\alpha_D - \frac{\sin\alpha_D\mu st_c}{2(\mu^2+\lambda^2)^{3/2}}\right\} - \sin\alpha_D(c_3'\theta_0 + c_4'\lambda)\left\{1 - \frac{\lambda st_c}{2(\mu^2+\lambda^2)^{3/2}}\right\}$$

$$\frac{\partial a_1}{\partial \hat{w}} = \frac{-\dfrac{s\sin\alpha_D}{2(\mu^2+\lambda^2)^{1/2}}\{c_2(c_3'\theta_0 + c_4'\lambda) - c_4(c_1'\theta_0 + c_2'\lambda)\}}{\Delta} \tag{91}$$

Differentiating equations (75) . . . . (78) with respect to θ_0 gives

$$\frac{\partial t_c}{\partial \theta_0} = (c_1'\theta_0 + c_2'\lambda)\frac{\partial \mu}{\partial \theta_0} + c_1 + c_2\frac{\partial \lambda}{\partial \theta_0} \tag{92}$$

$$\frac{\partial a_1}{\partial \theta_0} = (c_3'\theta_0 + c_4'\lambda)\frac{\partial \mu}{\partial \theta_0} + c_3 + c_4\frac{\partial \lambda}{\partial \theta_0} \tag{93}$$

$$\frac{\partial \mu}{\partial \theta_0} = -\hat{V}\sin\alpha_D\frac{\partial a_1}{\partial \theta_0} \tag{94}$$

$$\frac{\partial \lambda}{\partial \theta_0} = \hat{V}\cos\alpha_D\frac{\partial a_1}{\partial \theta_0} - \frac{s\dfrac{\partial t_c}{\partial \theta_0}}{2(\mu^2+\lambda^2)^{1/2}} + \frac{st_c}{2(\mu^2+\lambda^2)^{3/2}}\left(\mu\frac{\partial \mu}{\partial \theta_0} + \lambda\frac{\partial \lambda}{\partial \theta_0}\right). \tag{95}$$

These equations give

$$\frac{\partial t_c}{\partial \theta_0} = \frac{\left\{1 - \dfrac{\lambda st_c}{2(\mu^2+\lambda^2)^{3/2}}\right\}\left\{c_1 - \hat{V}\sin\alpha_D[c_1(c_3'\theta_0 + c_4'\lambda) - c_3(c_1'\theta_0 + c_2'\lambda)]\right\}}{\Delta}$$

$$\frac{-(c_1c_4 - c_2c_3)\left\{\hat{V}\cos\alpha_D - \dfrac{\hat{V}\sin\alpha_D\mu st_c}{2(\mu^2+\lambda^2)^{3/2}}\right\}}{\Delta} \tag{96}$$

$$\frac{\partial a_1}{\partial \theta_0} = \frac{\dfrac{s}{2(\mu^2+\lambda^2)^{1/2}}(c_1c_4 - c_2c_3) - c_3\left\{1 - \dfrac{\lambda st_c}{2(\mu^2+\lambda^2)^{3/2}}\right\}}{\Delta}. \tag{97}$$

The above derivatives, equations (83), (84), (91), (92), (96) and 97, can also be used for steep descent, except in the vortex ring region where the momentum theory, on which equation (82) is based, breaks down. However, even in this region these derivatives seem to give reasonable values.

For level flight good approximations to the derivatives are

$$\frac{\partial t_c}{\partial \hat{u}} = \frac{c_2\left\{\alpha_D + \dfrac{\mu s t_c}{2(\mu^2 + \lambda^2)^{3/2}}\right\} + \mu\{c_2(c_3'\theta_0 + c_4'\lambda) - c_4(c_1'\theta_0 + c_2'\lambda)\} + (c_1'\theta_0 + c_2'\lambda)\left\{1 - \dfrac{\lambda s t_c}{2(\mu^2 + \lambda^2)^{3/2}}\right\}}{\Delta} \tag{98}$$

$$\frac{\partial a_1}{\partial \hat{u}} = \frac{c_4\left\{\alpha_D + \dfrac{\mu s t_c}{2(\mu^2 + \lambda^2)^{3/2}}\right\} + (c_3'\theta_0 + c_4'\lambda)\left\{1 - \dfrac{\lambda s t_c}{2(\mu^2 + \lambda^2)^{3/2}} + \dfrac{c_2 s}{2(\mu^2 + \lambda^2)^{1/2}}\right\}}{\Delta} \tag{99}$$

$$\frac{\partial t_c}{\partial \hat{w}} = \frac{c_2}{\Delta} \tag{100}$$

$$\frac{\partial a_1}{\partial \hat{w}} = \frac{c_4}{\Delta} \tag{101}$$

$$\frac{\partial t_c}{\partial \theta_0} = \frac{c_1\left\{1 - \dfrac{\lambda s t_c}{2(\mu^2 + \lambda^2)^{3/2}}\right\} - \mu(c_1 c_4 - c_2 c_3)}{\Delta} \tag{102}$$

$$\frac{\partial a_1}{\partial \theta_0} = \frac{c_3\left\{1 - \dfrac{\lambda s t_c}{2(\mu^2 + \lambda^2)^{3/2}}\right\} + \dfrac{s}{2(\mu^2 + \lambda^2)^{1/2}}(c_1 c_4 - c_2 c_3)}{\Delta} \tag{103}$$

where the approximation to Δ is

$$\Delta = 1 - \frac{\lambda s t_c}{2(\mu^2 + \lambda^2)^{3/2}} + \frac{c_2 s}{2(\mu^2 + \lambda^2)^{1/2}} - c_4\mu\,. \tag{104}$$

APPENDIX II

Calculation of Rate-of-Roll and Rate-of-Pitch Derivatives

Consider the system of axes in Fig. 6. In the mutually perpendicular set of unit vectors **i**, **j**, **k**, **k** is parallel to the rotor-hub axis and **i** lies in the plane of flapping. Relative to the helicopter this system rotates about **k** with angular velocity Ω. In the other mutually perpendicular set of unit vectors **x**, **y**, **z**, **x** always is fixed in the blade and **y** always coincides with **j**. The **x**, **y**, **z** system therefore rotates relative to the **i**, **j**, **k** system with angular velocity $-\dot{\beta}$ about **j**. Finally since the helicopter is rolling and pitching about its longitudinal and lateral axes with rates p and q respectively the angular velocity of the blade can be represented by the vector

$$\mathbf{A} = \{\Omega \sin\beta - p\cos\psi\cos\beta + q\sin\psi\cos\beta\}\,\mathbf{x} + \{p\sin\psi + q\cos\psi - \dot{\beta}\}\,\mathbf{y} + \{\Omega\cos\beta - p\cos\psi\sin\beta - q\sin\psi\sin\beta\}\,\mathbf{z} \equiv A_x\mathbf{x} + A_y\mathbf{y} + A_z\mathbf{z}\,. \tag{105}$$

The moments of inertia about **x**, **y**, **z** can be taken as 0, I_1, I_1. Therefore the angular momentum of the blade is

$$\mathbf{H} = I_1 A_y \mathbf{y} + I_1 A_z \mathbf{z} \tag{106}$$

and the rate of change of angular momentum is

$$\frac{d\mathbf{H}}{dt} = \frac{\partial \mathbf{H}}{\partial t} + \mathbf{A} \wedge \mathbf{H}. \tag{107}$$

Expanding equation (107), and equating the component about **j** to the aerodynamic moment M_A, gives the flapping equation

$$M_A = I_1\{\ddot{\beta} + \Omega^2\beta - 2p\Omega\cos\psi + 2q\Omega\sin\psi\}. \tag{108}$$

The total pitching moment on the helicopter of the rotor forces is

$$C_m = h\{t_c(a_1 - B_1) + h_c\} \tag{109}$$

and the rolling moment

$$C_l = h\{t_c(b_1 + A_1) + C_y\}. \tag{110}$$

We have now to calculate t_c, h_c, a_1 and b_1 in terms of p and q.

The pitch angle in the tip-path plane is

$$\theta = \theta_0 - a_1\sin\psi + b_1\cos\psi. \tag{111}$$

The relative wind perpendicular to the blade span (in the sense of increasing incidence) for a blade element distance xR from the hub is

$$U_P = \Omega R(\lambda - \mu a_0\cos\psi + x\hat{p}\sin\psi + x\hat{q}\cos\psi) \tag{112}$$

where $\hat{p} = p/\Omega$ and $\hat{q} = q/\Omega$

and along the chord

$$U_T = \Omega R(\mu\sin\psi + x). \tag{113}$$

The blade incidence is

$$\alpha = \theta + \phi = \theta + \frac{\lambda - \mu a_0\cos\psi + x\hat{p}\sin\psi + x\hat{q}\cos\psi}{\mu\sin\psi + x} \tag{114}$$

therefore the elementary lift is

$$dL = \tfrac{1}{2}\rho a c\Omega^2R^2(\mu\sin\psi + x)^2(\theta + \phi)\,dr. \tag{115}$$

Expanding equation (115), taking the mean value round the disc, *i.e.* with respect to ψ, and integrating between $x = 0$ and $x = B$ results finally in a thrust coefficient

$$t_c = \frac{a}{4}\{\tfrac{2}{3}B\theta_0(B^2 + \tfrac{3}{2}\mu^2) + B^2\lambda - \mu a_1 B^2 + \tfrac{1}{2}B\mu\hat{p}\} \tag{116}$$

or in terms of λ_{nf} (λ referred to the no-feathering axis which does not change incidence with q)

$$t_c = \frac{aB}{4}\{\tfrac{2}{3}\theta_0(B^2 + \tfrac{3}{2}\mu^2) + B\lambda_{nf} + \tfrac{1}{2}\mu\hat{p}\} \tag{117}$$

since

$$\lambda_{nf} = \lambda - \mu a_1.$$

Also, from Fig. 11,

$$dH = -dL\,a_0\cos\psi - (dL\phi - dD)\sin\psi. \tag{118}$$

Proceeding as above we obtain for the in-plane force coefficient

$$h_c = \tfrac{1}{4}\mu\delta - \frac{aB}{4}\left\{\frac{B^2}{3}a_0b_1 - \tfrac{1}{2}B\mu a_0 + \tfrac{1}{3}B^2a_0\hat{q} - \tfrac{1}{2}B\lambda a_1 + B\lambda\hat{p} + \mu\theta_0\lambda - \right.$$
$$\left. - \tfrac{3}{8}B\mu\hat{p}a_1 + \tfrac{1}{8}B\mu\hat{q}b_1 + \tfrac{1}{3}B^2\theta_0\hat{p}\right\} \tag{119}$$

and therefore, in terms of λ_{nf},

$$c_m = \tfrac{1}{4}\mu\delta h + \frac{aBh}{4}\left\{\tfrac{2}{3}\theta_0(B^2 + \tfrac{3}{2}\mu^2)(a_1 - B_1) + \tfrac{3}{2}B\lambda_{nf}a_1 - \frac{B^2}{3}a_0b_1 + \right.$$
$$+ \tfrac{1}{2}B\mu a_0 - \tfrac{1}{3}B^2a_0\hat{q} - B\lambda_{nf}B_1 + \tfrac{1}{2}B\mu a_1^2 - B\lambda_{nf}\hat{p} -$$
$$- \mu\theta_0\lambda_{nf} - \mu^2\theta_0a_1 - \tfrac{1}{8}B\mu a_1\hat{p} - \tfrac{1}{8}B\mu\hat{q}b_1 -$$
$$\left. - \tfrac{1}{3}B^2\theta_0\hat{p} - \tfrac{1}{2}\mu\hat{p}\right\}. \tag{120}$$

Calling the lateral force Y and its coefficient C_y (positive in the direction of the retreating blade), we have

$$dY = -dLa_0\sin\psi + (dL\phi - dD)\cos\psi \tag{121}$$

and in a similar manner to the calculation of C_m we have

$$C_l = \frac{aBh}{4}\left\{\tfrac{2}{3}\theta_0(B^2 + \tfrac{3}{2}\mu^2)(A_1 + b_1) + B\lambda_{nf}(A_1 + b_1) + \tfrac{1}{2}B\mu A_1\hat{p} - \right.$$
$$- \tfrac{3}{2}\mu a_0\theta_0 - \frac{B}{8}\mu a_1\hat{q} + \tfrac{5}{8}B\mu b_1\hat{p} + \frac{B}{3}q\theta_0 + \frac{B}{2}\lambda_{nf}b_1 +$$
$$\left. + \frac{B}{2}\mu a_1b_1 - \frac{B^2}{3}a_0\hat{p} + \frac{B^2}{3}a_0a_1 - \mu a_0\lambda_{nf}\right\}. \tag{122}$$

The moment of lift of a blade element about the flapping hinge is

$$dM_A = dLxR. \tag{123}$$

Equation (123) is integrated by using equation (115) and M_A, together with the relation

$$\beta = a_0 - a_1\cos\psi - b_1\sin\psi, \tag{124}$$

is substituted in equation (108).

Equating coefficients of $\sin\psi$ gives

$$a_1 = \frac{2\mu(\frac{4}{3}B\theta_0 + \lambda_{nf})}{B^2 - \frac{1}{2}\mu^2} - \frac{16\hat{q}}{\gamma B^2(B^2 - \frac{1}{2}\mu^2)} + \frac{B^2\hat{p}}{B^2 - \frac{1}{2}\mu^2}. \tag{125}$$

Equating coefficients of $\cos\psi$ gives

$$b_1 = \frac{\frac{4}{3}B\mu a_0}{B^2 + \frac{1}{2}\mu^2} - \frac{16\hat{p}}{\gamma B^2(B^2 + \frac{1}{2}\mu^2)} - \frac{B^2\hat{q}}{B^2 + \frac{1}{2}\mu^2}. \tag{126}$$

Now C_m and C_l depend on a_1 and b_1 which in turn depend on $\hat{q}$, therefore the derivatives with respect to $\hat{q}$ must be written

$$m_q = \left(\frac{\partial C_m}{\partial \hat{q}}\right)_{\hat{u},\hat{w}} = \left(\frac{\partial C_m}{\partial \hat{q}}\right)_{a1,b1} + \left(\frac{\partial C_m}{\partial a_1}\right)_{b1,\hat{q}}\left(\frac{\partial a_1}{\partial \hat{q}}\right) + \left(\frac{\partial C_m}{\partial b_1}\right)_{a1,q}\left(\frac{\partial b_1}{\partial \hat{q}}\right) \tag{127}$$

and

$$l_p = \left(\frac{\partial C_l}{\partial \hat{p}}\right)_{\hat{r},\hat{v}} = \left(\frac{\partial C_l}{\partial \hat{p}}\right)_{a1,b1} + \left(\frac{\partial C_l}{\partial a_1}\right)_{b1,\hat{p}}\left(\frac{\partial a_1}{\partial \hat{p}}\right) + \left(\frac{\partial C_l}{\partial b_1}\right)_{a1,\hat{p}}\left(\frac{\partial b_1}{\partial \hat{p}}\right) \tag{128}$$

where the suffices indicate those variables kept constant during differentiation.

We find on differentiating equations (120), (122), (125) and (126) and substituting in (127) and (128) that the first and third terms on the right-hand sides of (127) and (128) cancel almost exactly, provided also that the term $\mu(A_1 + b_1)$ in (128) is very small, which it should be in trimmed flight. Thus we have

$$(m_q)_r = -\frac{4ah}{\gamma(B^2 - \frac{1}{2}\mu^2)}\{\tfrac{2}{3}B\theta_0 + \tfrac{3}{2}\lambda - \tfrac{1}{2}\mu a_1\} \tag{129}$$

and

$$(l_p)_r = -\frac{4ah}{\gamma B(B^2 + \frac{1}{2}\mu^2)}\{\tfrac{2}{3}\theta_0(B^2 + \tfrac{3}{2}\mu^2) + \tfrac{3}{2}B\lambda - B\mu a_1\} \tag{130}$$

Similar expressions, if required, can be obtained for x_q and y_p but these are usually negligibly small.

It is interesting to note that although the disc incidence changes due to precession when the helicopter is steadily pitching the incidence of the no-feathering axis does not change so that there is a corresponding variation of cyclic pitch angle in the tip-path plane which keeps the thrust constant, i.e. $z_q = 0$. This can be inferred from equations (116) and (117).

APPENDIX III

Calculation of $\partial t_c/\partial\hat{w}$ for a Rotor Fitted with δ_3-hinges

The relation between feathering and flapping for a blade attached to a δ_3-hinge is

$$(\theta)_{\delta 3} = \theta_0 + C\beta_s. \tag{131}$$

If

$$\beta_s = a_0 - a_{1s}\cos\psi - b_{1s}\sin\psi \tag{132}$$

the feathering in the tip-path plane is

$$\theta = \theta_0 + Ca_0 - Ca_{1s}\cos\psi - Cb_{1s}\sin\psi - a_1\sin\psi + b_1\cos\psi \tag{133}$$

and the incidence at a blade element is

$$\alpha = \theta + \frac{\lambda - \mu a_0\cos\psi}{\mu\sin\psi + x} \tag{134}$$

therefore

$$dT = \tfrac{1}{2}\rho ac\Omega^2R^3(\mu\sin\psi + x)^2\left(\theta + \frac{\lambda - \mu a_0\cos\psi}{\mu\sin\psi + x}\right)dx. \tag{135}$$

Expanding (109), taking the mean value with respect to ψ and integrating between $x = 0$ and $x = B$ gives a thrust coefficient

$$(t_c)_{\delta 3} = c_1(\theta_0 + Ca_0) + c_2\lambda \tag{136}$$

assuming Cb_{1s} is small compared with a_1.

By considering the flapping moment equation we obtain

$$a_1 = c_3(\theta_0 + Ca_0) + c_4\lambda \tag{137}$$

and

$$a_0\left\{1 - \frac{\gamma C}{2}(1 + \mu^2)\right\} = \left\{\tfrac{1}{4}\theta_0(1 + \mu^2) + \tfrac{1}{3}(\lambda - \mu a_1)\right\} \tag{138}$$

From (136), (137) and (138) and neglecting some small terms in μ^2 we get

$$\left(\frac{\partial t_c}{\partial\hat{w}}\right)_{\delta 3} = \frac{\partial t_c}{\partial\hat{w}}\left\{1 + \frac{Cc_1\gamma}{6c_2\left(1 - \frac{\gamma C}{8}\right)}\right\} \tag{139}$$

where $\dfrac{\partial t_c}{\partial\hat{w}}\left(= c_2\dfrac{\partial\lambda}{\partial\hat{w}}\right)$ is the thrust derivative without δ_3-hinge effect.

TABLE 1

Particulars of example helicopter (basically Bristol 173)

Weight	13,000 lb
Rotor radius	25 ft
Rotor speed	26 rad/sec
Solidity	0·04
h_F	0·22
h_R	0·424
$l_R + l_F$	1·62
C.G. range from $l_F = l_R$ (fully back) to $l_R - l_F = 0{\cdot}1\ (l_F + l_R)$ (fully forward)	
k_1	0·286
k_2	0·143
Fuselage drag	300 lb at 100 ft/sec
Moment of inertia in pitch	85,000 slugs ft^2
Lock's inertia number for rotor blade	8
δ	0·016

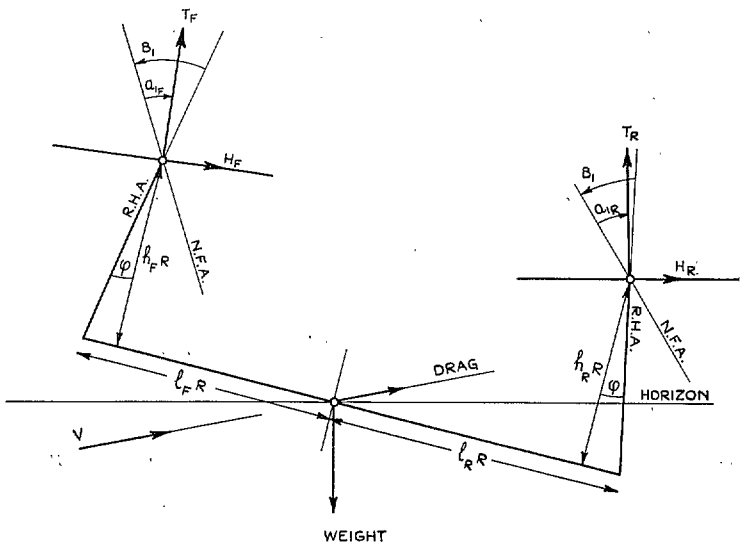

FIG. 1. Nomenclature diagram.

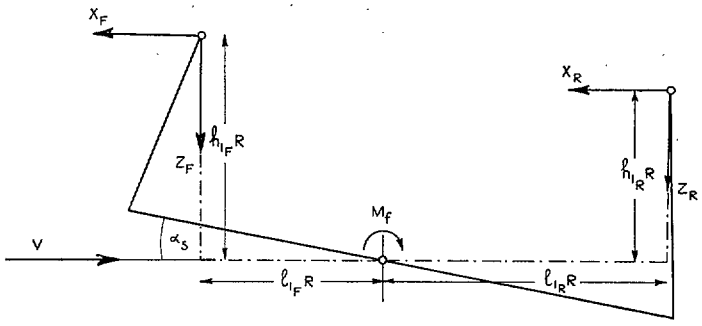

FIG. 2. Force and moment diagram.

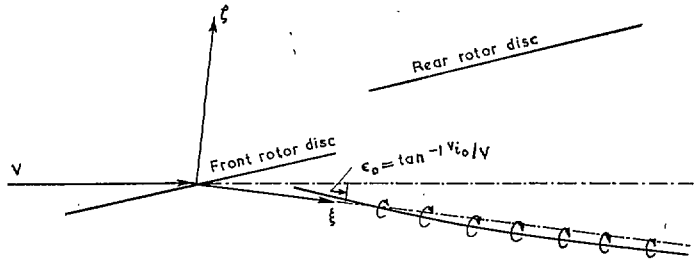

FIG. 3. Reference axes for downwash pattern.

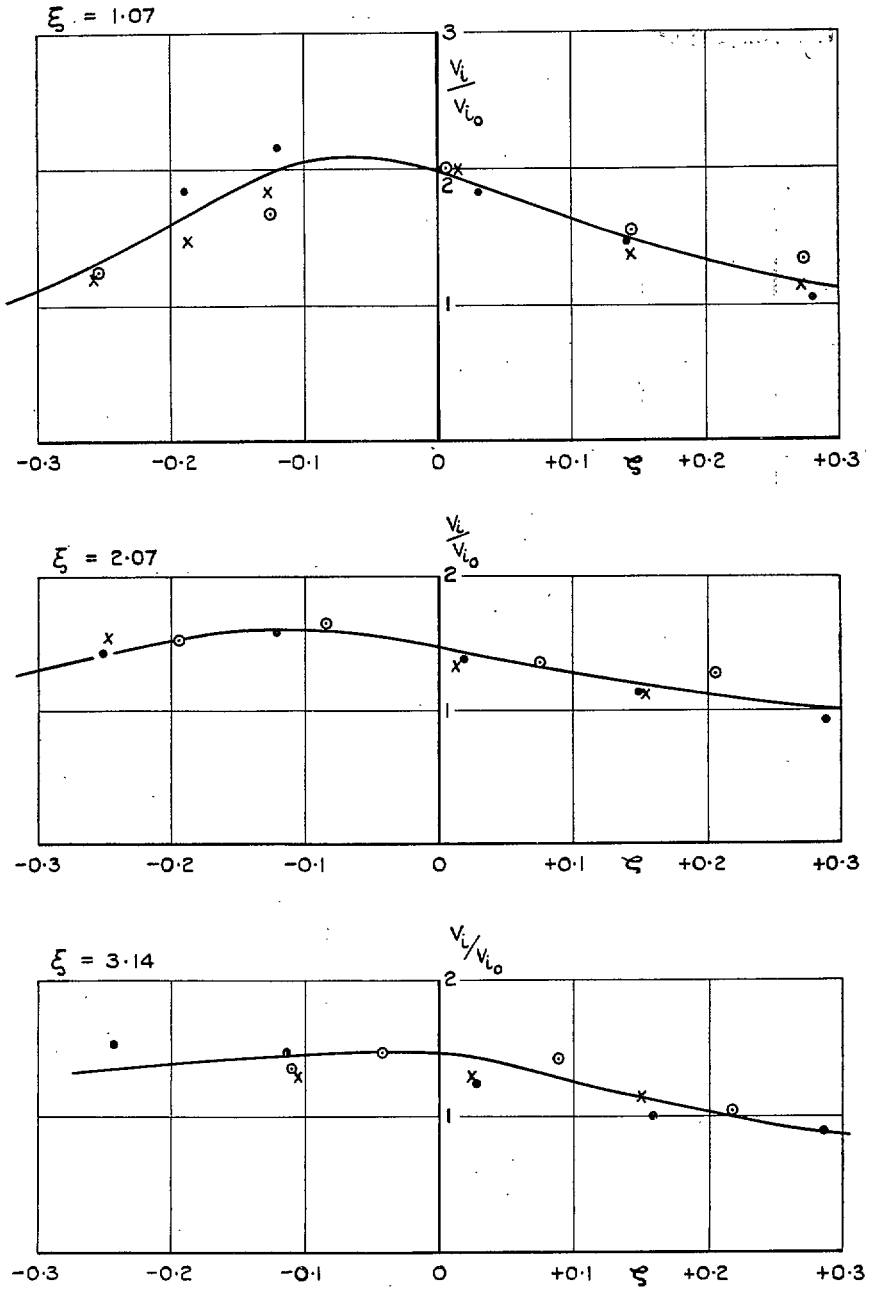

FIG. 4. Longitudinal and vertical distribution of mean lateral induced velocity behind front rotor.

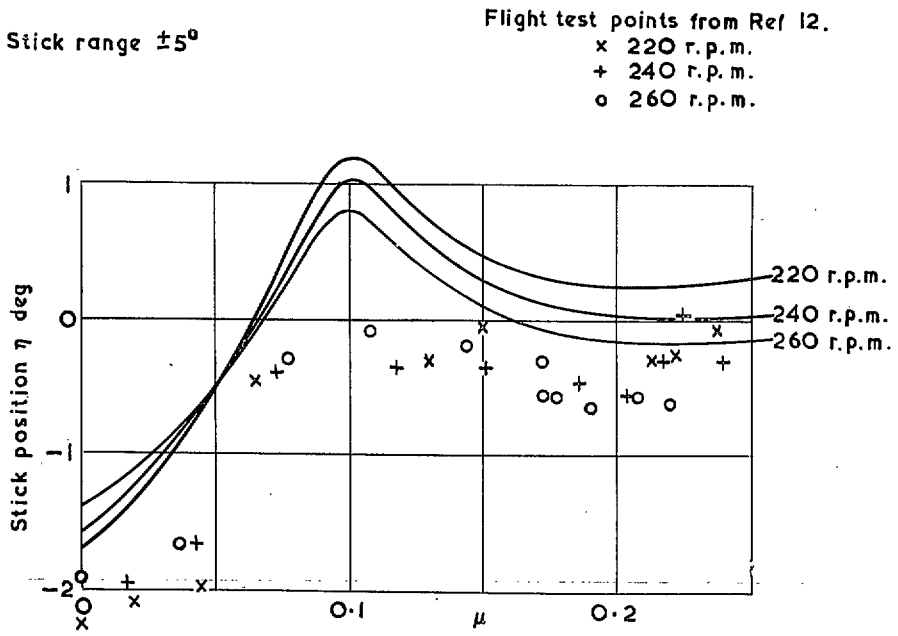

FIG. 5(a). Comparison of theoretical trim curves with flight test points. (Bristol 192.)

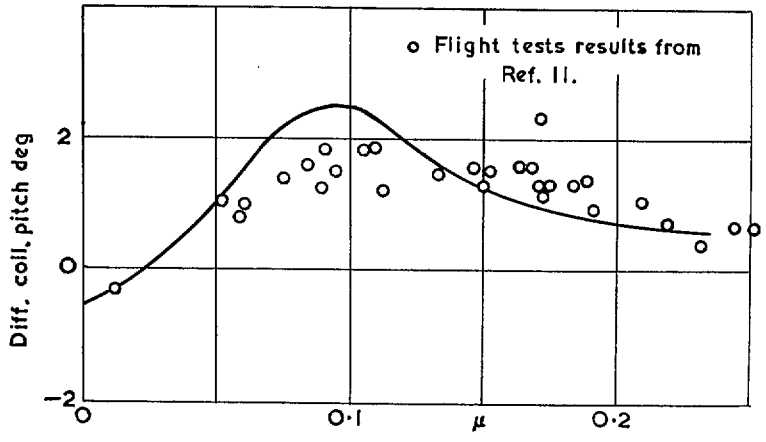

FIG. 5(b). Comparison of theoretical trim curves with flight test points. (Helicopter of ref. 11.)

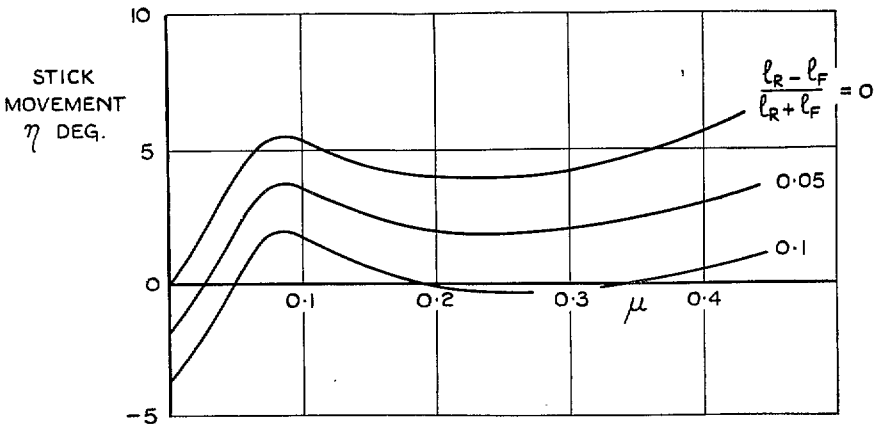

FIG. 6. Level flight trim curves for $\varphi = 0°$.

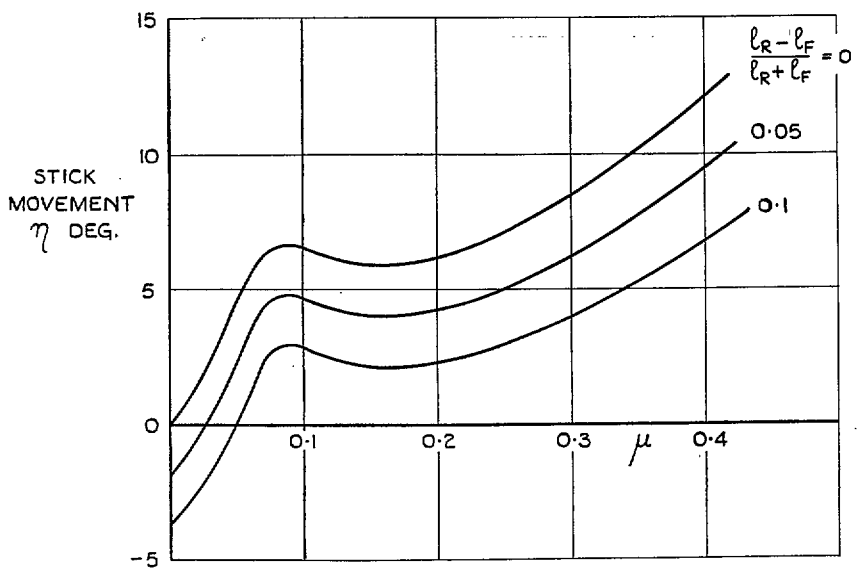

FIG. 7. Level flight trim curves for $\varphi = 1°$.

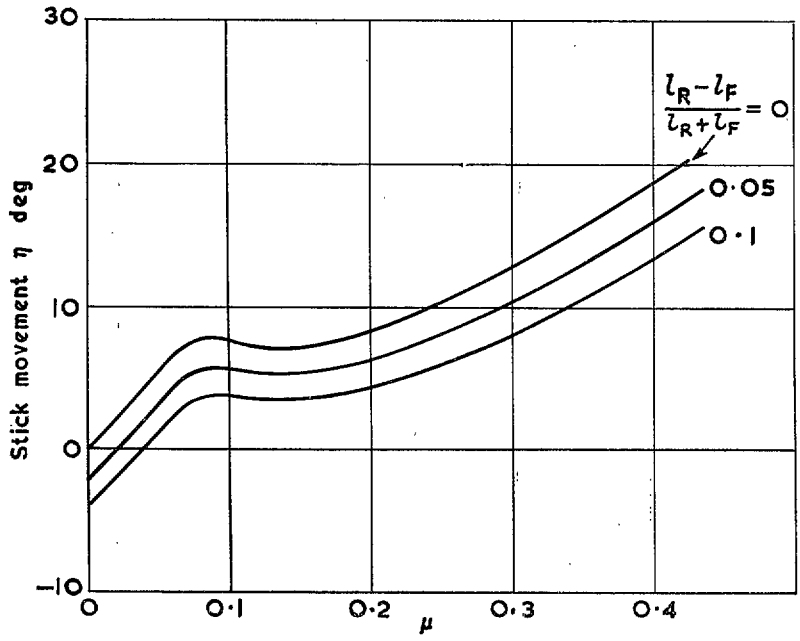

FIG. 8. Level flight trim curves for $\varphi = 2°$.

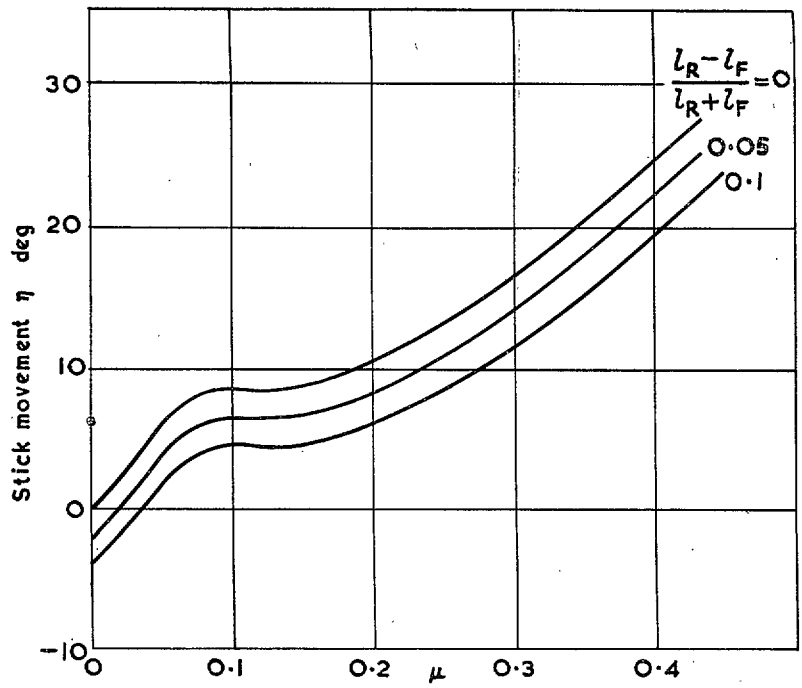

FIG. 9. Level flight trim curves for $\varphi = 3°$.

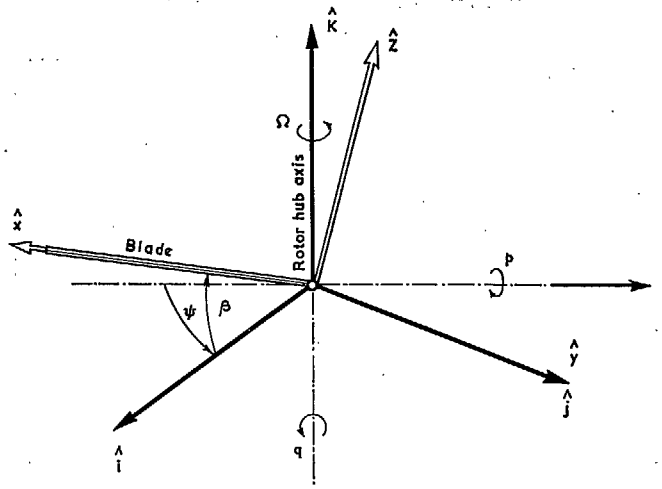

FIG. 10. Axes used for calculating rate of pitch derivatives.

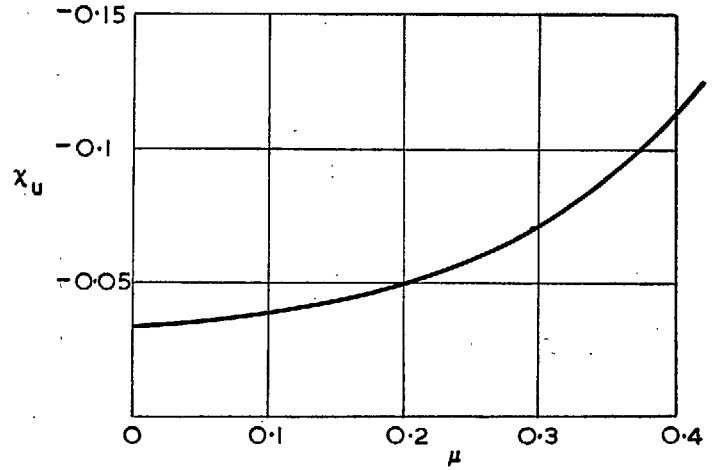

FIG. 12. Variation of χ_u with μ.

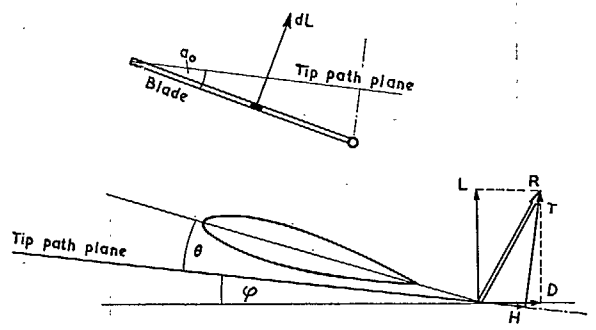

FIG. 11. Force diagram for blade element.

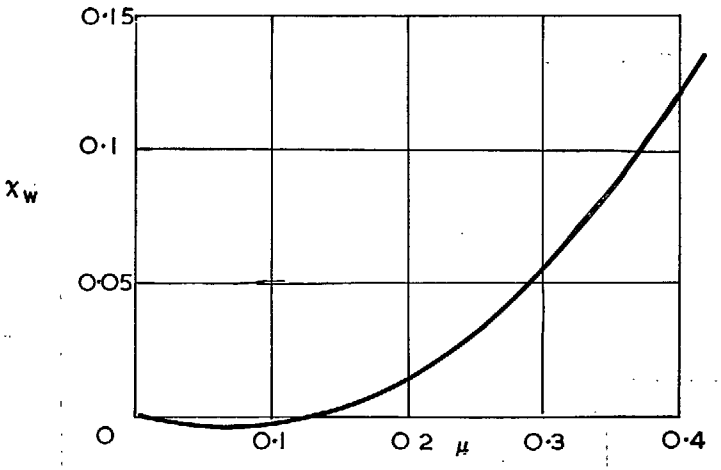

FIG. 13. Variation of χ_w with μ.

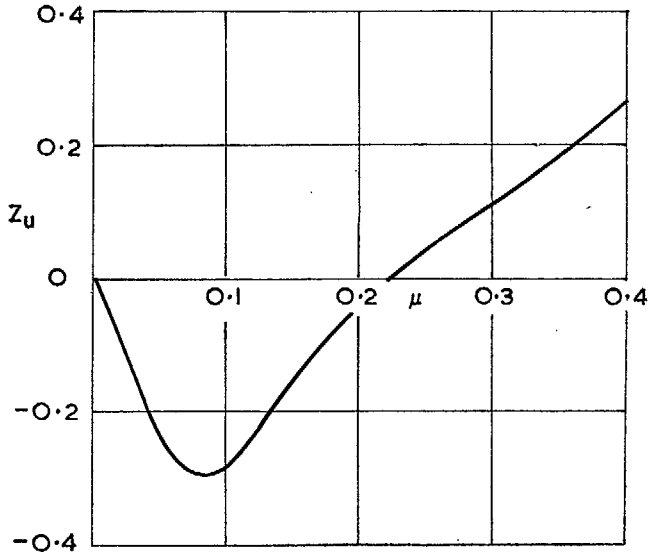

FIG. 14. Variation of Z_u with μ.

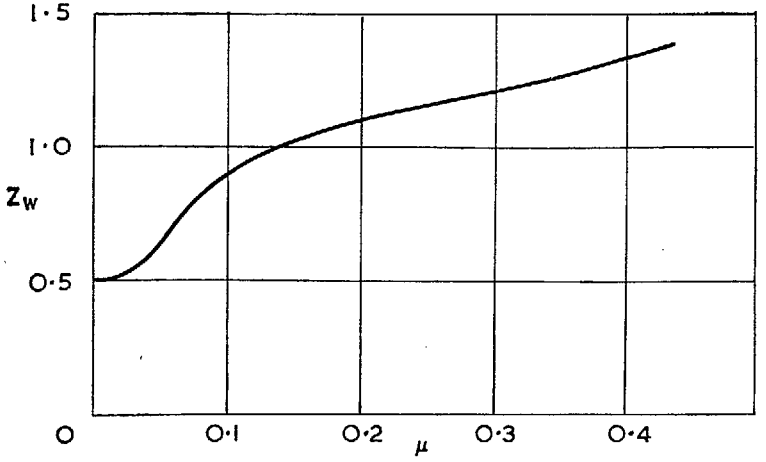

FIG. 15. Variation of Z_w with μ.

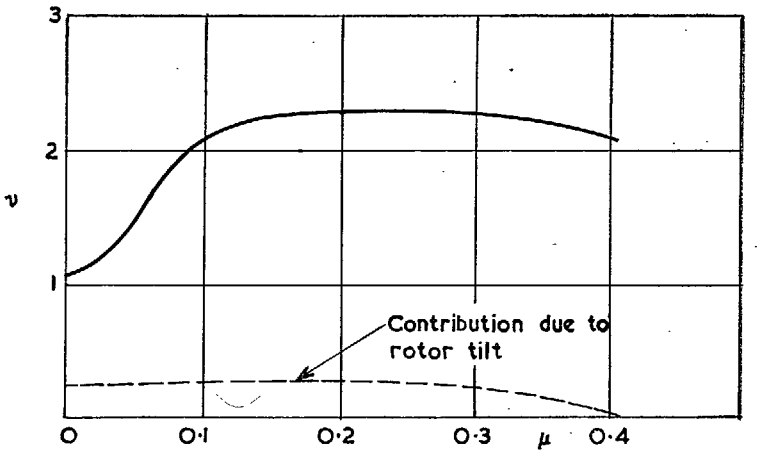

FIG. 16. Variation of damping in pitch, ν, with μ.

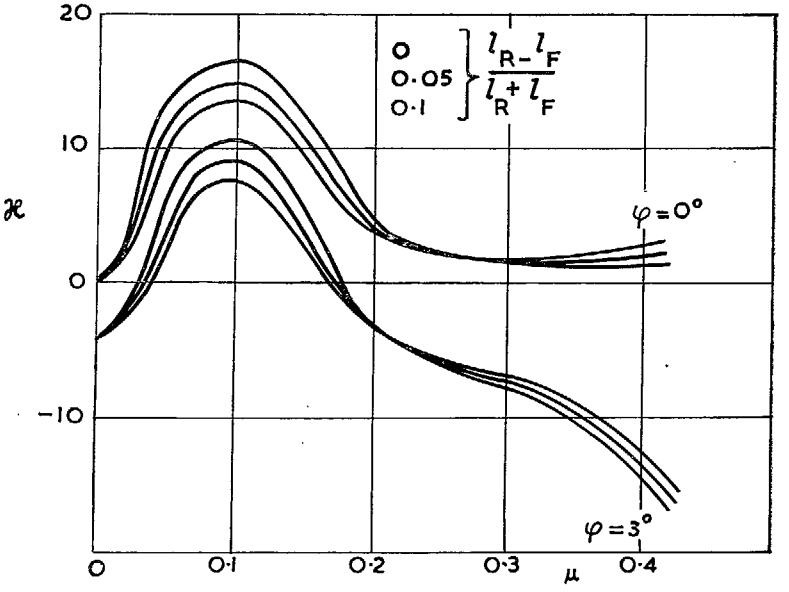

FIG. 17. Variation of $\mathcal{H}$ with μ.

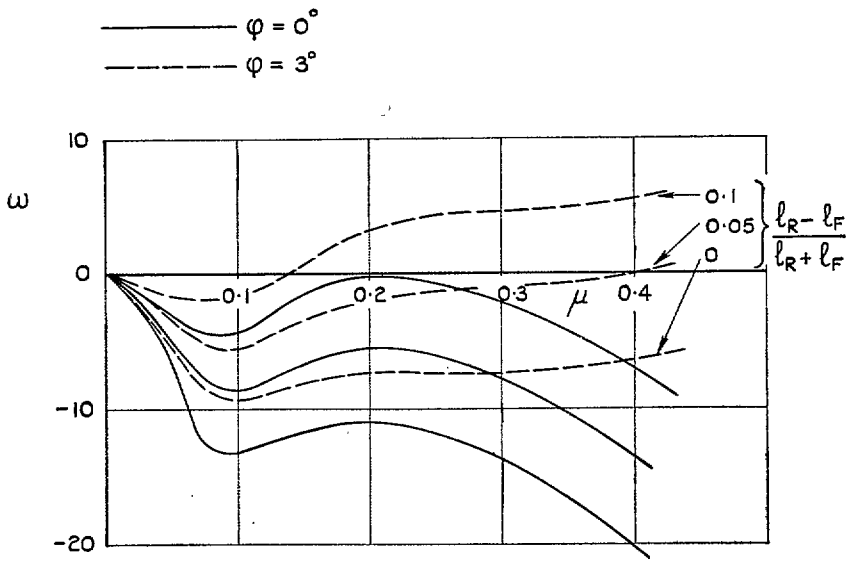

FIG. 18. Variation of w with μ.

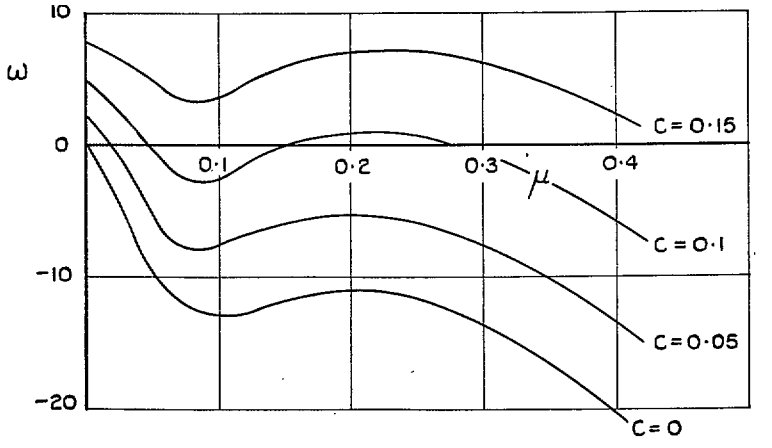

FIG. 19. Effect of δ_3-hinge on w.

$$\left(\varphi = 0, \frac{l_R - l_F}{l_R + l_F} = 0\right).$$

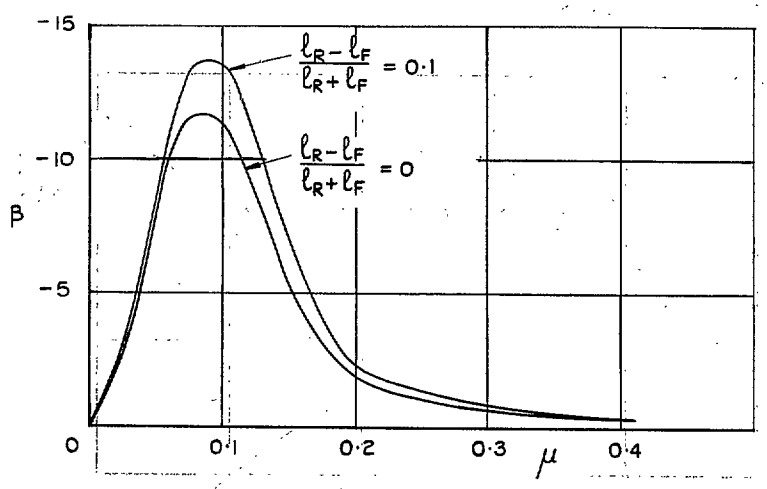

FIF. 20. Variation of downwash lag derivative β with μ.

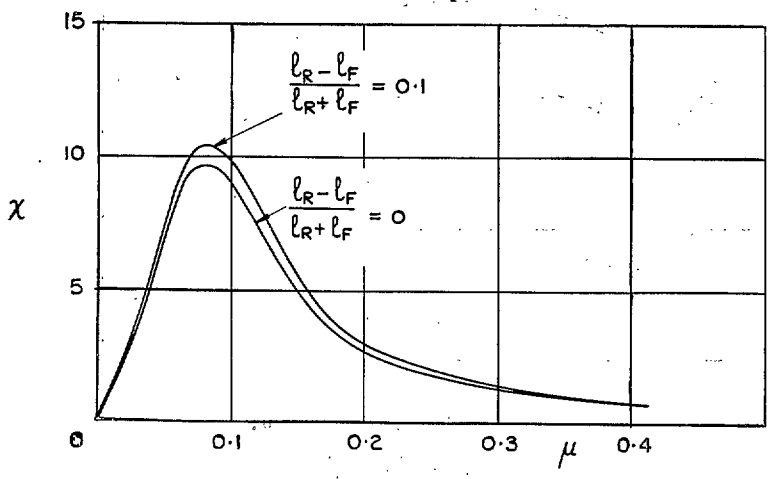

FIG. 21. Variation of downwash lag derivative χ with μ

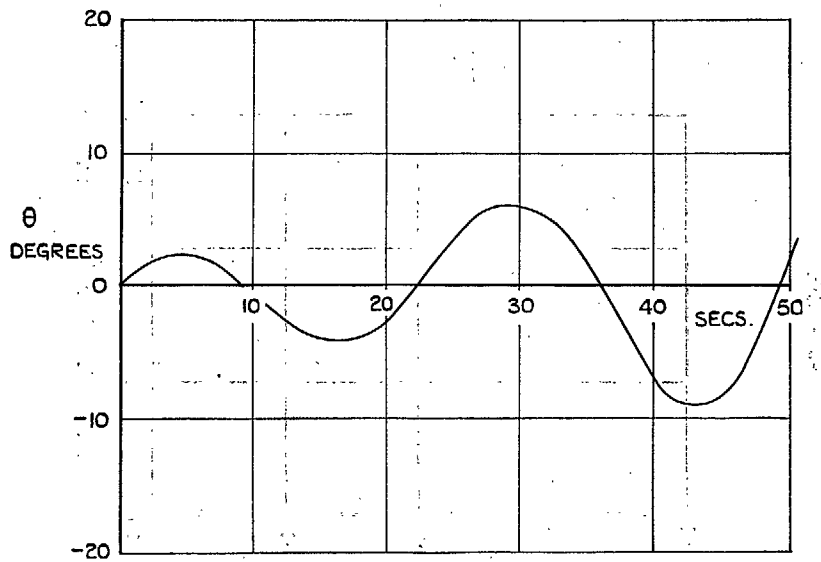

FIG. 22(a). Typical oscillation in hovering ($\varphi = 1°$ all C.G. positions. No δ_3-hinge).

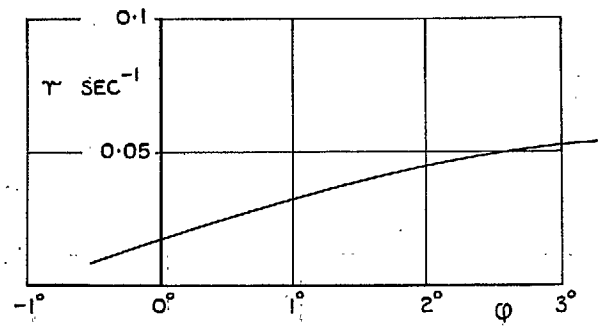

FIG. 22(b). Damping factor of phugoid oscillation in hovering. (All C.G. positions.)

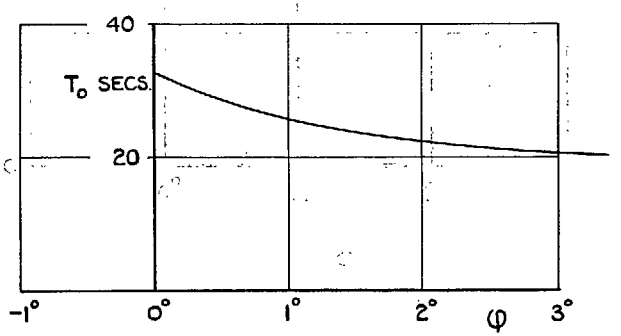

FIG. 22(c). Period of phugoid oscillation in hovering. (All C.G. positions.)

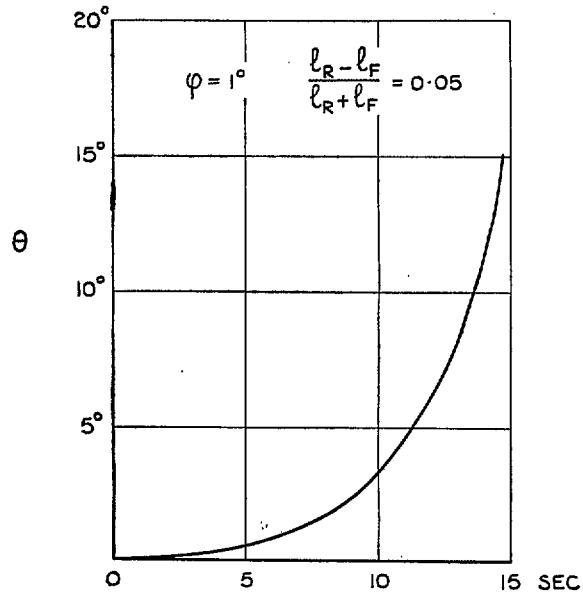

FIG. 23(a). Typical time history of longitudinal motion $\mu = 0{\cdot}1$. (No δ_3-hinge.)

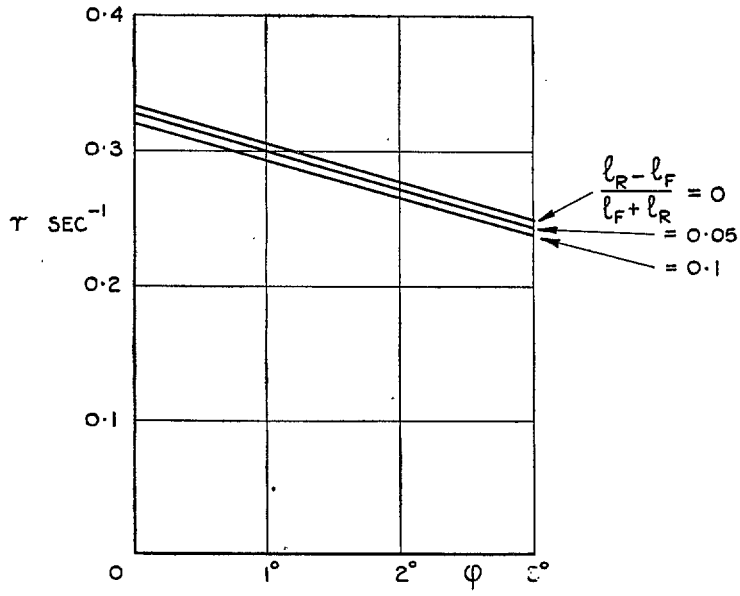

FIG. 23(b). Damping factor.

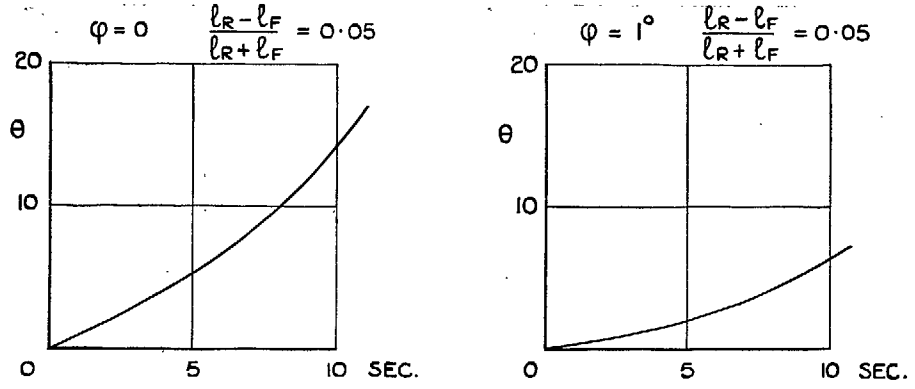

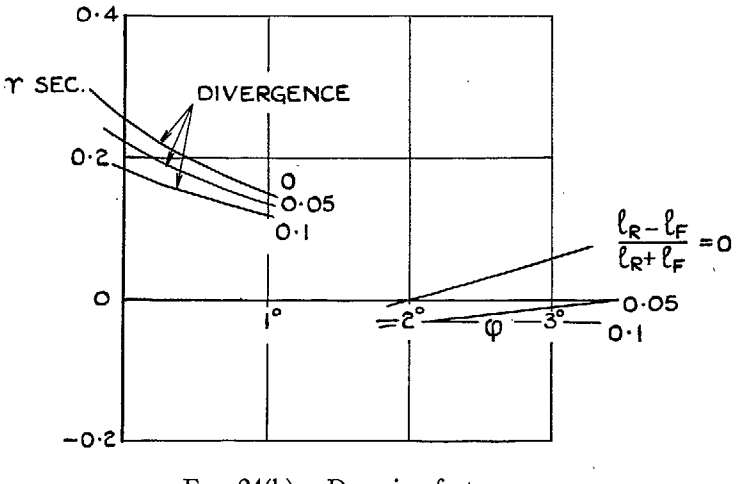

FIG. 24(b). Damping factor.

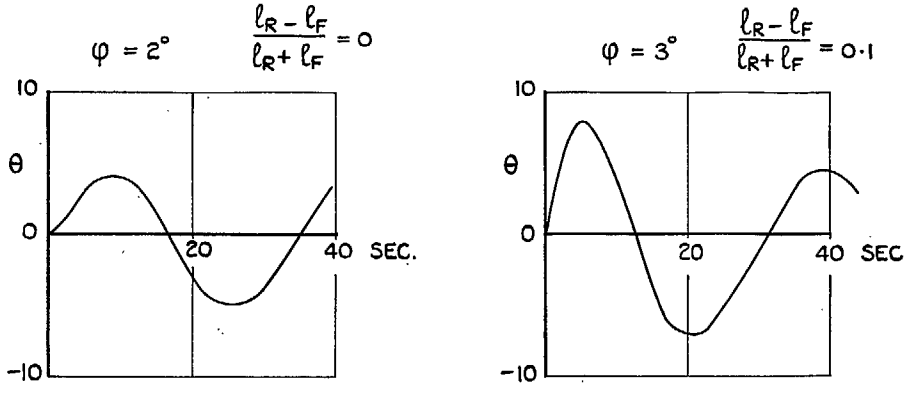

FIG. 24(a). Typical time histories of longitudinal motion $\mu = 0{\cdot}2$. (No δ_3-hinge.)

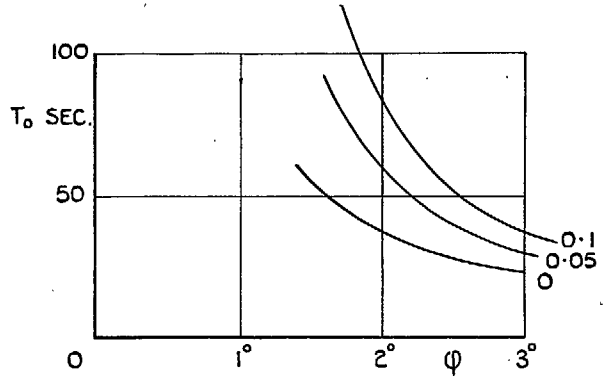

FIG. 24(c). Period of oscillation.

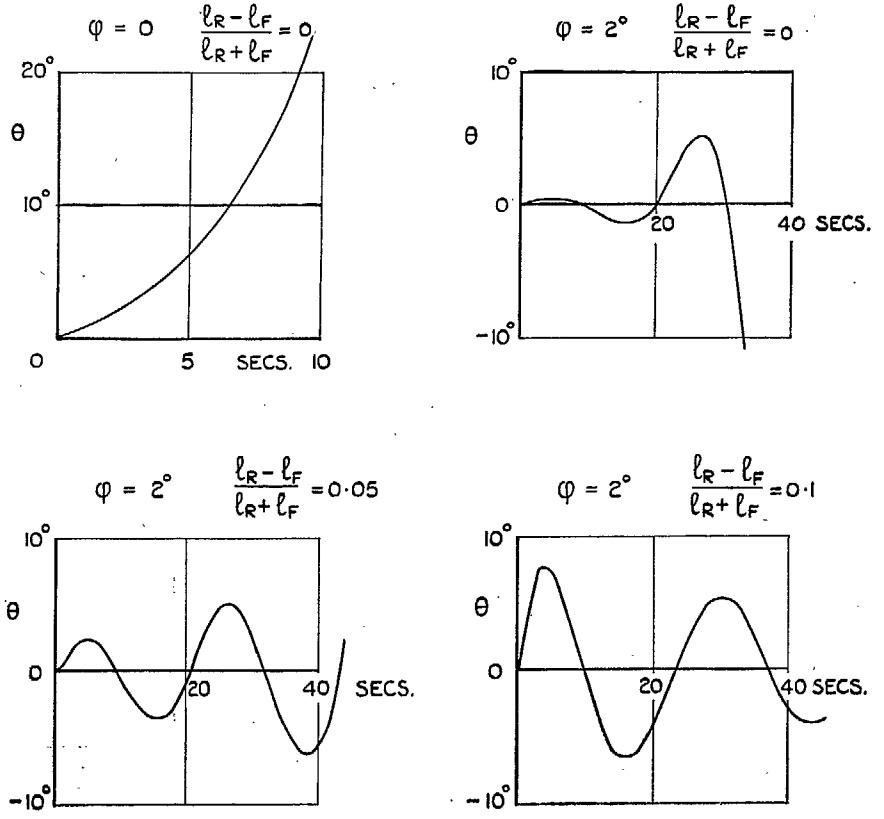

FIG. 25(a). Typical time histories of longitudinal motion $\mu = 0{\cdot}3$. (No δ_3-hinge.)

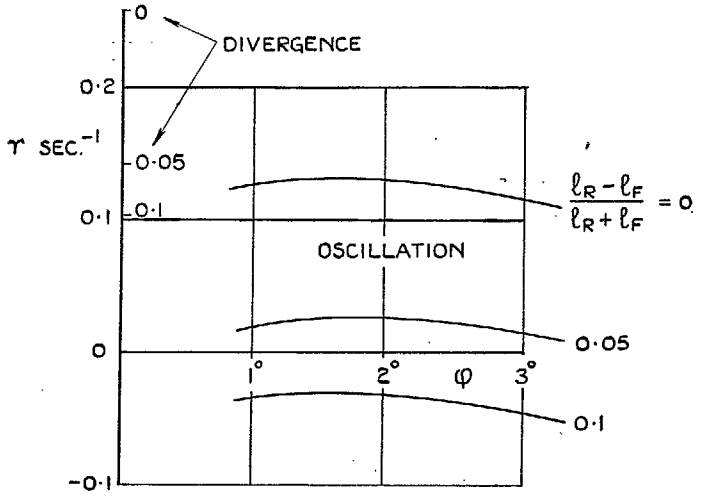

FIG. 25(b). Damping factor.

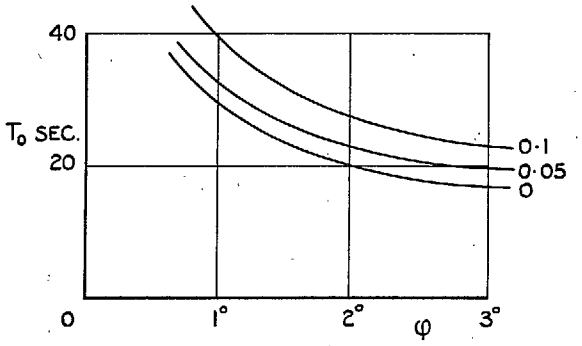

FIG. 25(c). Period of oscillation.

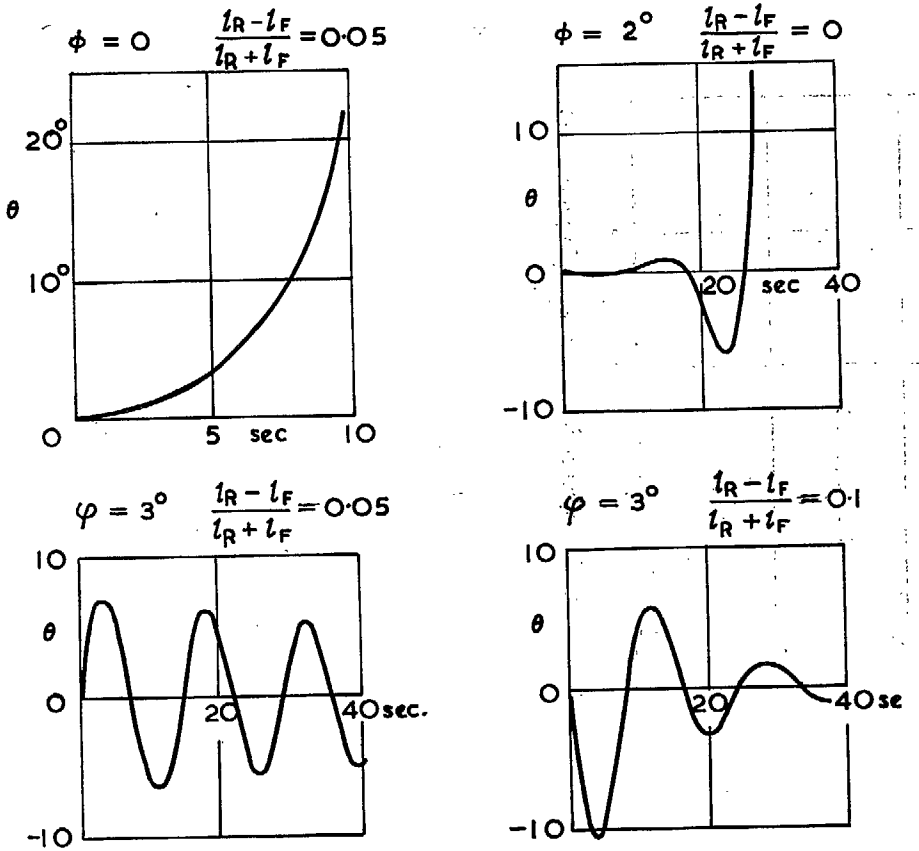

FIG. 26(a). Typical time histories of longitudinal motion $\mu = 0{\cdot}4$. (No δ_3-hinge.)

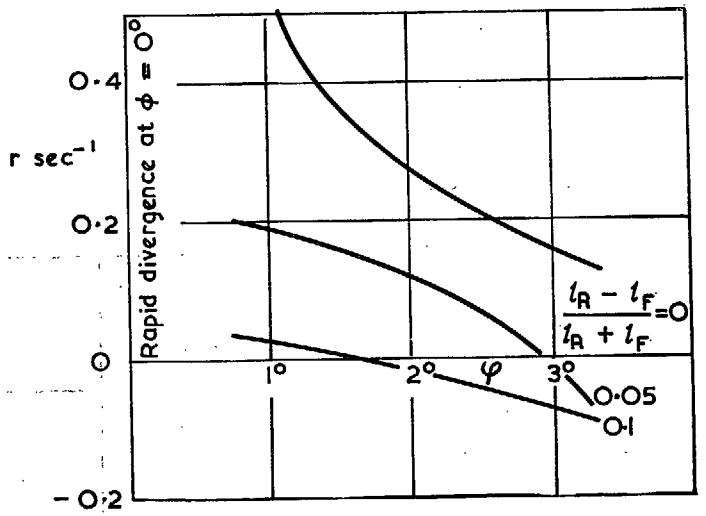

FIG. 26(b). Damping factor.

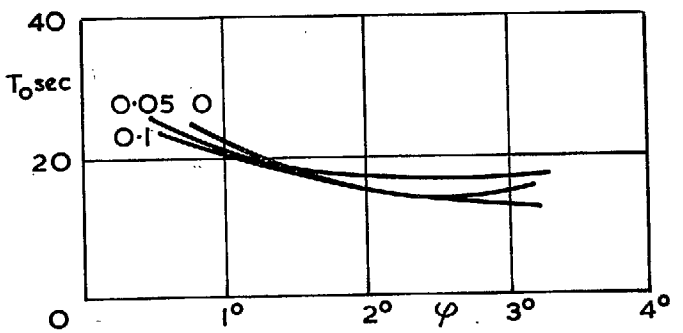

FIG. 26(c). Period of oscillation.

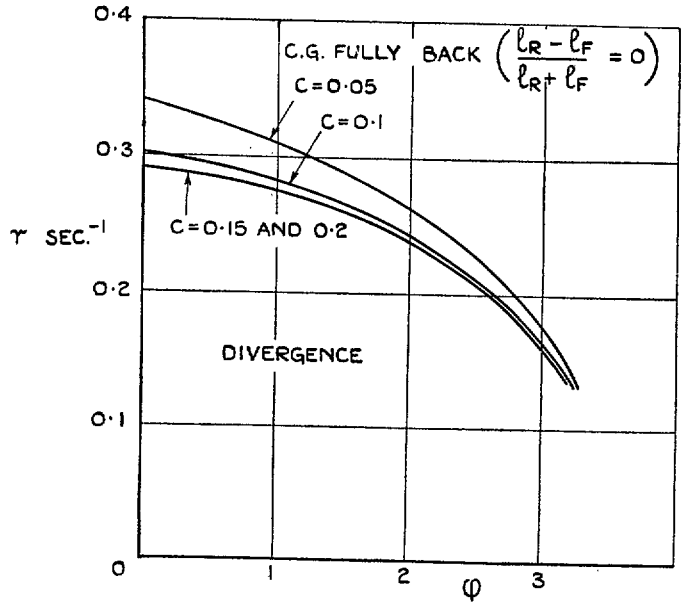

FIG. 27. Effect of δ_3-hinge on damping at $\mu = 0 \cdot 1$.

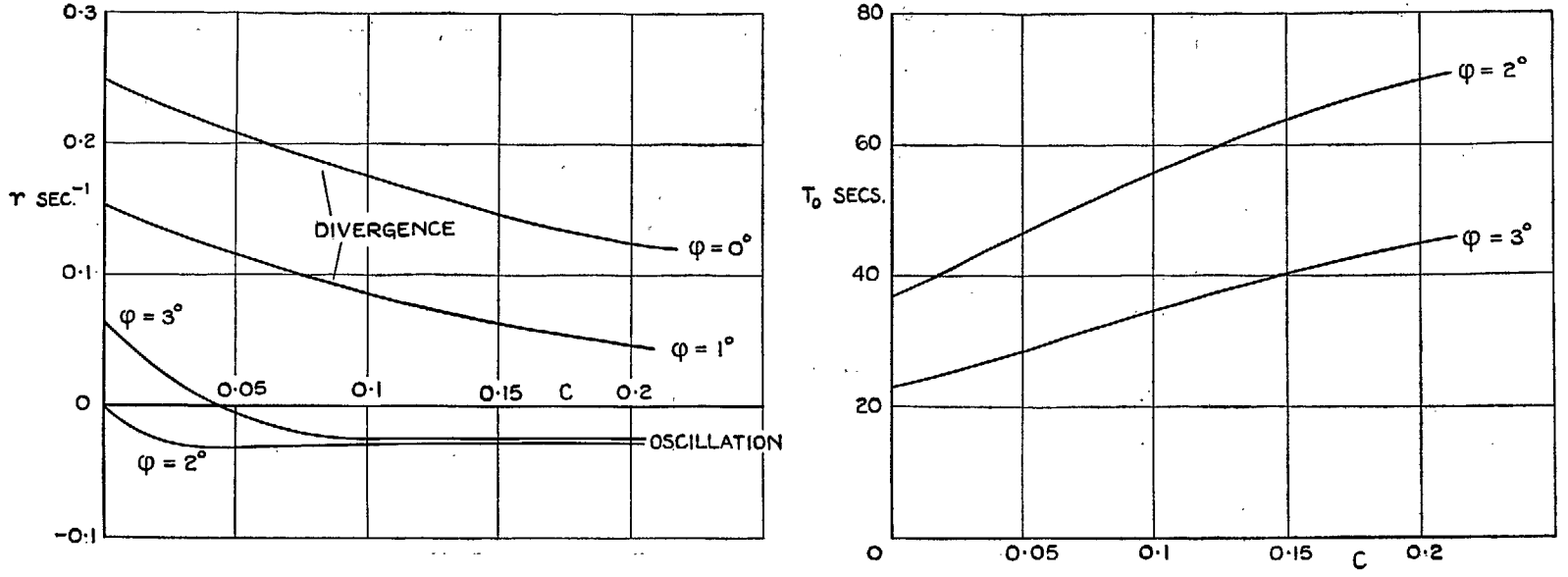

FIG. 28. Effect of δ_3-hinge on damping and period of longitudinal motion at $\mu = 0{\cdot}2$. $\left(\text{c.g. fully back } \frac{l_R - l_F}{l_R + l_F} = 0\right)$.

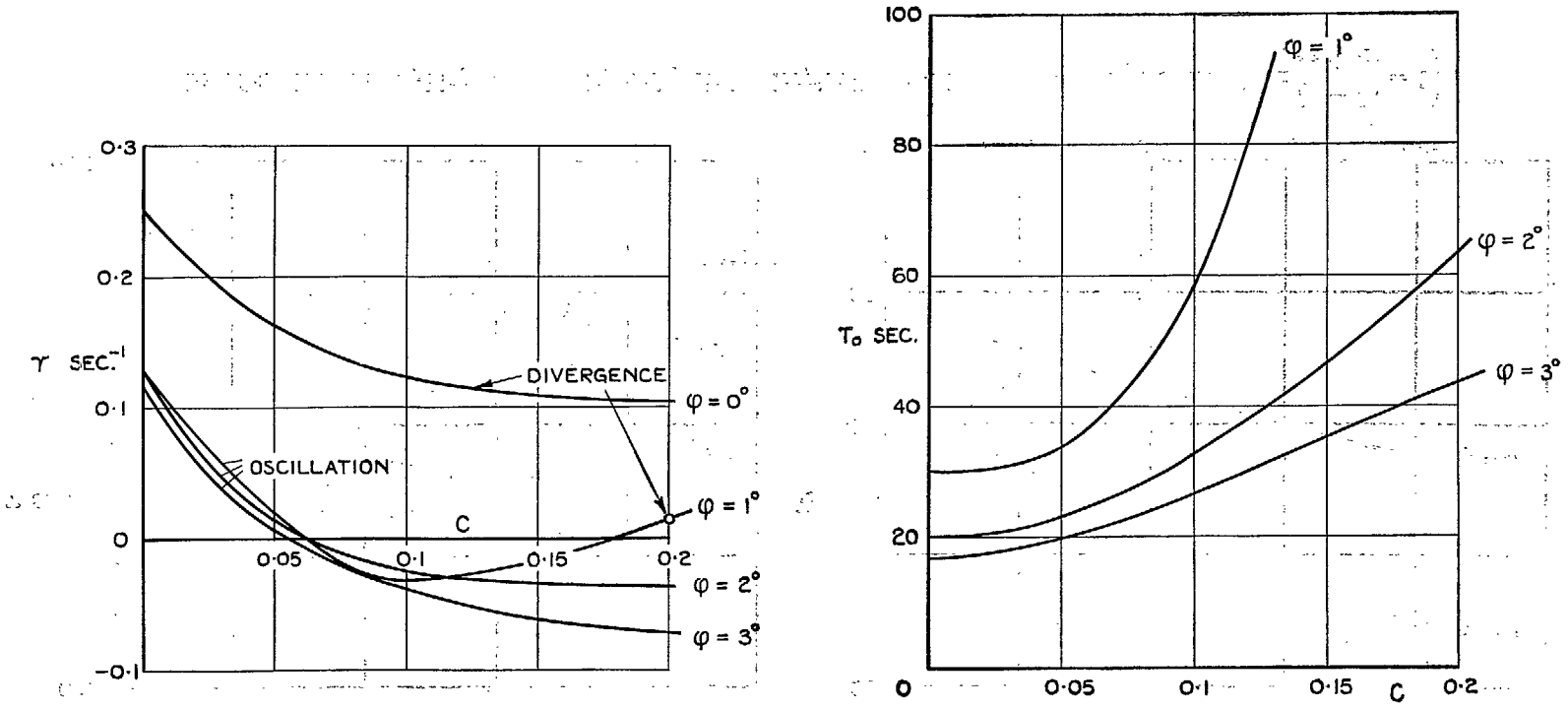

FIG. 29. Effect of δ_3-hinge on damping and period of longitudinal motion at $\mu = 0{\cdot}3$. $\left(\text{c.g. fully back } \frac{l_R - l_F}{l_R + l_F} = 0\right)$.

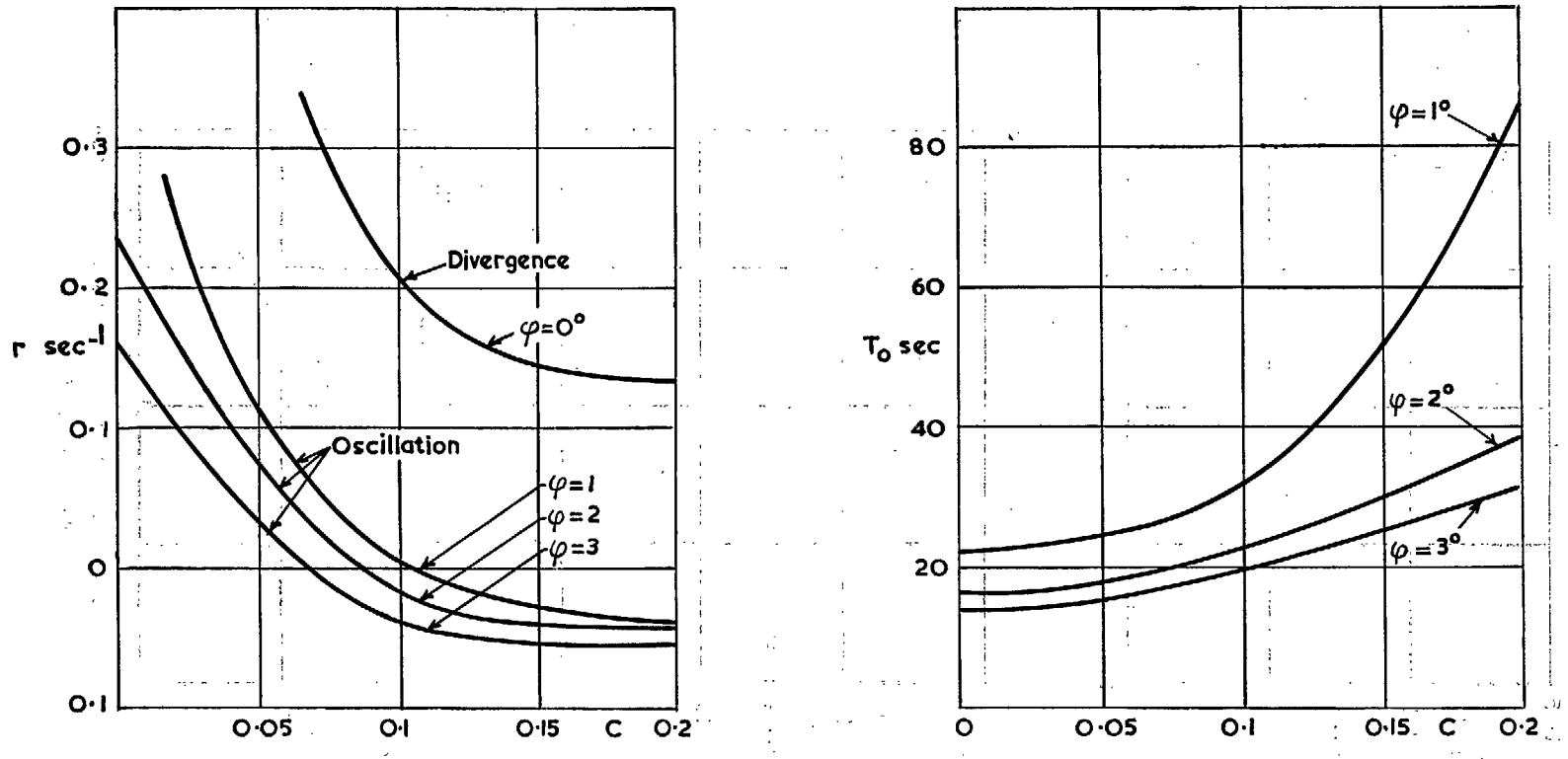

FIG. 30. Effect of δ_3-hinge on damping and period of longitudinal motion at $\mu = 0{\cdot}4$. $\left(\text{C.G. fully back } \frac{l_R - l_F}{l_R + l_F} = 0\right)$.

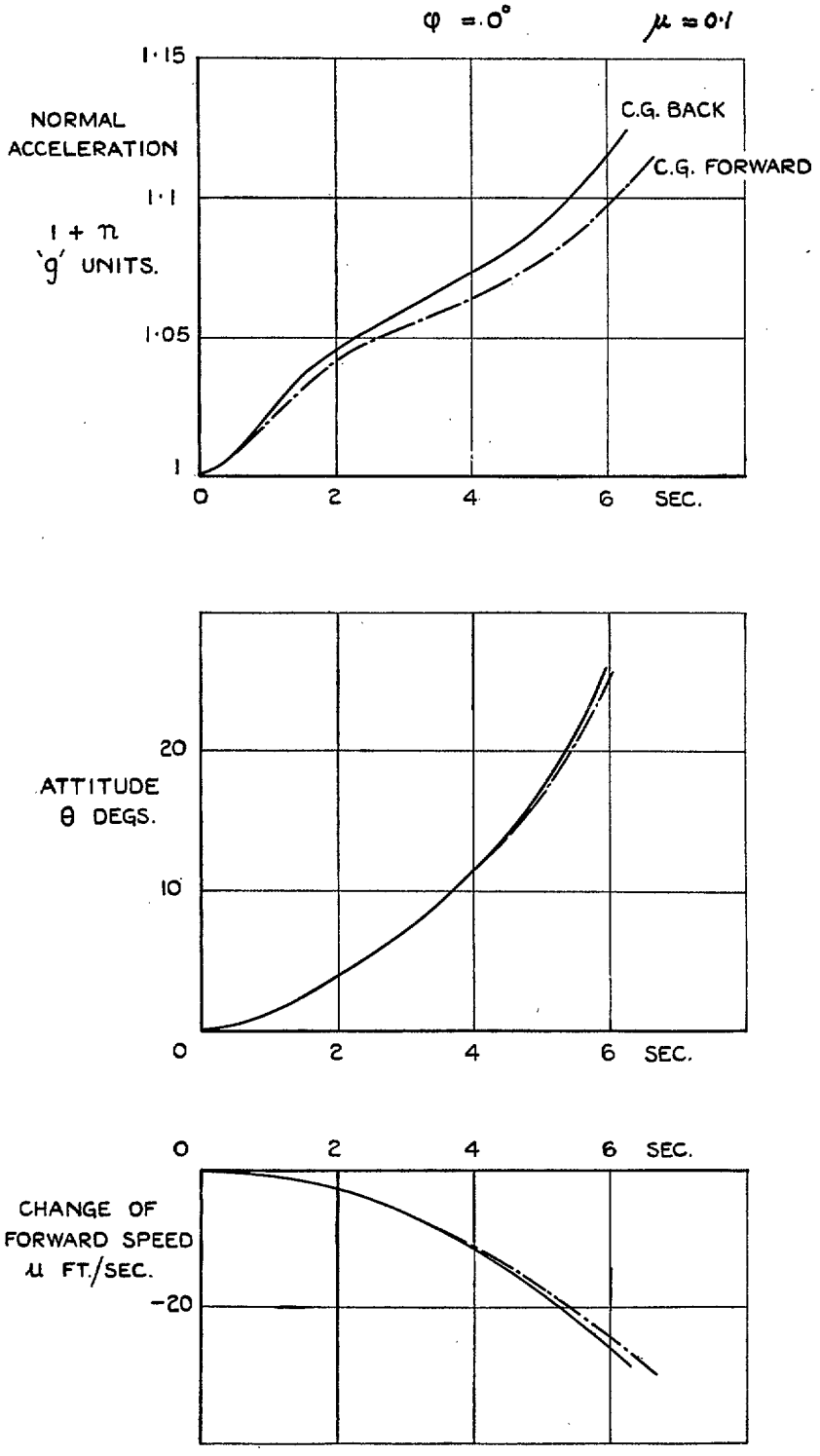

FIG. 31. Response to sudden backward stick displacement of 1°. ($\mu = 0{\cdot}1$, $\varphi = 0°$.)

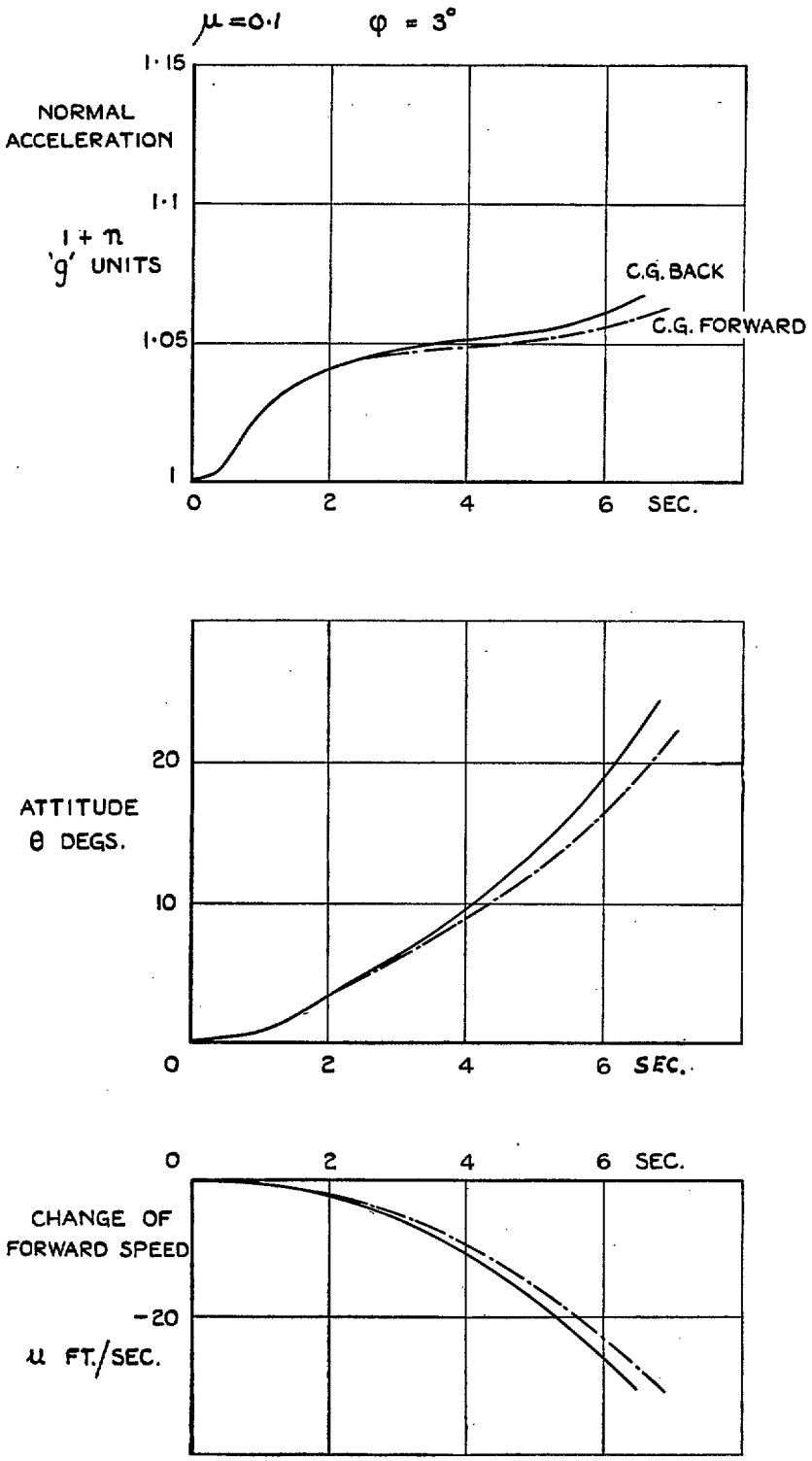

FIG. 32. Response to sudden backward stick displacement of 1°. ($\mu = 0{\cdot}1$, $\varphi = 3°$.)

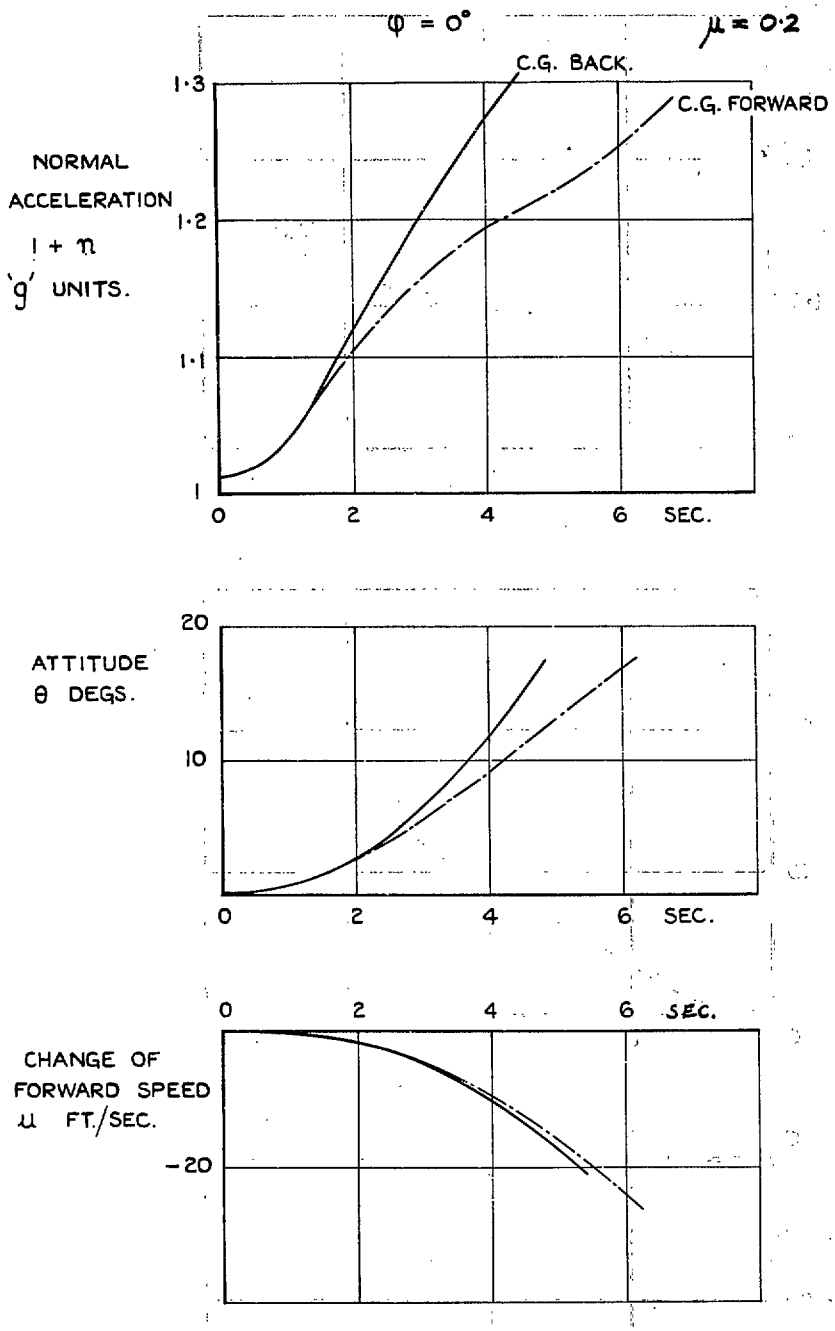

FIG. 33. Response to sudden backward stick displacement of 1°. ($\mu = 0{\cdot}2$, $\varphi = 0°$.)

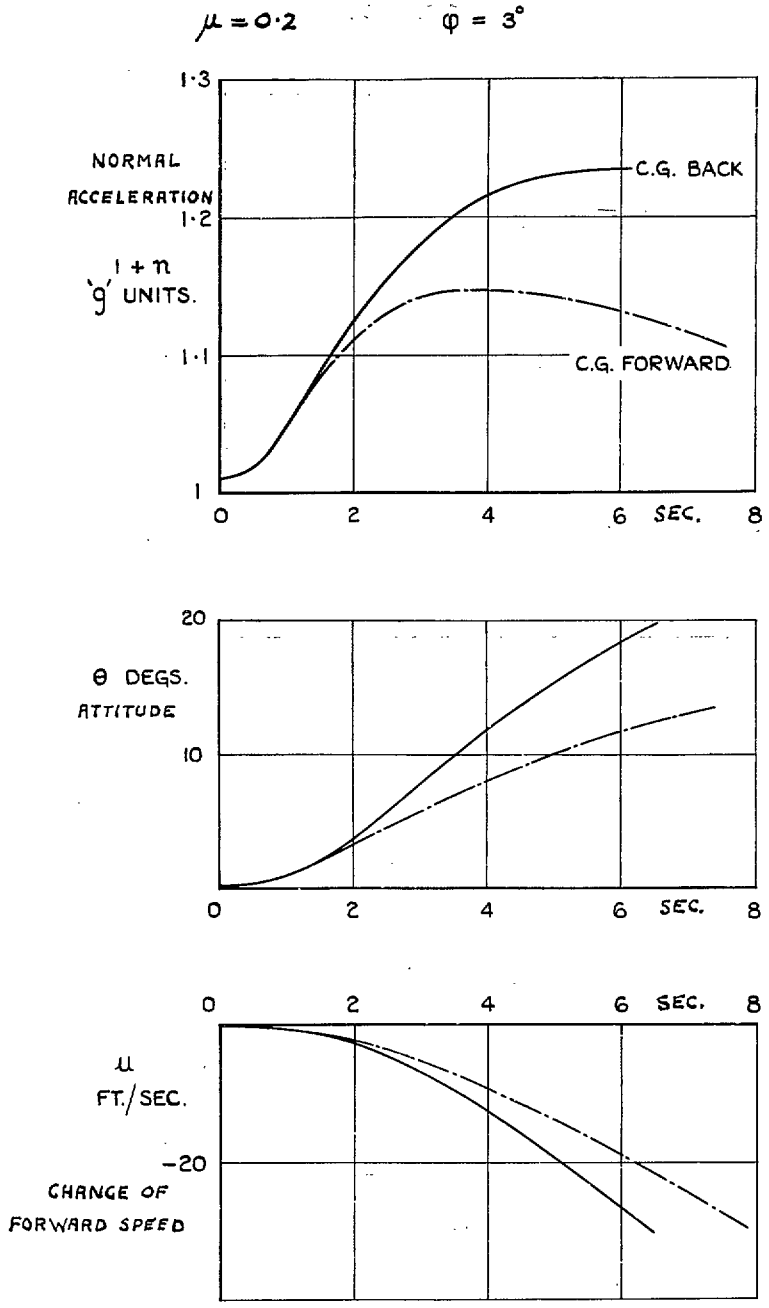

FIG. 34. Response to sudden backward stick displacement of 1°. ($\mu = 0{\cdot}2$, $\varphi = 3°$.)

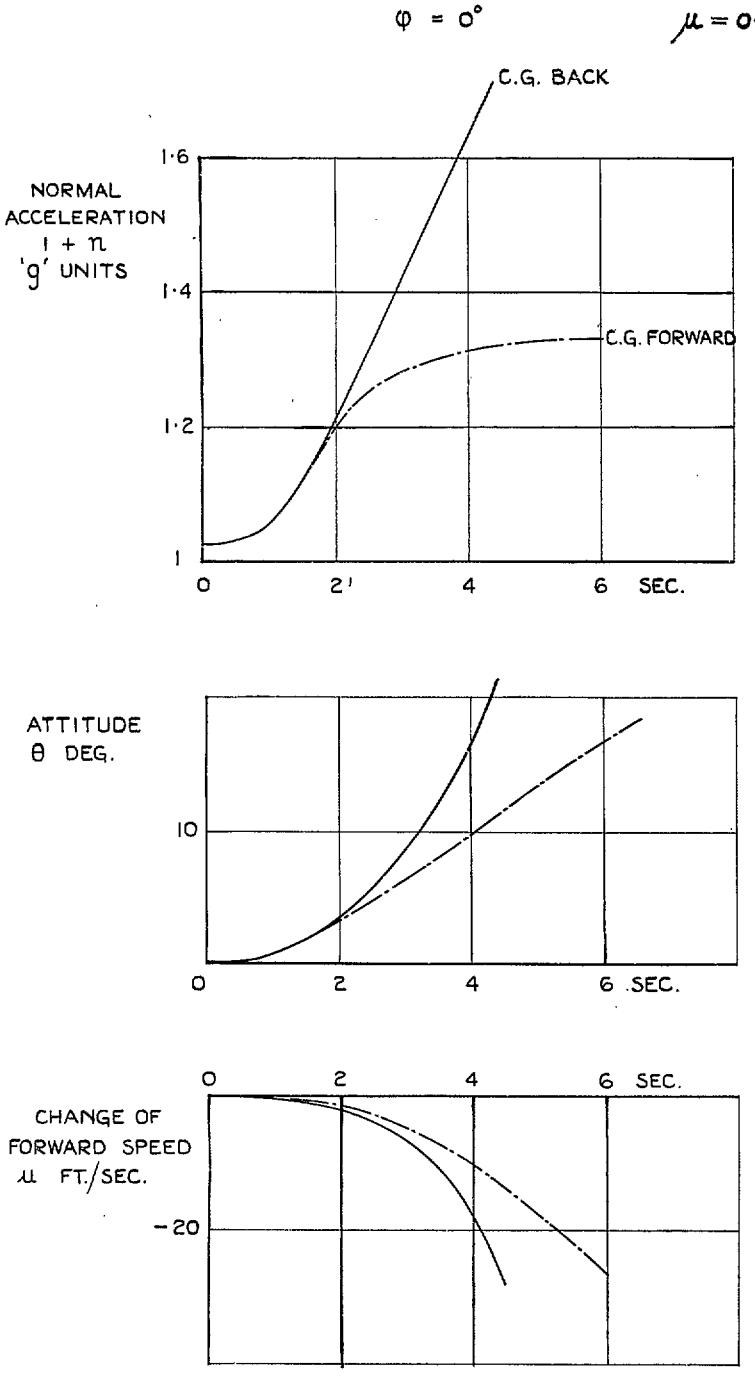

FIG. 35. Response to sudden backward stick displacement of 1°. ($\mu = 0{\cdot}3$, $\varphi = 0°$.)

$\mu = 0{\cdot}3$ $\varphi = 3°$

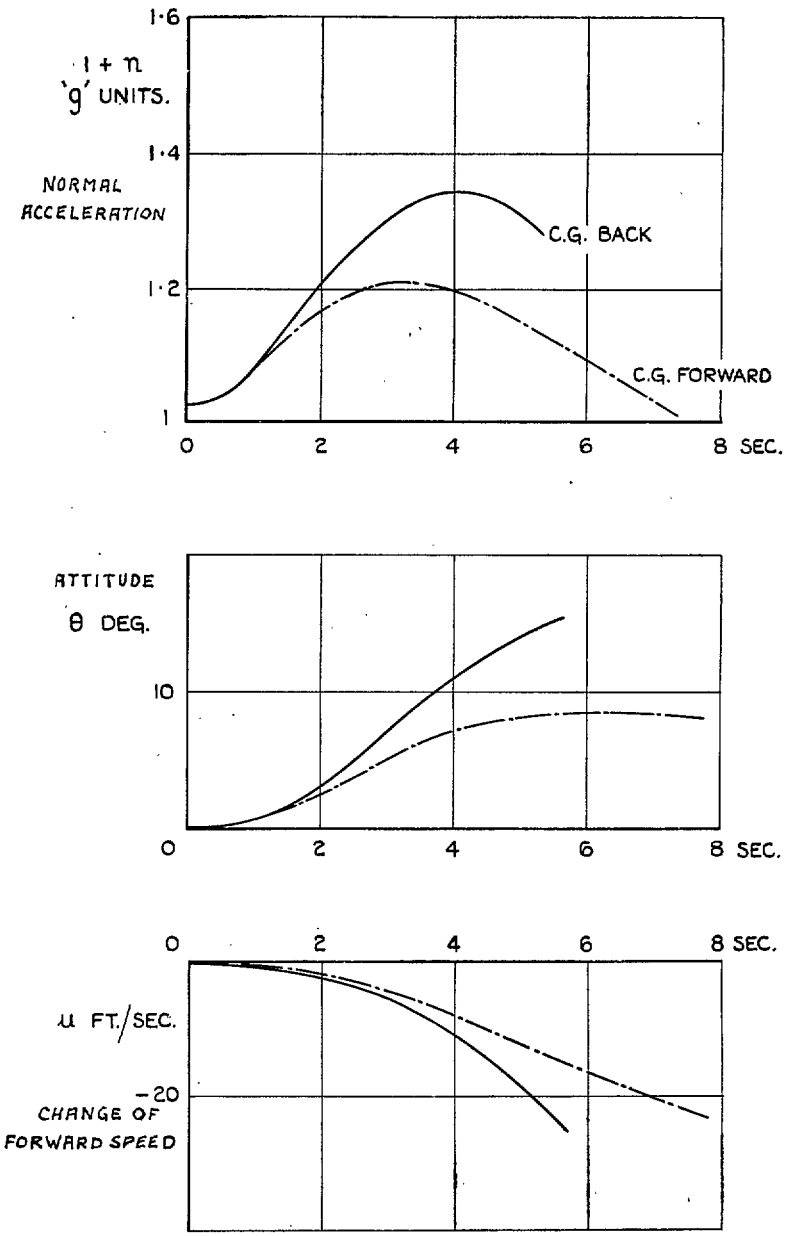

FIG. 36. Response to sudden backward stick displacement of 1°. ($\mu = 0{\cdot}3$, $\varphi = 3°$.)

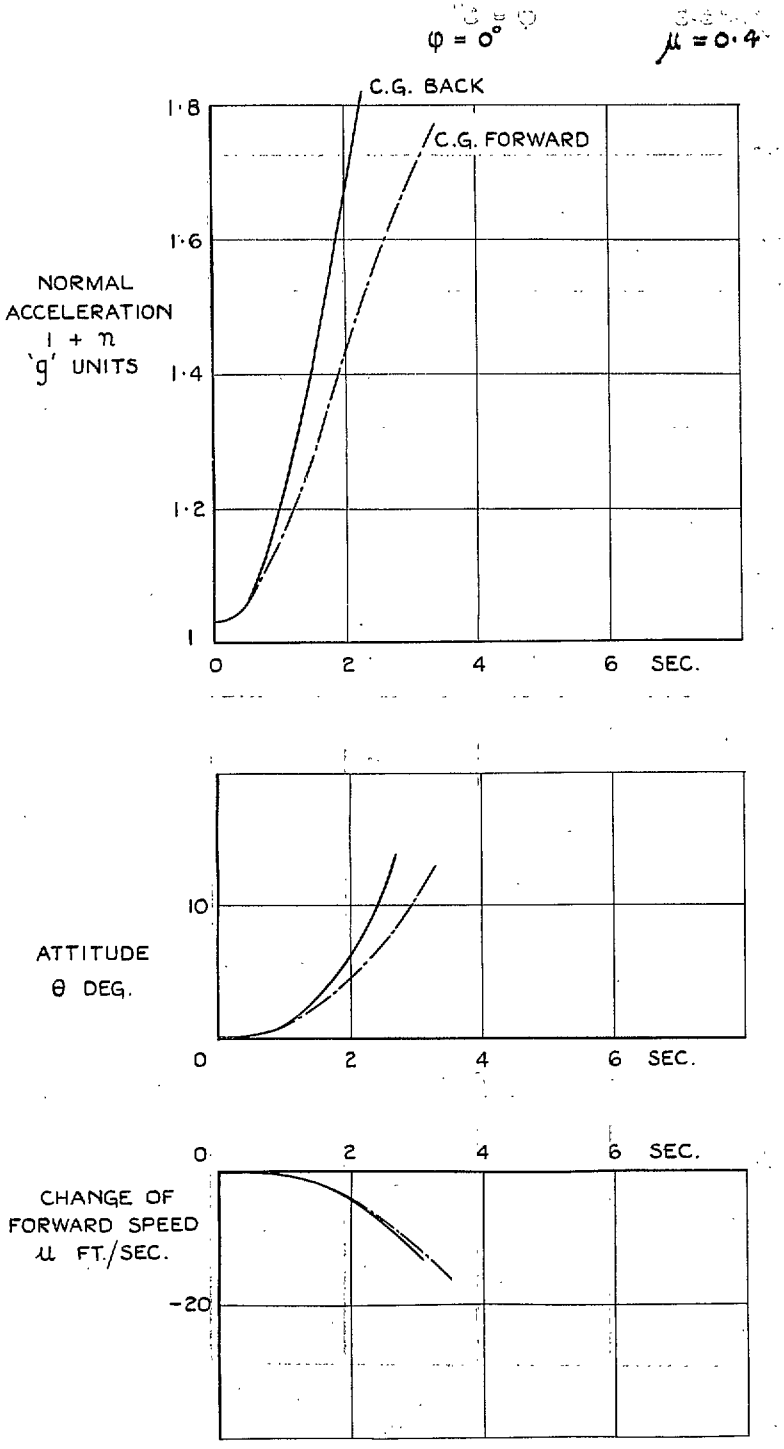

FIG. 37. Response to sudden backward stick displacement of 1°. ($\mu = 0{\cdot}4$, $\varphi = 0°$.)

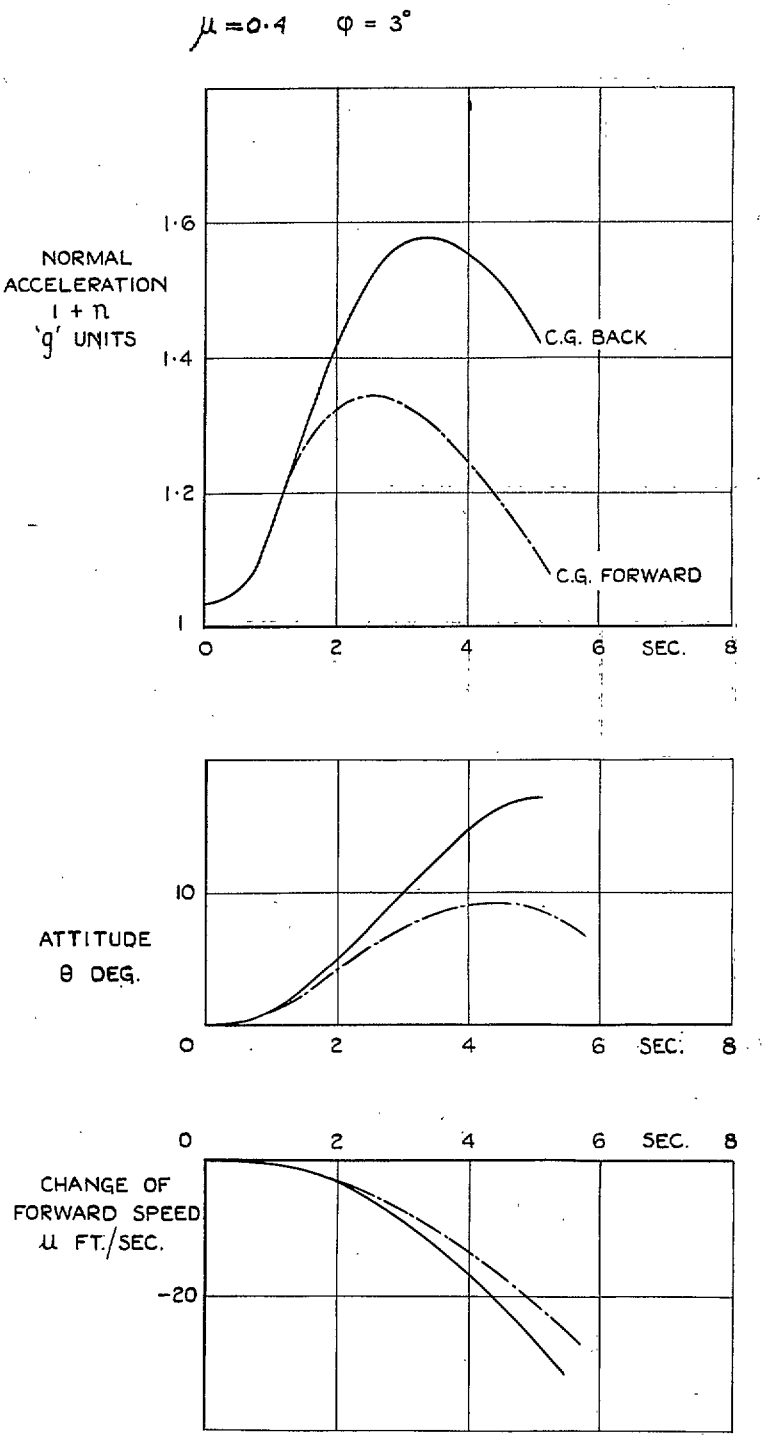

FIG. 38. Response to sudden backward stick displacement of 1°. ($\mu = 0{\cdot}4$, $\varphi = 3°$.)

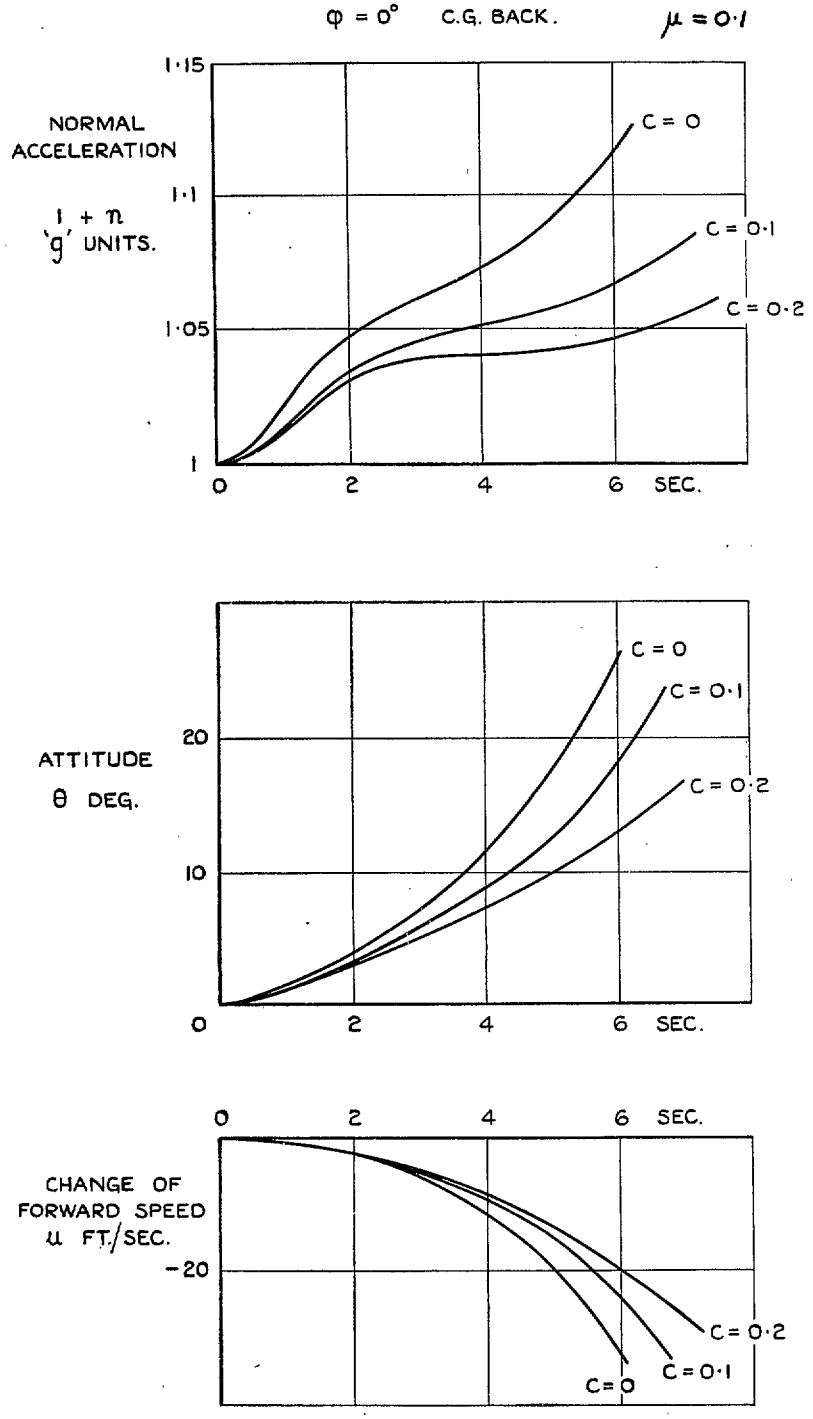

FIG. 39. Response to sudden backward stick displacement of 1°. (With δ_3-hinge. $\mu = 0{\cdot}1$, $\varphi = 0°$.)

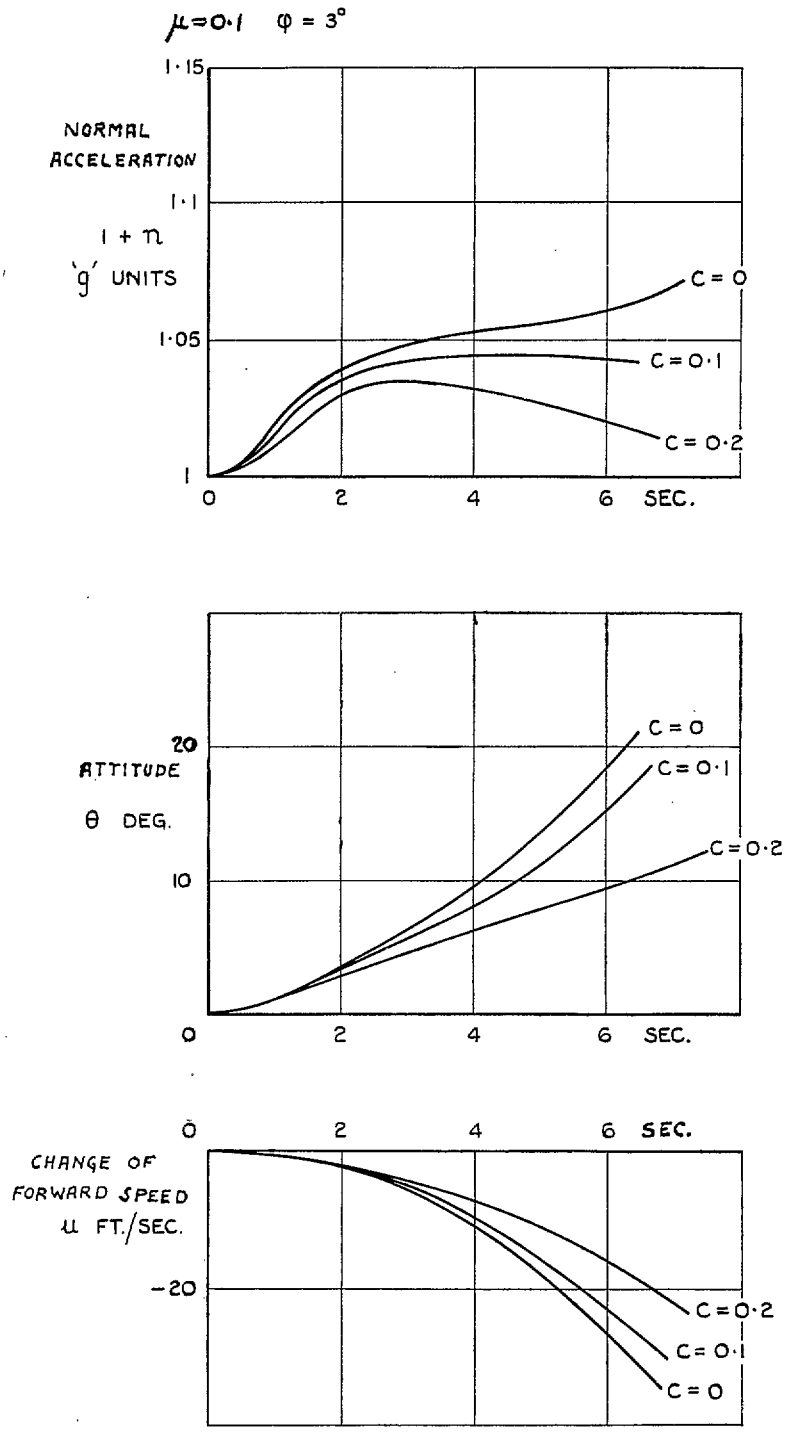

FIG. 40. Response to sudden backward stick displacement of 1°. (With δ_3-hinge. $\mu = 0{\cdot}1$, $\varphi = 3°$.)

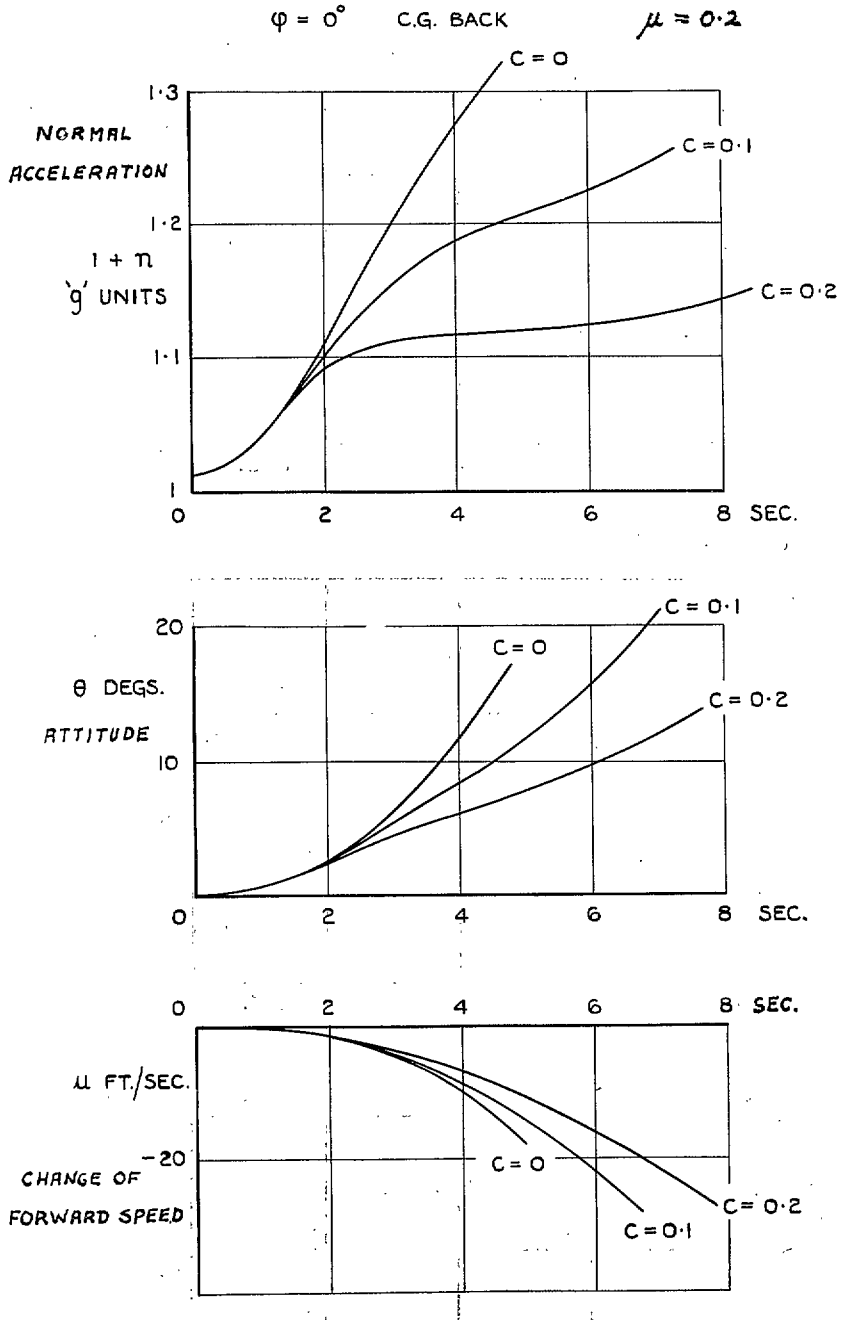

FIG. 41. Response to sudden backward stick displacement of 1°. (With δ_3-hinge. $\mu = 0{\cdot}2$, $\varphi = 0°$.)

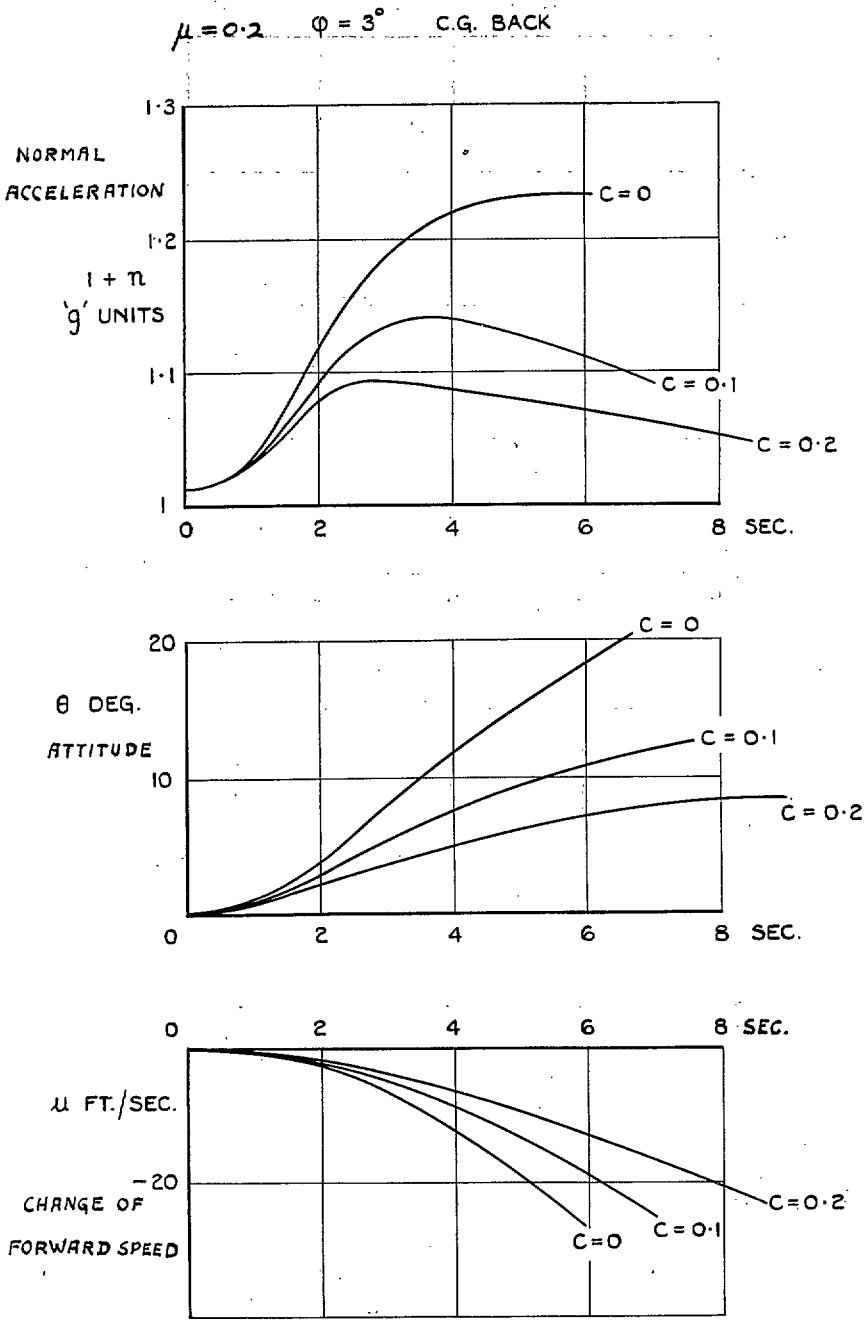

FIG. 42. Response to sudden backward stick displacement of 1°. (With δ_3-hinge. $\mu = 0{\cdot}2$, $\varphi = 3°$.)

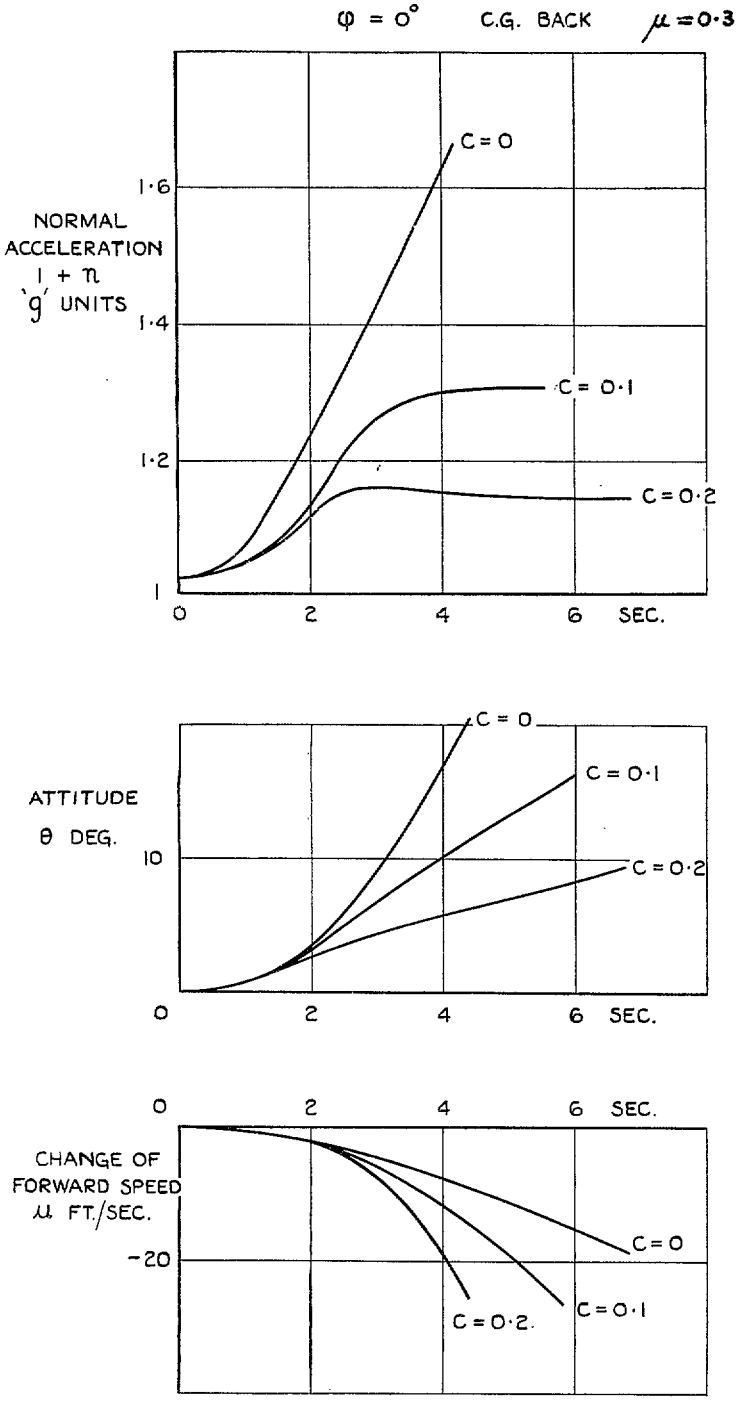

FIG. 43. Response to sudden backward stick displacement of 1°. (With δ_3-hinge. $\mu = 0{\cdot}3$, $\varphi = 0°$.)

$\mu = 0{\cdot}3$ $\varphi = 3°$ C.G. BACK

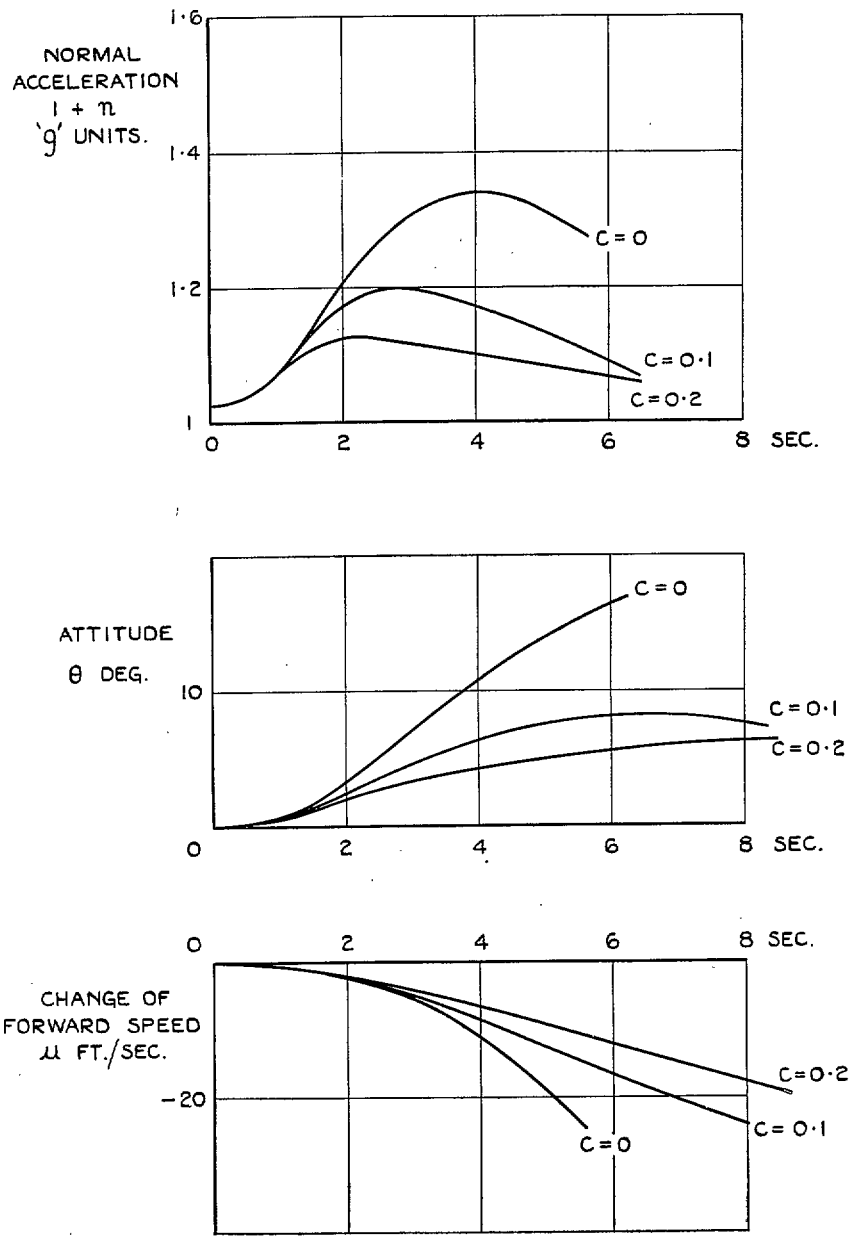

FIG. 44. Response to sudden backward stick displacement of 1°. (With δ_3-hinge. $\mu = 0{\cdot}3$, $\varphi = 3°$.)

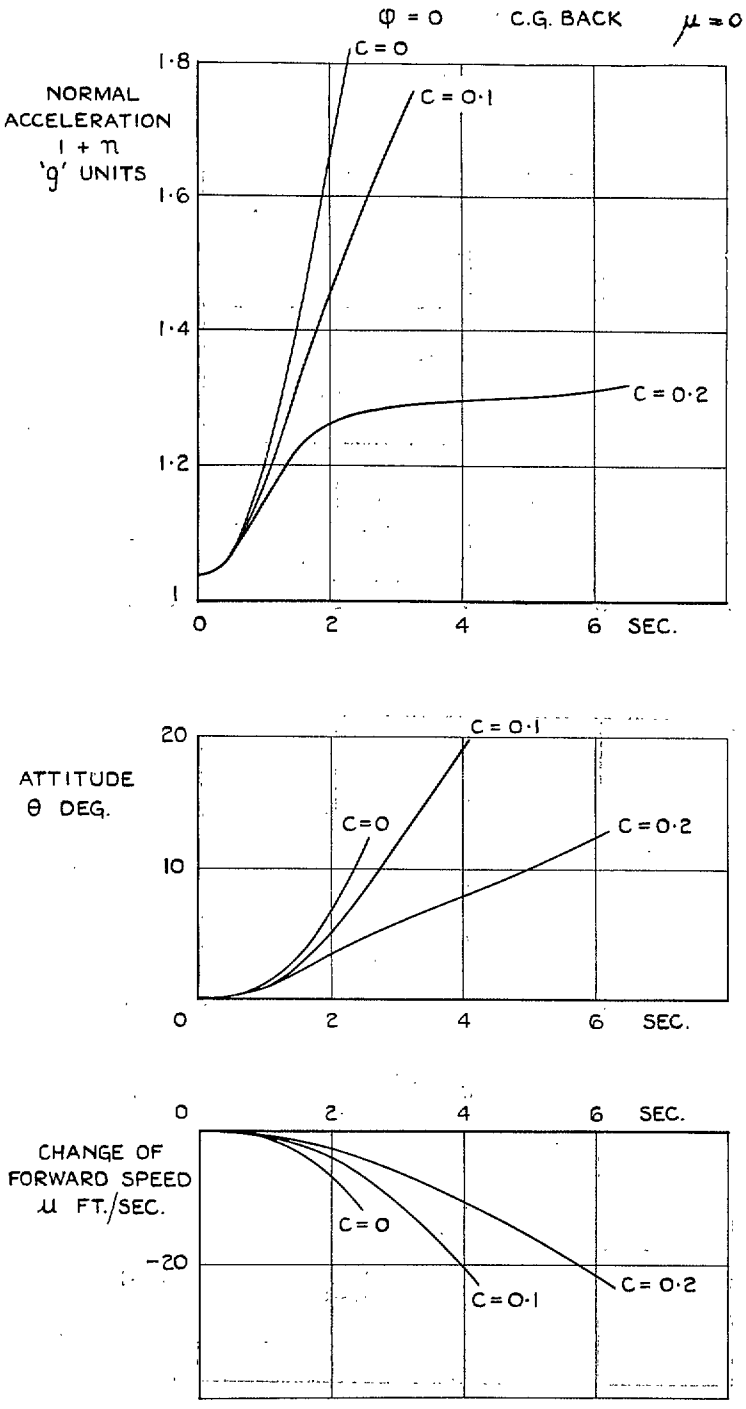

FIG. 45. Response to sudden backward stick displacement of 1°. (With δ_3-hinge. $\mu = 0{\cdot}4$, $\varphi = 0°$.)

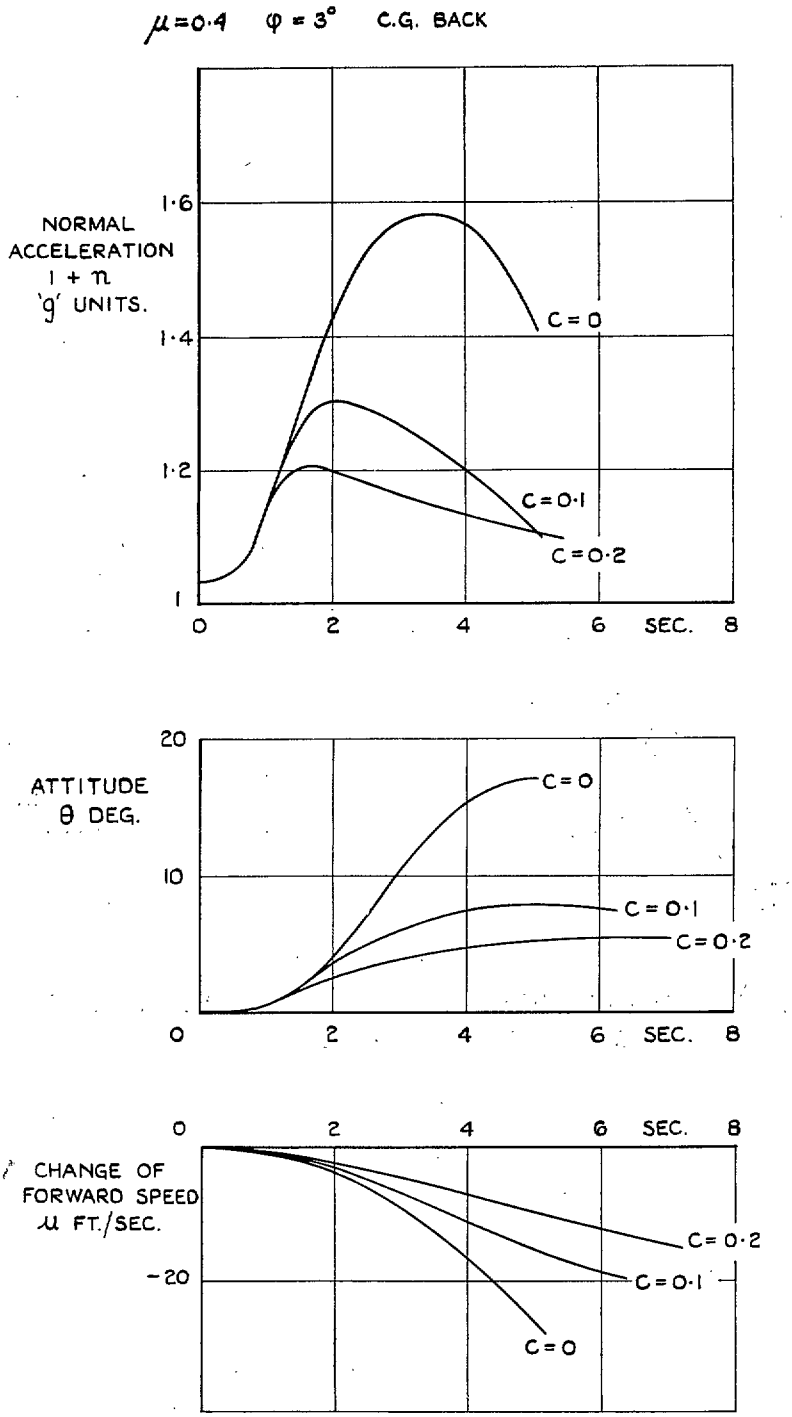

FIG. 46. Response to sudden backward stick displacement of 1°. (With δ_3-hinge. $\mu = 0{\cdot}4$, $\varphi = 3°$.)

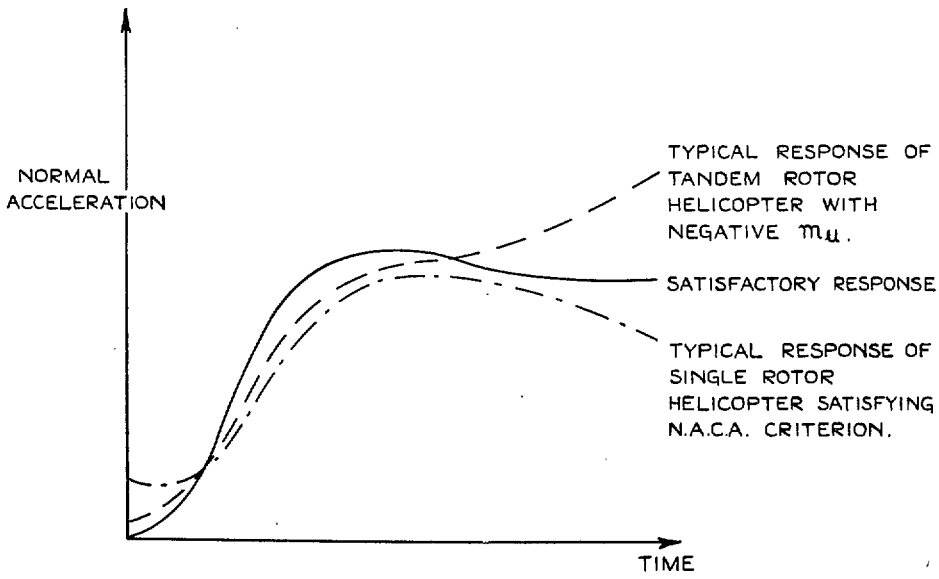

FIG. 47. Comparison of satisfactory response with typical responses of single and tandem-rotor helicopters.

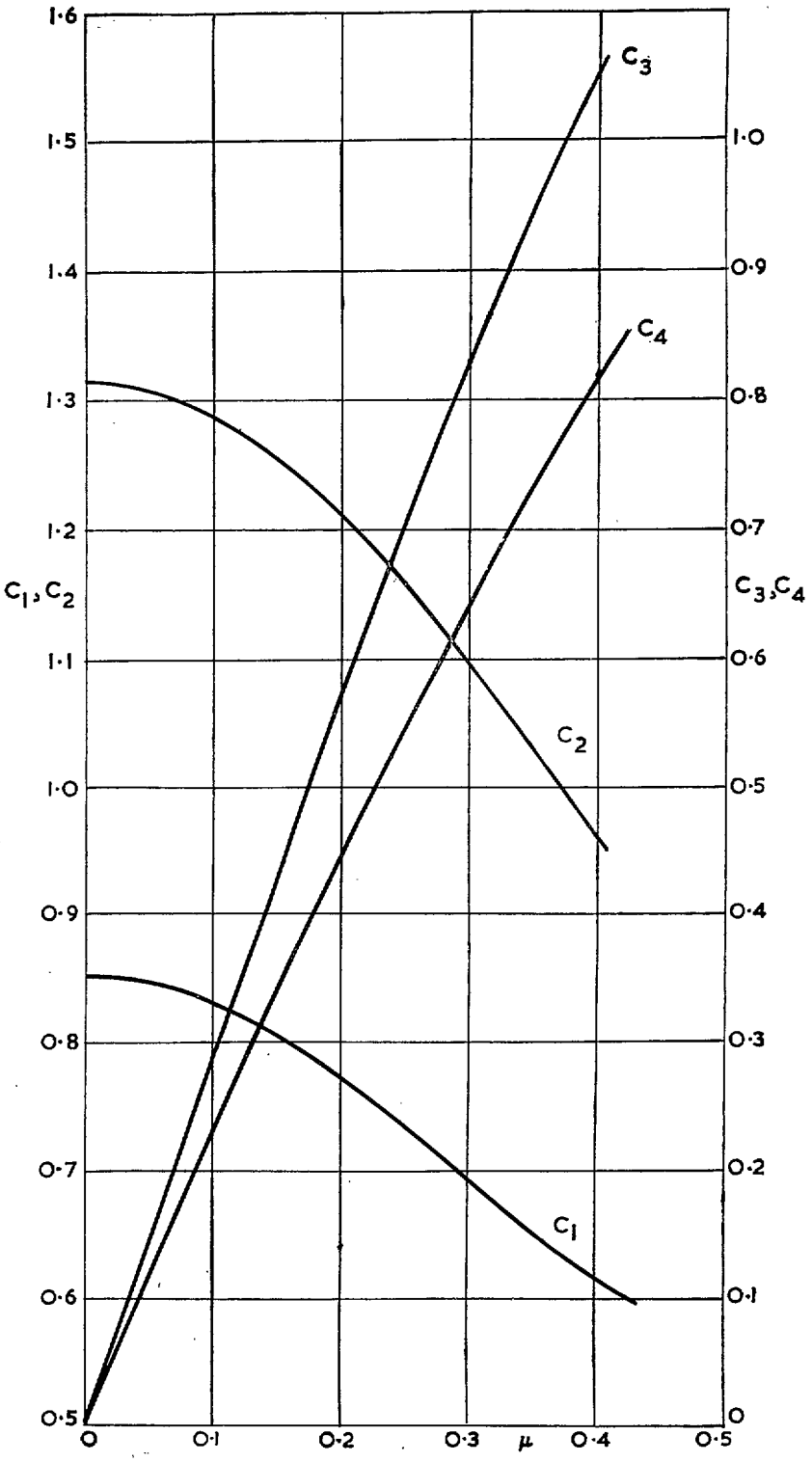

FIG. 48. Variation of the functions c_1, c_2, c_3 and c_4 with μ ($B = 0{\cdot}97$).

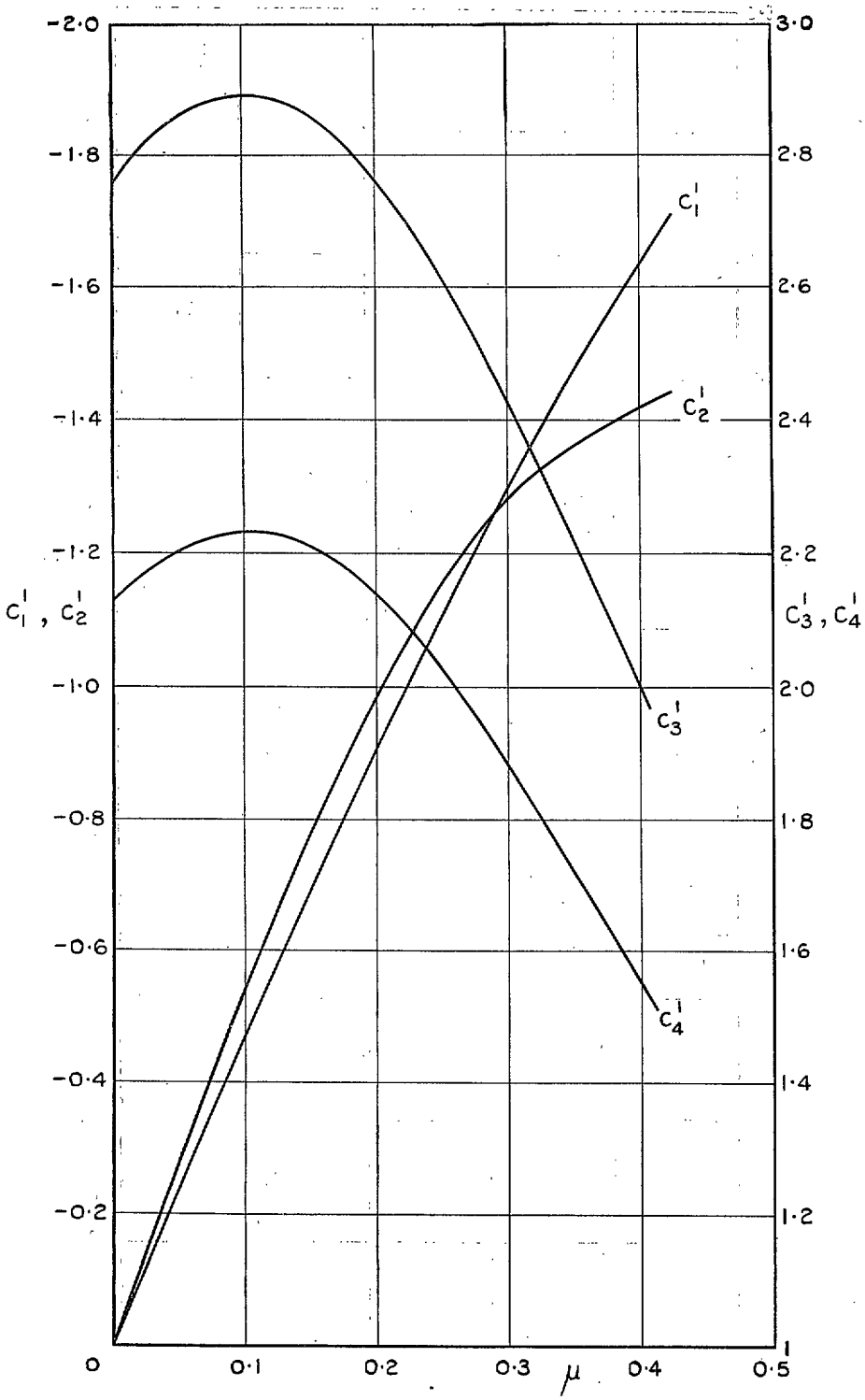

FIG. 49. Variation of $\frac{dc_1}{d\mu}$, $\frac{dc_2}{d\mu}$, $\frac{dc_3}{d\mu}$ and $\frac{dc_4}{d\mu}$ with μ ($B = 0{\cdot}97$).

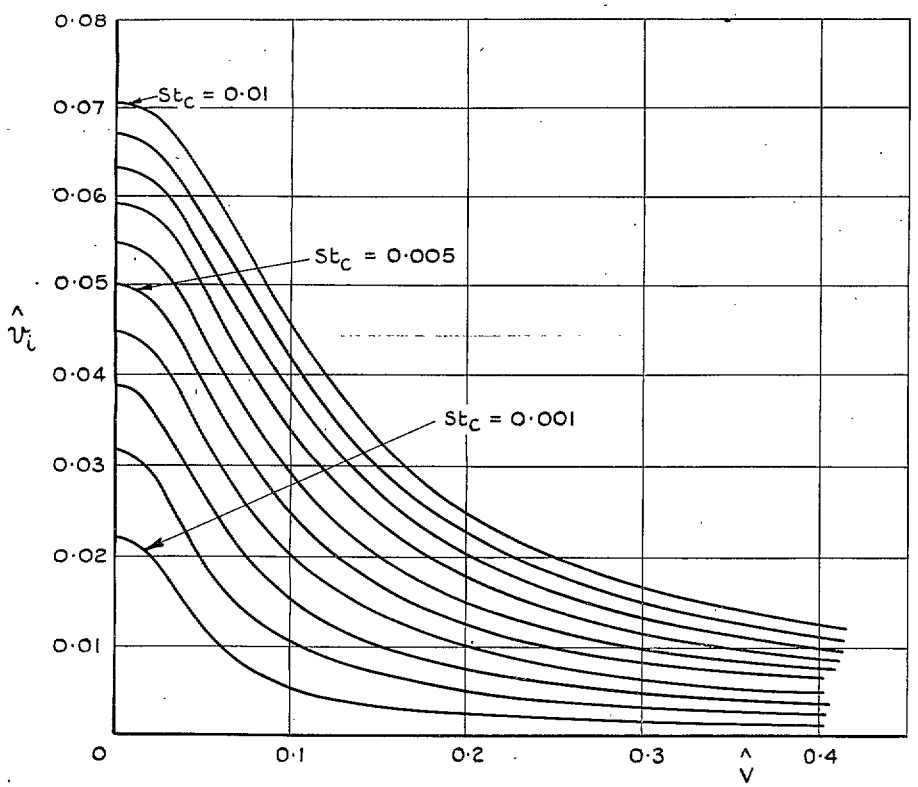

FIG. 50. Variation of dimensionless induced velocity with $\hat{V}$.

Part II

The Lateral Stability and Control of the Tandem-Rotor Helicopter

By A. R. S. Bramwell

Summary. The lateral stability and control of the tandem-rotor helicopter with a basic configuration similar to that of the Bristol 173 has been investigated. A method of calculating the derivatives is given. Values calculated for the HUP-1 helicopter show fairly good agreement with those obtained from flight measurements.

The stability investigation shows that a tall fin may provide an effective dihedral several times larger than that of the rotors and lead to an unstable Dutch-roll oscillation which becomes progressively worse with increase of speed. The corresponding spiral mode is stable. If the rotors provide the only contribution, the Dutch-roll oscillation is stable but the spiral mode may become unstable.

Simple approximations are given for the estimation of the damping and period of the stability modes and show quite close approximation to the more exact calculations.

---

1. *Introduction.* This Report is the second part of a study of the stability and control of the tandem-rotor helicopter and deals with the lateral motion. As in Ref. 2 which dealt with the longitudinal behaviour, a configuration similar to that of the Bristol 173 is used as an example.

The equations of motion used in the main part of the Report are referred to wind axes in the usual manner but it is shown that, for the tandem-rotor helicopter, it may be advantageous to refer the equations to the principal inertia axes for lateral stability studies. When these axes are used the derivatives are easier to calculate and, since product of inertia terms are absent, the terms in the stability quartic are easier to interpret.

The fuselage derivatives have been given special attention since they appear to be at least as important as the rotor derivatives especially in the case of l_v where the fin contribution may be several times that from the rotors.

As in fixed-wing aircraft stability studies, it is possible to obtain simple approximations to the damping and periods of the modes of motion.

2. *The Equations of Motion.* As usual, wind axes are used, the axes being fixed in the body with the x-axis directed initially parallel to the trimmed flight path, the y-axis directed to starboard and the z-axis pointing downwards. The equations of motion for small disturbances are then

$$\frac{W}{g}\dot{v} - Y_v v - Y_p p + \frac{W}{g}Vr - Y_r r - W\phi\cos\gamma_e - W\psi\sin\gamma_e = Y_\xi\xi + Y_\zeta\zeta \qquad (1)$$

$$- L_v v + A\dot{p} - L_p p - E\dot{r} - L_r r = L_\xi\xi + L_\zeta\zeta \qquad (2)$$

$$- N_v v - E\dot{p} - N_p p + C\dot{r} - N_r r = N_\xi\xi + N_\zeta\zeta. \qquad (3)$$

Previously issued as R.A.E. Report Naval 4 (A.R.C. 21,918).

Dividing equation (1) by $2\rho sA\Omega^2R^2$ and equations (2) and (3) by $2\rho sA\Omega^2R^3$ and moments of inertia A and C respectively the non-dimensional forms of the equations of motion become

$$\frac{d\hat{v}}{d\tau} - y_v\hat{v} - \frac{y_p}{\mu_2}\frac{d\phi}{d\tau} - t_c'\,\phi\cos\gamma_e + \left(\hat{V} - \frac{y_r}{\mu_2}\right)\frac{d\psi}{d\tau} - t_c'\psi\sin\gamma_e = y_\xi\xi + y_\zeta\zeta \tag{4}$$

$$-\frac{\mu_2 l_v}{i_A}\hat{v} + \frac{d^2\phi}{d\tau^2} - \frac{l_p}{i_A}\frac{d\phi}{d\tau} - \frac{i_E}{i_A}\frac{d^2\psi}{d\tau^2} - \frac{l_r}{i_A}\frac{d\psi}{d\tau} = \frac{\mu_2}{i_A}l_\xi\xi + \frac{\mu_2}{i_A}l_\zeta\zeta \tag{5}$$

$$-\frac{\mu_2 n_v}{i_C}\hat{v} - \frac{i_E}{i_C}\frac{d^2\phi}{d\tau^2} - \frac{n_p}{i_C}\frac{d\phi}{d\tau} + \frac{d^2\psi}{d\tau^2} - \frac{n_r}{i_C}\frac{d\psi}{d\tau} = \frac{\mu_2}{i_C}n_\xi\xi + \frac{\mu_2}{i_C}n_\zeta\zeta. \tag{6}$$

The scheme for the conversion of the force and moment derivatives and moments of inertia of equations (1), (2) and (3) to the non-dimensional derivatives and coefficients of inertia of equations (4), (5) and (6) is given in the table of Section 2 of Ref. 1 except that, as in Ref. 2, A is replaced by $2A$.

Solution of equations (4), (5) and (6), when the control terms on the right-hand side are zero, by the usual substitution $\hat{v} = \hat{v}_0 e^{\lambda\tau}$, etc. gives the frequency equation

$$\lambda(A'\lambda^4 + B'\lambda^3 + C'\lambda^2 + D'\lambda + E') = 0 \tag{7}$$

where

$$A' = 1 - \frac{i_E^2}{i_A i_C}$$

$$B' = -y_v\left(1 - \frac{i_E^2}{i_A i_C}\right) - \left(\frac{l_p}{i_A} + \frac{n_r}{i_C} + \frac{i_E}{i_A i_C}l_r + \frac{i_E}{i_A}\frac{n_p}{i_C}\right) \tag{8}$$

$$C' = y_v\left(\frac{l_p}{i_A} + \frac{n_r}{i_C} + \frac{i_E}{i_C}\frac{l_r}{i_A} + \frac{i_E}{i_A}\frac{n_p}{i_C}\right) + \left(\frac{l_p}{i_A}\frac{n_r}{i_C} - \frac{l_r}{i_A}\frac{n_p}{i_C}\right) + \frac{\mu_2 l_v}{i_A}\left\{\frac{i_E}{i_C}\left(\hat{V} - \frac{y_r}{\mu_2}\right) - \frac{y_p}{\mu_2}\right\} + \frac{\mu_2 n_v}{i_C}\left\{\left(\hat{V} - \frac{y_r}{\mu_2}\right) - \frac{i_E}{i_A}\frac{y_p}{\mu_2}\right\} \tag{9}$$

$$D' = -y_v\left(\frac{l_r}{i_A}\frac{n_p}{i_C} - \frac{l_p}{i_A}\frac{n_r}{i_C}\right) + \frac{\mu_2 l_v}{i_A}\left\{\frac{n_p}{i_C}\left(\hat{V} - \frac{y_r}{\mu_2}\right) + \frac{n_r}{i_C}\frac{y_p}{\mu_2} - t_c'\cos\gamma_e + \frac{i_E}{i_C}t_c'\sin\gamma_e\right\} - \frac{\mu_2 n_v}{i_C}\left\{\frac{l_p}{i_A}\left(\hat{V} - \frac{y_r}{\mu_2}\right) + \frac{l_p}{i_A}\frac{y_p}{\mu_2} - t_c'\sin\gamma_e + \frac{i_E}{i_A}t_c'\cos\gamma_e\right\} \tag{10}$$

$$E' = \frac{\mu_2 l_v}{i_A}\left(\frac{n_p}{i_C}t_c'\sin\gamma_e + \frac{n_r}{i_C}t_c'\cos\gamma_e\right) - \frac{\mu_2 n_v}{i_C}\left(\frac{l_p}{i_A}t_c'\sin\gamma_e + \frac{l_r}{i_A}t_c'\cos\gamma_e\right). \tag{11}$$

The zero root given by equation (7) implies that the aircraft has no preference for a particular heading.

3. *The Lateral Stability Derivatives.* 3.1. *The Rotor Derivatives.* When a rotor is placed in a stream of air of velocity V the rotor disc, relative to the no-feathering axis, will tilt backwards with angle a_1, and sideways towards the advancing side with angle b_1. The resultant tilt will be of amount $(a_1^2 + b_1^2)^{1/2}$ and at angle $\psi_0 = \tan^{-1} b_1/a_1$ towards the advancing blade, ψ_0 being measured from

the rear-most position of the blade. If a small side-wind of velocity v blows from the retreating side of the disc the relative wind will appear to come from a new direction at angle $\epsilon = \tan^{-1} v/V \cos \alpha_D$ in the plane of the disc relative to the original direction. The new sideways flapping component $b_1 + \delta b_1$, will be given by

$$\begin{aligned} b_1 + \delta b_1 &= (a_1^2 + b_1^2)^{1/2} \sin (\psi_0 + \epsilon) \\ &= (a_1^2 + b_1^2)^{1/2} \{\sin \psi_0 \cos \epsilon + \sin \epsilon \cos \psi_0\} \\ &= b_1 + a_1 \epsilon, \text{ for small } \epsilon \end{aligned}$$

therefore

$$\delta b_1 = a_1 \epsilon = \frac{a_1 v}{V \cos \alpha_D}$$

therefore

$$\frac{\partial b_1}{\partial \hat{v}} = \frac{a_1}{\mu} = \frac{2(\frac{4}{3} B\theta_0 + \lambda)}{B^2 + \frac{3}{2}\mu^2} \tag{12}$$

using the familiar expression for a_1.

It should be noted that the sign of b_1 for a given direction of tilt depends on the sense of rotation of the rotor and that $\partial b_1/\partial \hat{v}$ will be of opposite sign if the side-wind blows from the advancing side. However, there will be no confusion if it is remembered that the disc always tilts away from the side-wind.

In addition, a side-wind will also cause a sideways component of the in-plane H-force. This component will be

$$h_c \epsilon = \frac{h_c v}{V \cos \alpha_D}$$

therefore

$$\begin{aligned} \frac{\partial}{\partial \hat{v}} \left(\frac{h_c v}{V \cos \alpha_D} \right) &= \frac{h_c}{\mu} \\ &\simeq \tfrac{1}{4}\delta. \end{aligned} \tag{13}$$

The front and rear rotor contributions to the side-force will then be

$$(y_v)_F = -\tfrac{1}{2} \left(t_{c\,F} \frac{a_{1\,F}}{\mu} + \tfrac{1}{4}\delta \right) \tag{14}$$

$$(y_v)_R = -\tfrac{1}{2} \left(t_{c\,R} \frac{a_{1\,R}}{\mu} + \tfrac{1}{4}\delta \right). \tag{15}$$

These side forces will result in contributions to the moment derivatives

$$(l_v)_r = (y_v)_F h_{1\,F} + (y_v)_R h_{1\,R} \tag{16}$$

and

$$(n_v)_r = (y_v)_F l_{1\,F} - (y_v)_R l_{1\,R}. \tag{17}$$

From Ref. 2 we find that the side-force contributions due to roll are

$$(y_p)_F = -\tfrac{1}{2} \left(t_{c\,F} - \frac{B^2 a \lambda_F}{8} \right) \frac{16}{\gamma B^2 (B^2 + \frac{3}{2}\mu^2)} \tag{18}$$

$$(y_p)_R = -\tfrac{1}{2} \left(t_{c\,R} - \frac{B^2 a \lambda_R}{8} \right) \frac{16}{\gamma B^2 (B^2 + \frac{3}{2}\mu^2)}. \tag{19}$$

The total rotor contributions to the moment due to roll derivatives are therefore

$$(l_p)_r = (y_p)_F h_{1F} + (y_p)_R h_{1R} \tag{20}$$

$$(n_p)_r = (y_p)_F l_{1F} - (y_p)_R l_{1R}. \tag{21}$$

When the tandem-rotor helicopter rotates in yaw side-winds (of opposite signs) will be imposed on the front and rear rotors and we find that

$$(y_r)_F = -\tfrac{1}{2}t_{cF} l_{1F} a_{1F}/\mu \tag{22}$$

$$(y_r)_R = +\tfrac{1}{2}t_{cR} l_{1R} a_{1R}/\mu. \tag{23}$$

The total rotor contributions to the moment due to yaw are then

$$(l_r)_r = (y_r)_F h_{1F} + (y_r)_R h_{1R} \tag{24}$$

$$(n_r)_r = (y_r)_F l_{1F} - (y_r)_R l_{1R}. \tag{25}$$

It is useful to note that $(y_r)_r = (n_v)_r$.

(It is unfortunate that the standard symbols for rate of yaw and suffix for rotor contribution are the same, namely r. However, when r appears outside a bracket throughout this Report it refers to the contribution of both rotors.)

3.2. *Fuselage Derivatives.*

3.2.1. $(y_v)_f$

It is difficult to make a theoretical estimate of $(y_v)_f$ but the wind-tunnel tests of Refs. 3 and 9 should give a reasonably accurate value for a typical fuselage. An analysis of these results shows that the fuselage contribution can be represented by

$$(y_v)_f = \frac{-0{\cdot}3\mu S_B}{sA}. \tag{26}$$

3.2.2. $(l_v)_f$

The calculation of l_v due to a fin is usually of secondary importance for the fixed-wing aircraft but for the helicopter without a wing the fin contribution to l_v may be far greater than that of the rotors and is therefore of great importance.

If the fin effect is calculated in the manner of Ref. 4 we have

$$(l_v)_f = -V_f a_f F(\alpha)\hat{V} \tag{27}$$

where the interference factor, κ_{FY}, of Ref. 4 is taken to be unity.

In the notation of this Report (*see* Fig. 2) V_f becomes

$$V_f = \frac{A_f}{4sA}$$

and

$$F(\alpha) = h_f \cos\alpha_s - l_f \sin\alpha_s.$$

a_f can be calculated from Ref. 4 but a more accurate value can probably be obtained from Ref. 5.

No tandem-rotor helicopter flying at present has a wing but wings may be fitted to future designs. The calculation of l_v due to a wing may be calculated from Refs. 4 and 6.

Again, we are in difficulty with notation. We would like to use the symbols f or F to denote the fin contribution to the derivatives but they have already been used to denote fuselage and front rotor respectively.

However, in lateral stability work, the term 'fin effect' is meant to include all those fuselage effects which act like a fin and so there will be no ambiguity throughout this Report if the suffix f is used to denote the fin contribution.

3.2.3. $(n_v)_f$

The method of Ref. 7 has been used for estimating $(n_v)_f$ but care must be taken to convert the non-dimensional values given there to those which correspond to the tandem-rotor helicopter. Thus the values of $n_{v\,B}$ of Ref. 7 must be multiplied by $\hat{V}S_B\, l_B/4sAR$ and the values of $n_{v\,W}$ by $\hat{V}Sb/4sAR$. For the fin itself Ref. 7 uses the results of Ref. 5, *i.e.* the fin contribution, in the notation of this Report, will be $a_f\, A_f\, l_f\, \hat{V}/4sA$.

3.2.4. *The moment derivatives due to rate of roll and rate of yaw.* These derivatives, like $(l_v)_f$, may be considerable for the helicopter and have been calculated by strip theory, as follows.

Let x be the distance above the centre of area of an elementary strip, parallel to the flight path, of chord C and width dx. A rate of roll p will change the incidence of the strip by $p\{F(\alpha) + x\}/V$ and the rolling moment of the fin will then be

$$(C_l)_f = -\frac{\frac{1}{2}\rho a_f p R^2}{V}\int_{x_1}^{x_2} c\,\{F(\alpha) + x\}^2\,dx$$

giving

$$(l_p)_f = -\frac{a_f A_f \hat{V}\,\{F^2(\alpha) + h_{fg}{}^2\}}{4sA} \tag{28}$$

where h_{fg} is the radius of gyration of the fin about an axis through its centroid parallel to the flight path or, approximately, parallel to the aircraft datum line.

Similarly we derive

$$(n_p)_f = \frac{a_f \hat{V} A_f l_f F(\alpha)}{4sA} \tag{29}$$

$$(l_r)_f = \frac{a_f \hat{V} A_f l_f F(\alpha)}{4sA} = (n_p)_f \tag{30}$$

$$(n_r)_f = -\frac{a_f \hat{V} A_f l_f^2}{4sA}\,. \tag{31}$$

3.2.5. *Control moment derivatives.* Adopting the notation for fixed-wing aircraft, an angular displacement of the cyclic stick to port, ξ, produces equal changes of cyclic pitch, $k_1\xi$, on front and rear rotors such that both tilt to port. A displacement, ζ, of the rudder bar, with the left foot forward, produces tilts, $k_2\zeta$, of both rotors, the front rotor tilting to port and the rear rotor to starboard. The control angle notation has been used for stick and rudder displacements rather than the rotor disc displacement because of the possible confusion arising from the signs of the lateral tilt and cyclic pitch application for counter rotating rotors, as mentioned in Section 3.1.

In non-dimensional form the control force and moment derivatives will then be

$$y_\xi = -k_1 t_c' \tag{32}$$

$$y_\zeta = -k_2 (t_{cF} - t_{cR}) \tag{33}$$

$$l_\xi = -k_1 (t_{cF} h_{1F} + t_{cR} h_{1R}) \tag{34}$$

$$l_\zeta = -k_2 (t_{cF} h_{1F} - t_{cR} h_{1R}) \tag{35}$$

$$n_\xi = -k_1 (t_{cF} l_{1F} - t_{cR} l_{1R}) \tag{36}$$

$$n_\zeta = -k_2 (t_{cF} l_{1F} + t_{cR} l_{1R}). \tag{37}$$

3.3. *Comparison of Theoretical Derivatives with Estimates from Flight Tests.* The trim equations in level flight for a given steady sideslip angle $\beta(=\hat{v}/\mu)$ are obtained from equations (4), (5) and (6) of Section 2 by omitting the acceleration and rate terms and putting $\gamma_e = 0$, giving

$$\mu\beta y_v + t_c'\phi = -(y_\xi \xi + y_\zeta \zeta) \tag{38}$$

$$\mu\beta l_v = -(l_\xi \xi + l_\zeta \zeta) \tag{39}$$

$$\mu\beta n_v = -(n_\xi \xi + n_\zeta \zeta). \tag{40}$$

Thus by measuring the control angles (assuming the control derivatives are known from equations (32) to (37)) and the angle of bank for a given sideslip angle the derivatives y_v, l_v and n_v can be obtained. A number of such measurements for the Vertol HUP-1 tandem-rotor helicopter is given in Ref. 8. From these measurements the derivatives were calculated and the results for y_v and l_v, together with the theoretical values are shown in Figs. 3 and 4 where it is seen that the agreement is quite good. On the other hand n_v has not been shown as agreement was extremely poor; it was unfortunate that the fuselage of the HUP-1 is very short and 'stubby' whilst the fin section has a thickness/chord ratio of 35 per cent and a trailing edge angle of about 45 deg. Thus the fuselage and fin contributions to n_v were both difficult to estimate accurately and since the total n_v is the difference between these comparatively large quantities it is not surprising that the theoretical estimate should be so poor. The estimation of n_v for a comparatively slender fuselage, such as that of the Bristol 192 which closely resembles fixed-wing aircraft practice, should be far more reliable.

4. *Discussion of Derivatives.* The estimated derivatives for the Bristol 173 helicopter are shown in Figs. 5(a) to 5(g). The force-rate derivatives y_p and y_r have been omitted as they are negligibly small.

4.1. y_v

The rotor contribution is roughly proportional to a_1/μ which is almost constant throughout the speed range. The fuselage contribution which varies linearly with speed is very much larger at all but the lower speeds so that for most of the speed range the rotor contribution can be neglected.

4.2. l_v

The rotor contribution is again roughly constant with speed for the reason given above in 4.1. The fin contribution increases rapidly with speed and above $\mu = 0{\cdot}2$ is already larger than the rotor

contribution. Thus it will be seen that the fin has a powerful dihedral effect compared with that of the rotors but without a corresponding effect on the damping in roll (Section 4.4). It will be shown later that this may lead to a very unstable Dutch-roll oscillation at the higher speeds.

It should be noted that, although the force derivative on the fin is linear, the moment derivative rises more rapidly than this since the fin height relative to the wind-axis increases with the increasing nose-down attitude in pitch.

4.3. n_v

The rotor contribution is usually negligible and the total n_v depends almost entirely on the fuselage and fin contributions. However, it is interesting to note that setting the C.G. forward increases the front rotor thrust and tilt and decreases the rear rotor thrust and tilt thus causing the rotor contribution to be unstable.

4.4. l_p

The rotor provides nearly all the damping in roll, a small contribution arising from the fin at higher speeds. It will be seen later that it would be desirable to be able to increase l_p considerably but presumably this could only be done by fitting a small wing.

4.5. n_p

This derivative hardly warrants discussion as it is usually unimportant and, in any case, appears in combination with other derivatives in such a way that its effect can always be eliminated by slight changes in the others.

4.6. l_r and n_r

These derivatives will be discussed together as their most important effect is their appearance in the constant term, E, of the stability quartic. In level flight E is proportional to $l_v n_r - n_v l_r$. Now n_r is negative and so is l_v, usually, so that the first term contributes to the stability of the spiral mode. On the other hand l_r is positive and n_v must be positive for positive weathercock stability so that the second term represents spiral instability. However, as can be seen from Figs. 5(f) and 5(g) both l_r and n_r increase with speed, although not necessarily in the same ratio, and the effect of one tends to cancel the effect of the other. Therefore the spiral stability depends mainly on the choice of l_v and n_v being, in any case, easier to control than l_r and n_r which depend mainly on fin and rotor heights.

5. *Discussion of Stick-Fixed Stability.* 5.1. *Approximate Roots of Stability Quartic.* Before discussing the stability in detail, it is worth while obtaining approximations to the roots of equation (7) to see more clearly the dependence of the motions on certain derivatives or combinations of derivatives.

Dividing equation (7) through by A' we obtain

$$\lambda^4 + B\lambda^3 + C\lambda^2 + D\lambda + E = 0. \tag{41}$$

Now the coefficient D is always several times larger than E so that to a good approximation one root of equation (41) is $\lambda_1 = -E/D$. This is the spiral root, familiar also to fixed-wing aircraft practice, and since D is usually positive a stable mode requires that E is also positive *i.e.* $l_v n_r - n_v l_r > 0$. Comparisons between this approximation and more exact calculations are shown in Fig. 8 where agreement is seen to be extremely good.

Dividing equation (41) by $(\lambda + E/D)$ leaves a cubic which can be written approximately as

$$\lambda^3 + B\lambda^2 + (C - BE/D)\,\lambda + D = 0. \tag{42}$$

In fixed-wing aircraft practice the coefficient B is large enough (compared with the other coefficients) to take as a good approximation $\lambda_2 = -B$ but this is not always true for the helicopter as is shown at the higher values of μ in Fig. 9. Also, Newton's process of approximation which is often used to obtain a better value of λ_2 is slowly convergent or may even be divergent at the higher values of μ. However, another iterative process, which seems to work quite well, consists of writing equation (42) as

$$\lambda^3 = -\{B\lambda^2 + (C - BE/D)\,\lambda + D\} \tag{43}$$

and substituting $\lambda = -B$ (or a better approximation, if known) into the right-hand side of equation (43) and taking the cube-root, this latter value being used as the next approximation and the process repeated until the desired accuracy is obtained. This process can be carried out quickly on a slide-rule. Since this root is roughly equal to $-B$ and since B consists very largely of the term l_p/i_A, this root can be regarded roughly as representing the damping of the rolling motion. Let α be the value of the root obtained from the above process. Dividing equation (42) by $(\lambda + \alpha)$ leaves a quadratic $(\lambda^2 + \beta\lambda + \gamma)$ so that to a good approximation

$$(\lambda + E/D)\,(\lambda + \alpha)\,(\lambda^2 + \beta\lambda + \gamma) \equiv \lambda^4 + B\lambda^3 + C\lambda^2 + D\lambda + E.$$

Equating the constant terms and the terms in λ^2 gives

$$\beta = C/\alpha - D/\alpha^2 - E/D. \text{ (neglecting } E/D \text{ compared with } \alpha) \tag{44}$$

and

$$\gamma = D/\alpha. \tag{45}$$

If we take $\alpha = B$, which is a good approximation for $\mu < 0{\cdot}3$, then $\gamma = D/B$, an approximation used in fixed-wing aircraft work giving for the time of oscillation

$$T_0 = 2\pi\hat{t}\,\sqrt{(B/D)} \tag{46}$$

assuming β is fairly small.

5.2. *Lateral (Dutch Roll) Oscillation.* 5.2.1. *Damping of oscillation.* The damping of the lateral oscillation of the complete helicopter is shown in Fig. 6 where it can be seen that the oscillation becomes rapidly unstable with speed. That this is due to excessive dihedral effect is shown by the lower curves in which the value of l_v used in the calculations is that from the rotors only. The beneficial effect of increasing l_p is shown in Fig. 10 where doubling the existing l_p greatly improves the stability. Unfortunately it does not appear possible to increase l_p considerably except by fitting a wing and the only other way of obtaining a damped oscillation is to prevent the fin and tailplane contributing too much to l_v. This might be done by fitting a tailplane which has anhedral or possibly by a retractable fin which, in the extended position, is placed below the aircraft centre line.

We can examine the effect of l_p and l_v on the damping of the oscillation by referring to the expression for β, equation (44). Since α, D and E are almost always positive a damped oscillation can only be achieved if C is positive and the term C/α (or approximately C/B) is larger than the sum of the other two.

Now numerical calculations show that the coefficients A', B', C', D' and E' of equations (8) to (11) can be written approximately

$$A' = 1 - \frac{i_E^2}{i_A i_C} \tag{47}$$

$$B' = -\frac{l_p}{i_A} \tag{48}$$

$$C' = \frac{l_p}{i_A}\left(y_v + \frac{n_r}{i_C}\right) + \hat{V}\left(\frac{\mu_2 l_v}{i_A}\frac{i_E}{i_C} + \frac{\mu_2 n_v}{i_C}\right). \tag{49}$$

$$D' = -\frac{\mu_2 l_v}{i_A} t_c' - \frac{\mu_2 n_v}{i_C}\frac{l_p}{i_A}\hat{V} \tag{50}$$

$$E' = \frac{\mu_2}{i_A i_C}(l_v n_r - n_v l_r). \tag{51}$$

The separate terms in β are approximately

$$\frac{C}{B} = -\left(y_v + \frac{n_r}{i_C}\right) - \frac{\hat{V} i_A}{l_p}\left(\frac{\mu_2 l_v}{i_A}\cdot\frac{i_E}{i_C} + \frac{\mu_2 n_v}{i_C}\right) \tag{52}$$

$$\frac{D}{B^2} = -\left(\frac{\mu_2 l_v}{l_p^2} i_A t_c' + \frac{\mu_2 n_v}{i_C}\cdot\frac{i_A}{l_p}\hat{V}\right)\left(1 - \frac{i_E^2}{i_A i_C}\right) \tag{53}$$

$$\frac{E}{D} = -\frac{(l_v n_r - n_v l_r)}{l_v t_c' i_C + n_v l_p \hat{V}}. \tag{54}$$

Taking the effect of l_p first, all other derivatives remaining constant, the terms in β all decrease with increasing l_p except the constant positive term $-\left(y_v + \frac{n_r}{i_C}\right)$ and the term $\frac{E}{D}$. Thus as l_p increases β tends to the value $-\left(y_v + \frac{n_r}{i_C}\right) - \frac{E}{D}$ which except, perhaps, at hovering and very low speeds is positive and increases with speed, *i.e.* the stability improves.

Turning now to the effect of l_v, the most important terms are D/B^2 and the second term of C/B. When l_v and l_p are negative and n_v positive, *i.e.* when they represent positive static stability, D/B^2 is positive and contributes to instability of the Dutch roll. This term increases with increase of l_v and usually increases rapidly with speed also. The second term of C/B also contributes to instability increasing rapidly with speed due to the term $\frac{\mu_2 l_v}{i_A}\cdot\frac{i_E}{i_C}$ which becomes negative, as the longitudinal principal axis assumes a nose-down attitude, and overwhelms the weathercock stability term $\frac{\mu_2 n_v}{i_C}$. Since i_E is determined by the mass and fuselage attitude and cannot be varied easily it follows that too large a value of l_v, especially at high speeds again leads to instability. These effects can be seen clearly in Fig. 6. Thus as far as the Dutch roll damping is concerned we wish to make n_v as large as possible and keep l_v and i_E as small as possible, assuming i_E is positive as is almost certain for a helicopter at all but the lower speeds.

The reduction of damping with increase of i_E is often described as a destabilizing 'product of inertia effect'. This effect is not easy to see physically, compared with those from aerodynamic terms, and in any case the magnitudes of the product of inertia terms depend on the axes chosen.

Another interpretation of the term involving i_E can be obtained by writing down the equations of motion of the helicopter referred to its principal axes. These are given in Appendix 1 where the term corresponding to $\left(\frac{\mu_2 l_v}{i_A} \cdot \frac{i_E}{i_C} + \frac{\mu_2 n_v}{i_C}\right)$ has become $\left(-\frac{\mu_2 l_v}{i_{A0}} \sin\vartheta + \frac{\mu_2 n_v}{i_{C0}} \cos\vartheta\right)$. The latter term is seen to be the sum of the terms $-\frac{\mu_2 l_v}{i_{A0}}$ and $\frac{\mu_2 n_v}{i_{C0}}$ resolved about the yawing axis of the wind-axes system and therefore represents a kind of weathercock stability—it is not a true weathercock *moment* since both terms are divided by their corresponding inertias. Nevertheless, it can be seen that when the fuselage takes up a nose-down attitude (negative ϑ) a negative l_v (the usual dihedral sense) acts partly like a negative weathercock stability and since $\frac{\mu_2 l_v}{i_A}$ is usually several times larger than $\frac{\mu_2 n_v}{i_C}$ it is quite easy for the whole term to become negative. Thus the deterioration of stability which is often regarded as a 'product of inertia effect' can be interpreted simply as a transformation of the dihedral effect into negative weathercock stability. This interpretation is especially appropriate to a helicopter since the moment derivatives (except those from a wing) are directly related to the fuselage geometry (and therefore to the principal axes) so that when referred to these axes will be almost independent of attitude. Since helicopter moment derivatives are simpler to calculate when referred to these axes their use in the study of helicopter lateral stability may be an advantage.

5.2.2. *Period of oscillation.* The approximate expression for the period of lateral oscillation is $T_0 = 2\pi\hat{t}\sqrt{(B/D)}$. This approximation gives good agreement with more exact calculations, except perhaps at the highest values of μ, as Fig. 7 shows. Using the approximations for B' and D' in equations (48) and (50) gives

$$\frac{B}{D} = \frac{1}{\frac{\mu_2 l_v}{l_p} t_c' + \frac{\mu_2 n_v}{i_C} \hat{V}}. \tag{55}$$

The two terms in the denominator are usually of the same order and since both increase with μ the period decreases as μ increases. If a wing is fitted l_p will be much larger and l_v possibly smaller and the time of oscillation would depend almost entirely on n_v. The approximation to the time of oscillation would then be

$$T_0 = 2\pi\hat{t}\sqrt{\left(\frac{i_C}{\mu_2 \hat{V} n_v}\right)} \tag{56}$$

an expression corresponding to one derived for fixed-wing aircraft, Ref. 10.

5.2.3. *Dutch Roll-yaw ratio.* If l_p, l_v and n_v are varied to improve the damping of the lateral oscillation or perhaps the spiral mode the ratio of amplitudes of roll to yaw in disturbed flight varies also. A simple approximate expression for this ratio is derived from equations (5) and (6) of Section 2, for zero control movement and neglecting n_p,

$$-\frac{\mu_2 l_v}{i_A}\hat{v} + \ddot{\phi} - \frac{l_p}{i_A}\dot{\phi} - \frac{i_E}{i_A}\ddot{\psi} - \frac{l_r}{i_A}\dot{\psi} = 0 \tag{57}$$

$$-\frac{\mu_2 n_v}{i_C}\hat{v} - \frac{i_E}{i_A}\ddot{\phi} + \ddot{\psi} - \frac{n_r}{i_C}\dot{\psi} = 0. \tag{58}$$

Now $\dot{\phi} = p = p_0 e^{\lambda\tau}$ and $\dot{\psi} = r = r_0 e^{\lambda\tau}$ where p_0 and r_0 are the (complex) amplitudes of the roll and yaw oscillations respectively and λ is complex in general. Substituting for $\dot{\phi}$ and $\dot{\psi}$ in equations (57) and (58) gives

$$-\frac{\mu_2 l_v}{i_A}\frac{\hat{v}_0}{r_0} + \lambda\frac{p_0}{r_0} - \frac{l_p}{i_A}\frac{p_0}{r_0} - \frac{i_E}{i_A}\lambda - \frac{l_r}{i_A} = 0 \tag{59}$$

$$-\frac{\mu_2 n_v}{i_C}\frac{\hat{v}_0}{r_0} - \frac{i_E}{i_C}\lambda\frac{p_0}{r_0} + \lambda - \frac{n_r}{i_C} = 0. \tag{60}$$

Eliminating $\hat{V}_0/r_0$ gives

$$\frac{p_0}{r_0} = \frac{\frac{\mu_2 n_v}{i_C}\left(\frac{i_E}{i_A}\lambda + \frac{l_r}{i_A}\right) + \frac{\mu_2 l_v}{i_A}\left(\lambda - \frac{n_r}{i_C}\right)}{\frac{\mu_2 n_v}{i_C}\left(\lambda - \frac{l_p}{i_A}\right) + \frac{\mu_2 l_v}{i_A}\frac{i_E}{i_C}\lambda}. \tag{61}$$

If the coefficient β of the Dutch-roll quadratic is small compared with γ then $\lambda^2 = -\gamma$ or $\lambda = i\delta$, say, equation (61) becomes

$$\frac{p_0}{r_0} = \frac{\frac{\mu_2 n_v}{i_C}\left(\frac{i_E}{i_A}i\delta + \frac{l_r}{i_A}\right) + \frac{\mu_2 l_v}{i_A}\left(i\delta - \frac{n_r}{i_C}\right)}{\frac{\mu_2 n_v}{i_C}\left(i\delta - \frac{l_p}{i_A}\right) + \frac{\mu_2 l_v}{i_A}\frac{i_E}{i_C}i\delta}. \tag{62}$$

Inserting typical values into equation (62) shows that many terms can be neglected when the modulus of p_0/r_0 is calculated and we have as quite a good approximation

$$\left|\frac{p_0}{r_0}\right| = \frac{\delta\mu_2\frac{l_v}{i_A}}{\frac{\mu_2 n_v}{i_C}\cdot\frac{l_p}{i_A}}. \tag{63}$$

It can be seen from Fig. 11 that the time of oscillation, and therefore δ, does not vary greatly with changes of l_p and l_v so that the Dutch-roll ratio can be said to be roughly proportional to l_v and inversely proportional to n_v and l_p. For the Bristol 173 the value of $|p_0/r_0|$ from equation (63) is $3{\cdot}75$ at $\mu = 0{\cdot}2$ and agrees well with more exact calculations from an analogue computer.

In fixed-wing aircraft practice a large ratio of roll in yaw is regarded as objectionable. From equation (63) this requires that, for a given l_p, l_v should not be too large compared with n_v, a combination required also for satisfactory damping of the Dutch-roll oscillation.

5.3. *The Spiral Mode.* Fig. 8 shows the damping of the spiral mode with μ for two configurations. Fig. 12 shows the effect of varying l_p and l_v on this mode. Since, approximately, $\lambda_1 = -E/D$ we can infer from the expression for E, what is shown in the Figures, that the larger the value of l_v the better the damping of the mode whilst increasing n_v tends to make the motion divergent. These derivatives have been shown to have the opposite effect on the Dutch-roll damping and, as for fixed-wing aircraft, the choice of l_v and n_v must often be a compromise between accepting some degree of instability of one or other, or even both, modes. Divergence of the spiral mode does not become very severe even for quite large changes in l_v and n_v and it is usual, in fixed-wing aircraft practice, to accept some spiral instability in order to achieve satisfactory damping of the Dutch roll.

6. *Control Response.* Fig. 14 shows the response of the helicopter to a sudden 1 deg lateral tilt of the rotor discs at $\mu = 0{\cdot}2$ for three values of l_p. In the original configuration the helicopter is about neutrally stable and reaches maximum bank angle in about 4 seconds and maximum rate of roll in about 1 second. If the stick were held in the displaced position for long enough the helicopter would roll from side to side with a period of about 8 seconds.

If l_p is increased the oscillation becomes stable and the angle of bank reaches a steady value but the maximum bank angle decreases and the time to reach it increases so that too much damping in roll for a given l_v may cause the aircraft to appear sluggish.

If l_v is increased for a given value of l_p, Fig. 15, we see that the maximum rate of roll is roughly the same for each case but that the maximum angle of bank is reduced and the time taken to reach it is also reduced. However, if l_v is increased too much the lateral oscillation becomes unstable and a steady bank angle is not reached. In these cases the rapid reversal of rate of roll is regarded as undesirable as it may prevent the pilot from banking the aircraft accurately. This effect becomes more pronounced at higher speeds where l_v increases and l_p falls off slightly.

7. *Conclusions.* 7.1. A method of calculating the aerodynamic derivatives of a tandem-rotor helicopter is given and shows fairly good agreement with values obtained from a series of flight tests.

7.2. The sideslip derivative, l_v, is greatly affected by a tall fin which may provide a contribution several times larger than that of the rotors. Since there is no corresponding increase of l_p, this leads to an unstable Dutch-roll oscillation at the higher speeds which becomes progressively worse as the speed increases. The corresponding spiral mode is stable.

7.3. If the rotors provide the only contribution to l_v, the Dutch roll is stable and the stability improves with speed. The spiral mode becomes unstable at the higher speeds.

7.4. The Dutch-roll characteristics could be improved by fitting a small wing or large tailplane. This would improve the damping in roll considerably and provide a control over l_v. Further, it has been shown that the Dutch-roll stability decreases as the fuselage attitude increases (in the nose-down sense) so that a clean fuselage, resulting in a small attitude, is beneficial. Considering, also, the remarks made in 7.2 it is evident that great care must be taken with the design of the fuselage. It may be that not all of these requirements can be satisfied together in which case auto-stabilization may be necessary.

7.5. Simple approximate expressions for the damping and period of the lateral modes can be derived from the coefficients of this quartic and give adequate agreement with more accurate calculations.

7.6. It may be an advantage to use equations of motion which are referred to the principal inertia axes of the helicopter rather than the wind axes. The coefficients of the stability quartic are no simpler but the derivatives are more closely related to the body axes than the wind axes and generally should be easier to calculate. Also, the product of inertia terms disappear and are replaced by aerodynamic terms which are easier to interpret physically.

LIST OF SYMBOLS

A		Moment of inertia about longitudinal wind axis, slugs ft^2
A_0		Moment of inertia about longitudinal principal axis, slugs ft^2
A		Area of one rotor disc
A'		Coefficient of λ^4 in stability quartic
A_f		Fin area, ft^2
a_1		Longitudinal backward flapping of rotor disc
a_f		Lift slope of fin
B'		Coefficient of λ^3 in stability quartic
B	$=$	B'/A'
B		Tip-loss factor (taken as 0·97)
b_1		Sideways flapping of rotor disc, positive when tilted to advancing side
b		Number of rotor blades
C		Moment of inertia about normal wind axis, slugs ft^2
C_0		Moment of inertia about normal principal axis, slugs ft^2
C'		Coefficient of λ^2 in stability quartic
C	$=$	C'/A'
C_l		Rolling-moment coefficient, $\dfrac{\text{rolling moment}}{2\rho s A\Omega^2 R^3}$
C_n		Yawing-moment coefficient, $\dfrac{\text{yawing moment}}{2\rho s A\Omega^2 R^3}$
c		Blade chord, ft
D'		Coefficient of λ in stability quartic
D	$=$	D'/A'
E		Product of inertia with respect to X and Z axes
E'		Constant term in stability quartic
E	$=$	E'/A'
$F(\alpha_s)$	$=$	$h_f \cos\alpha_s - l_f \sin\alpha_s$
$(h_{1F}R)$		Height of front rotor above line through C.G. parallel to flight path (*see* Fig. 1)
$(h_{1R}R)$		Height of rear rotor above line through C.G. parallel to flight path (*see* Fig. 1)
h_c		Coefficient of longitudinal rotor force parallel to tip-path plane
$h_{f_0}R$		Radius of gyration of fin about axis through C.G. parallel to flight path
i_{A0}, i_A, i_{C0}, i_C, i_E		Inertia coefficients $A_0 \Big/ \dfrac{W}{g} R^2$, etc.

k_1		Ratio between lateral stick displacement and cyclic pitch change
k_2		Ratio between rudder bar displacement and differential cyclic pitch change
L		Rolling moment, lb ft
L_v, L_p, L_r		Rolling-moment derivatives, $\partial L/\partial v$, $\partial L/\partial p$, $\partial L/\partial r$
l_v, l_p, l_r		Dimensionless rolling-moment derivatives, $\partial C_l/\partial \hat{v}$ $\partial C_l/\partial \hat{p}$ $\partial C_l/\partial \hat{r}$
$l_{1F}R$		Distance of front rotor from c.g. ft (*see* Fig. 1)
$l_{1R}R$		Distance of rear rotor from c.g. ft (*see* Fig. 1)
l_DR		Distance between rotors, ft
l_BR		Length of fuselage, ft
N		Yawing moment, lb ft
N_v, N_p, N_r		Yawing-moment derivatives $\partial N/\partial v$, $\partial N/\partial p$, $\partial N/\partial r$
n_v, n_p, n_r		Dimensionless yawing-moment derivatives $\partial C_n/\partial \hat{v}$, $\partial C_n/\partial \hat{p}$, $\partial C_n/\partial \hat{r}$
p		Rate of roll, rad/sec
$\hat{p}$		p/Ω
R		Rotor radius, ft
r		Rate of yaw, rad/sec
$\hat{r}$	=	r/Ω
S_B		Projected side area of fuselage, ft^2
s		Rotor solidity, $\dfrac{bc}{\pi R}$
T_0		Period of oscillation of Dutch roll
t_c'		$\dfrac{W}{2\rho s A \Omega^2 R^2}$
V		Trimmed flight velocity, ft/sec
$\hat{V}$		$V/\Omega R$
V_f	=	Fin area ratio, $A_f/4sA$
v		Lateral velocity of aircraft, ft/sec
$\hat{v}$		$v/\Omega R$
W		Weight of aircraft, lb
Y		Lateral force, lb
Y_v, Y_p, Y_r		Lateral force derivatives, $\partial Y/\partial v$, $\partial Y/\partial p$, $\partial Y/\partial r$
y_v, y_p, y_r		Dimensionless force derivatives
α		Value of a root of the stability quartic

α_D	Incidence of rotor disc, angle between relative wind and tip-path plane
α_s	Incidence of helicopter, angle between relative wind and datum line
β	Coefficient of λ in Dutch roll quadratic
γ	Constant term in Dutch roll quadratic
γ_e	Angle of climb, radians
δ	Drag coefficient of rotor blade
ζ	Displacement of rudder bar, positive for negative yawing moment
ϑ	Angle between trimmed flight path and undisturbed position of longitudinal principal axis
Θ	Angle between horizon and undisturbed position of longitudinal principal axis
θ_0	Collective pitch angle of rotor blades, radians
λ	Root of stability quartic
λ	Coefficient of flow normal to rotor disc
μ	Tip speed ratio, $V \cos \alpha_D/\Omega R$
μ_2	Relative density parameter, $W/2g\rho sAR$
ξ	Lateral displacement of stick, positive to port
ρ	Air density, slugs/ft^3
τ	Time in aerodynamic units
ϕ	Angle of bank, positive to starboard
ψ	Angle of yaw, positive to starboard
Ω	Angular velocity of rotor

Suffices

f	fuselage or fin contribution
F	front rotor
R	rear rotor
r	rotor contribution

REFERENCES

Ref. No.	*Author*	*Title, etc.*
1	A. R. S. Bramwell	Longitudinal stability and control of the single-rotor helicopter. R. & M. 3104.
2	A. R. S. Bramwell	Longitudinal stability and control of the tandem-rotor helicopter. Part I of this R. & M.
3	C. C. Smith Jr.	Static directional stability of tandem-helicopter fuselage. N.A.C.A. R.M. L50F29. TIL 2437.
4	I. Levačić	Rolling moment due to sideslip—Part III. A.R.C. 9987. Unpublished M.o.A. Report.
5	D. J. Lyons and P. L. Bisgood ..	An analysis of the lift slope of aerofoils of small aspect ratio, including fins, with design charts for aerofoils and control surfaces. A.R.C. 8540. Unpublished M.o.A. Report.
6	I. Levačić	Rolling moment due to sideslip—Part I. A.R.C. 8709. Unpublished M.o.A. Report.
7	P. L. Bisgood	Notes on the estimation of the yawing derivative due to sideslip. A.R.C. 9018. Unpublished M.o.A. Report.
8	J. H. Goldberg and R. R. Piper ..	Stability and control of tandem helicopters. Phases III and IV. Static and dynamic lateral stability and control. Princeton University Aeronautical Engineering Department Report No. 395.
9	J. L. Williams	Directional stability characteristics of two types of tandem helicopter fuselage models. N.A.C.A. Tech. Note 3201.
10	W. J. Duncan	*The principles of control and stability of aircraft.* Cambridge University Press. 1952.

APPENDIX

Equations of Motion Referred to Principal Axes

1. *Equations of Motion Referred to Principal Axes.* The equations of motion referred to the principal inertia axes are (*see* e.g. Ref. 10)

$$\frac{W}{g}(\dot{v} - pV\sin\vartheta + rV\cos\vartheta) = \Delta Y \tag{64}$$

$$A_0\dot{p} = \Delta L \tag{65}$$

$$C_0\dot{r} = \Delta N \tag{66}$$

where ϑ is the angle between the longitudinal principal axis and the direction of the trimmed flight path (positive when the axis is nose-up), and

$$\Delta Y = W(\phi\cos\Theta + \psi\sin\Theta) + Y_v v + Y_p p + Y_r r + Y_\xi\xi + Y_\zeta\zeta \tag{67}$$

$$\Delta L = L_v v + L_p p + L_r r + L_\xi\xi + L_\zeta\zeta \tag{68}$$

$$\Delta N = N_v v + N_p p + N_r r + N_\xi\xi + N_\zeta\zeta \tag{69}$$

where Θ is the angle between the longitudinal principal axis and the horizon (positive when axis is nose-up).

In non-dimensional form the equations (64) to (66) become

$$\frac{d\hat{v}}{d\tau} - y_v\hat{v} - \frac{y_p}{\mu_2}\frac{d\phi}{d\tau} - \hat{V}\sin\vartheta\frac{d\phi}{d\tau} - \frac{y_r}{\mu_2}\frac{d\psi}{d\tau} + \hat{V}\cos\vartheta\frac{d\psi}{d\tau} - t_c'\phi\cos\Theta - t_c'\psi\sin\Theta = y_\xi\xi + y_\zeta\zeta \tag{70}$$

$$-\frac{\mu_2 l_v}{i_{A0}}\hat{v} + \frac{d^2\phi}{d\tau^2} - \frac{l_p}{i_{A0}}\frac{d\phi}{d\tau} - \frac{l_r}{i_{A0}}\frac{d\psi}{d\tau} = \frac{\mu_2}{i_{A0}}l_\xi\xi + \frac{\mu_2}{i_{A0}}l_\zeta\zeta \tag{71}$$

$$-\frac{\mu_2 n_v}{i_{C0}}\hat{v} - \frac{n_p}{i_{C0}}\frac{d\phi}{d\tau} + \frac{d^2\psi}{d\tau^2} - \frac{n_r}{i_{C0}}\frac{d\psi}{d\tau} = \frac{\mu_2}{i_{A0}}n_\xi\xi + \frac{\mu_2}{i_{C0}}n_\zeta\zeta. \tag{72}$$

The frequency equation is the quintic

$$\lambda(A'\lambda^4 + B'\lambda^3 + C'\lambda^2 + D'\lambda + E') = 0$$

where

$$A' = 1$$

$$B' = -y_v - \frac{l_p}{i_{A0}} - \frac{n_r}{i_{C0}}$$

$$C' = y_v\left(\frac{l_p}{i_{A0}} + \frac{n_r}{i_{C0}}\right) + \left(\frac{l_p}{i_{A0}}\frac{n_r}{i_{C0}} - \frac{l_r}{i_{A0}}\frac{n_p}{i_{C0}}\right) - \frac{\mu_2 l_v}{i_{A0}}\left(\hat{V}\sin\vartheta + \frac{y_p}{\mu_2}\right) + \frac{\mu_2 n_v}{i_{C0}}\left(\hat{V}\cos\vartheta - \frac{y_r}{\mu_2}\right)$$

$$D' = -y_v\left(\frac{l_p}{i_{A0}}\frac{n_r}{i_{C0}} - \frac{l_r}{i_{A0}}\frac{l_p}{i_{C0}}\right) + \frac{\mu_2 l_v}{i_{A0}}\left\{\frac{n_p}{i_{C0}}\left(\hat{V}\cos\vartheta - \frac{y_r}{\mu_2}\right) + \frac{n_r}{i_{C0}}\left(\hat{V}\sin\vartheta + \frac{y_p}{\mu_2}\right) - t_c'\cos\Theta\right\} - \frac{\mu_2 n_v}{i_{C0}}\left\{\frac{l_p}{i_{A0}}\left(\hat{V}\cos\vartheta - \frac{y_r}{\mu_2}\right) + \frac{l_r}{i_{A0}}\left(\hat{V}\sin\vartheta + \frac{y_p}{\mu_2}\right) - t_c'\sin\Theta\right\}$$

$$E' = \frac{\mu_2 l_v}{i_{A0}}\left\{\frac{n_r}{i_{C0}}t_c'\cos\Theta - \frac{n_p}{i_{C0}}t_c'\sin\Theta\right\} - \frac{\mu_2 n_v}{i_{C0}}\left\{\frac{l_r}{i_{A0}}t_c'\cos\Theta - \frac{l_p}{i_{A0}}t_c'\sin\Theta\right\}.$$

2. *The Aerodynamic Derivatives with Respect to Principal Axes.* The forms of the rotor-moment and fuselage-moment derivatives of Section 3.2 remain the same except that the terms h_{1F}, h_{1R}, l_{1F} and l_{1R} are replaced by the constant values $(h_p)_F$, $(h_p)_R$, $(l_p)_F$ and $(l_p)_R$ respectively in the rotor-moment derivatives and $F(\alpha)$, l_f and h_{fg} are replaced by the constant values $(h_p)_f$, $(l_p)_f$ and $(h_p)_{fg}$ in the fuselage derivatives, the suffix $_p$ denoting measurements from or along the longitudinal principal axis.

TABLE 1

Particulars of the helicopter, similar to the Bristol 173, *used in the stability calculations*

Weight	13,000 lb
Rotor radius	25 ft
Solidity	0·04
Rotor speed	26 rad/sec
h_F	0·22
h_R	0·424
$l_F + l_R$	1·62
k_1	0·286
k_2	0·143
d_0	0·08
A_0 (principal moment of inertia in roll)	4,260 slugs ft²
B_0 (principal moment of inertia in pitch)	92,500 slugs ft²
C_0 (principal moment of inertia in yaw)	89,000 slugs ft²
Longitundial principal axis perpendicular to rotor hub axes when $\phi = 0$	
Lock's inertia number	8
l_f	0·72
h_{fg}	0·126
A_f	122 ft²
a_f	1·6

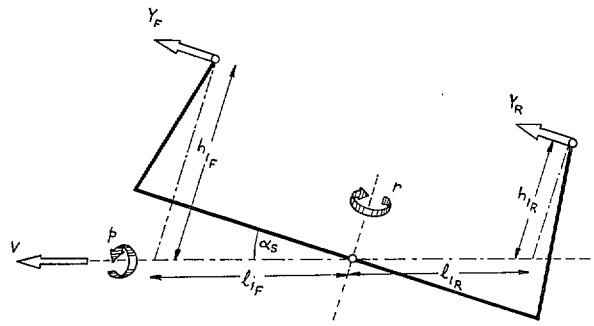

FIG. 1. Rotor force diagram for lateral stability.

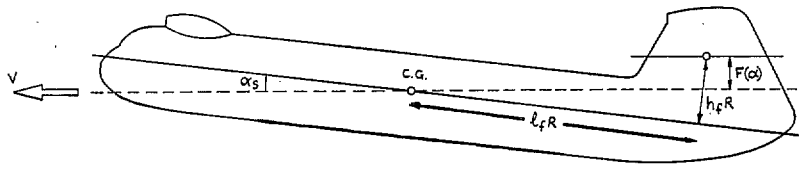

FIG. 2. Diagram defining fin dimensions.

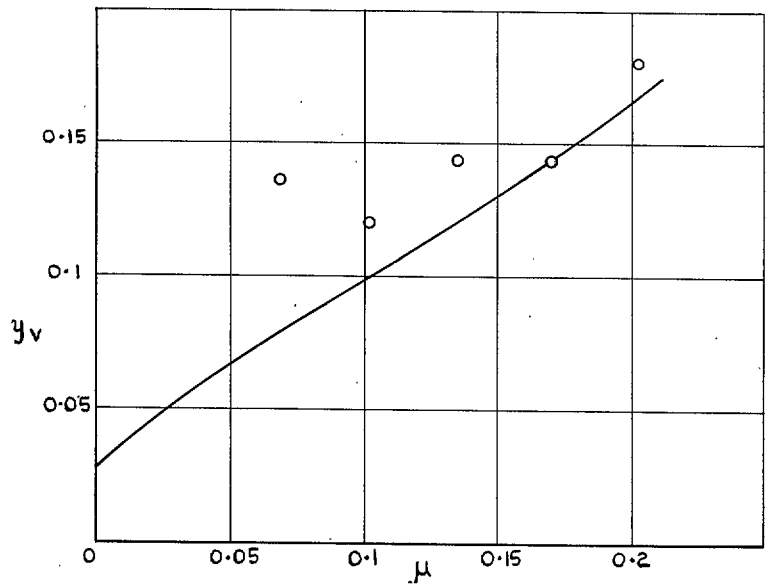

FIG. 3. Comparison of theoretical estimates of y_v with values obtained from flight tests of Ref. 8.

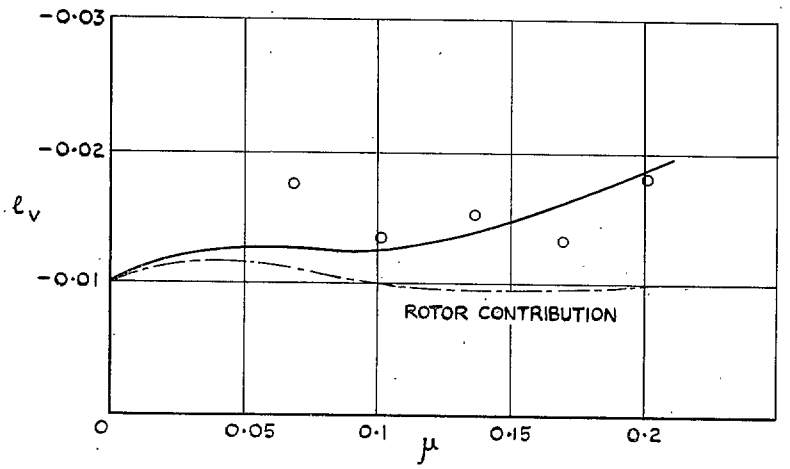

FIG. 4. Comparison of theoretical estimates of l_v with values obtained from flight tests of Ref. 8.

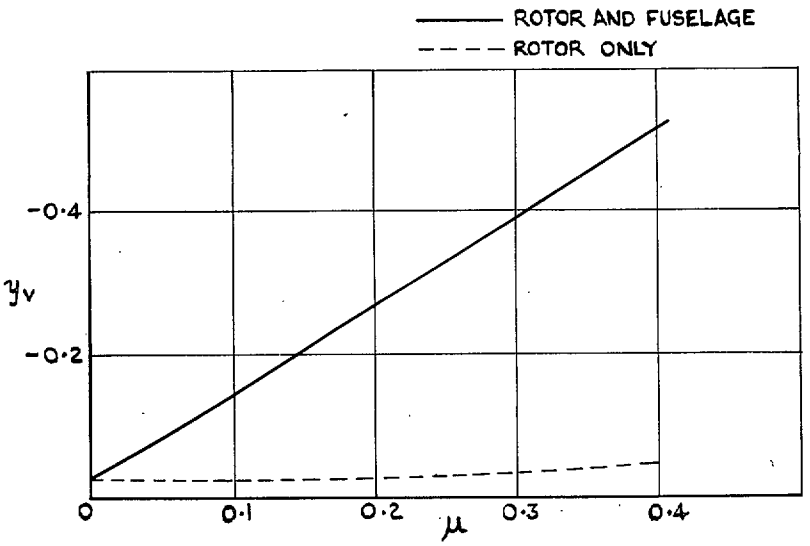

FIG. 5(a). Variation of y_v with μ.

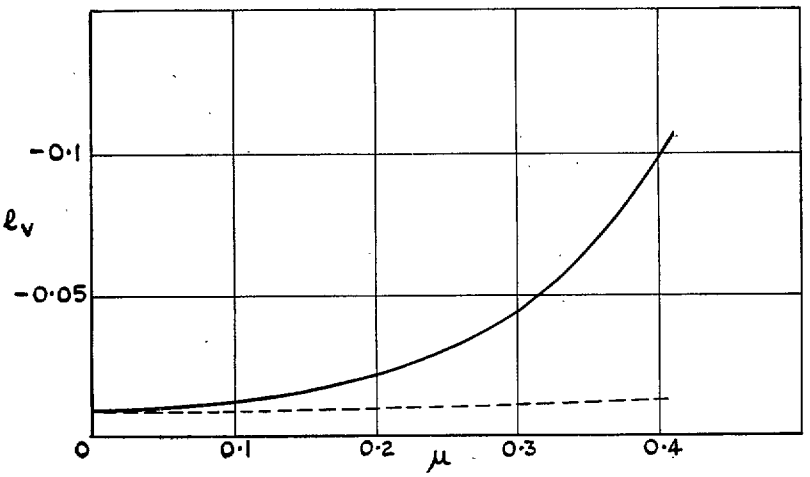

FIG. 5(b). Variation of l_v with μ.

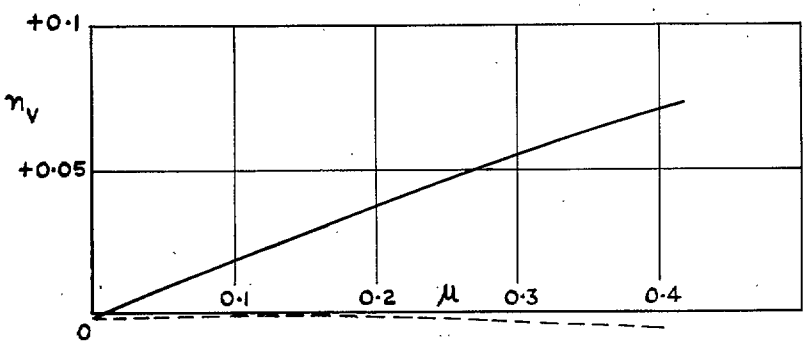

FIG. 5(c). Variation of n_v with μ.

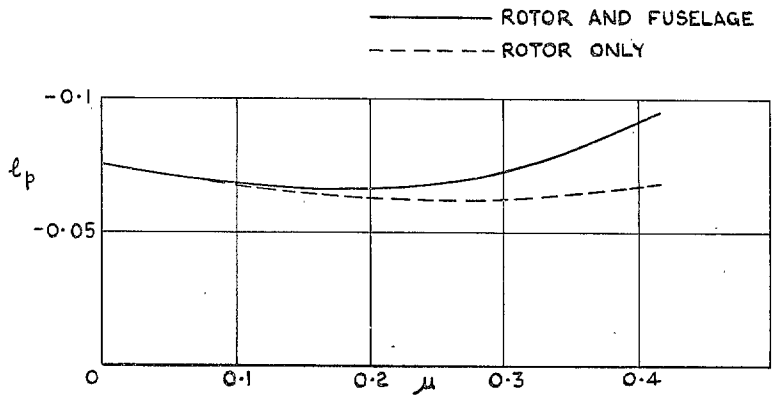

FIG. 5(d). Variation of l_p with μ.

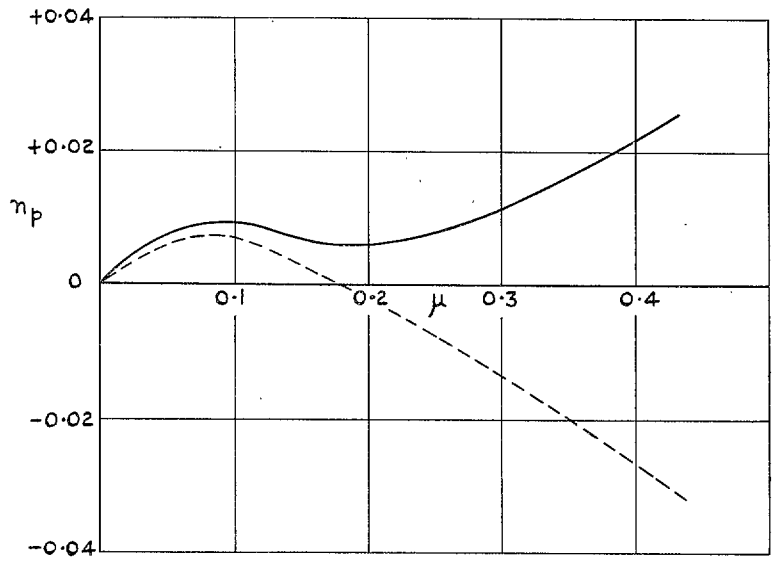

FIG. 5(e). Variation of n_p with μ.

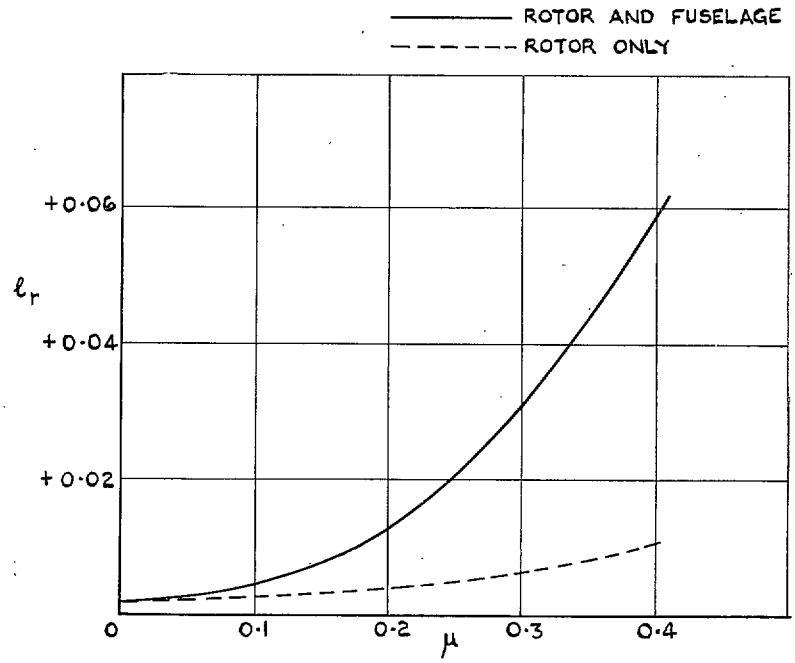

FIG. 5(f). Variation of l_r with μ.

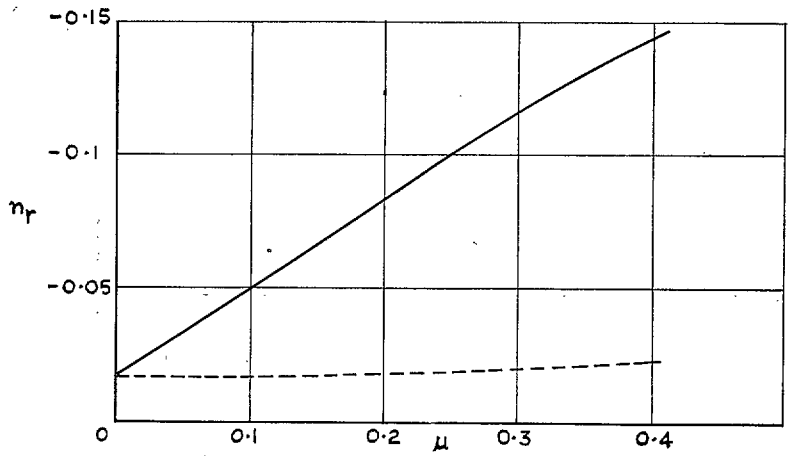

FIG. 5(g). Variation of n_r with μ.

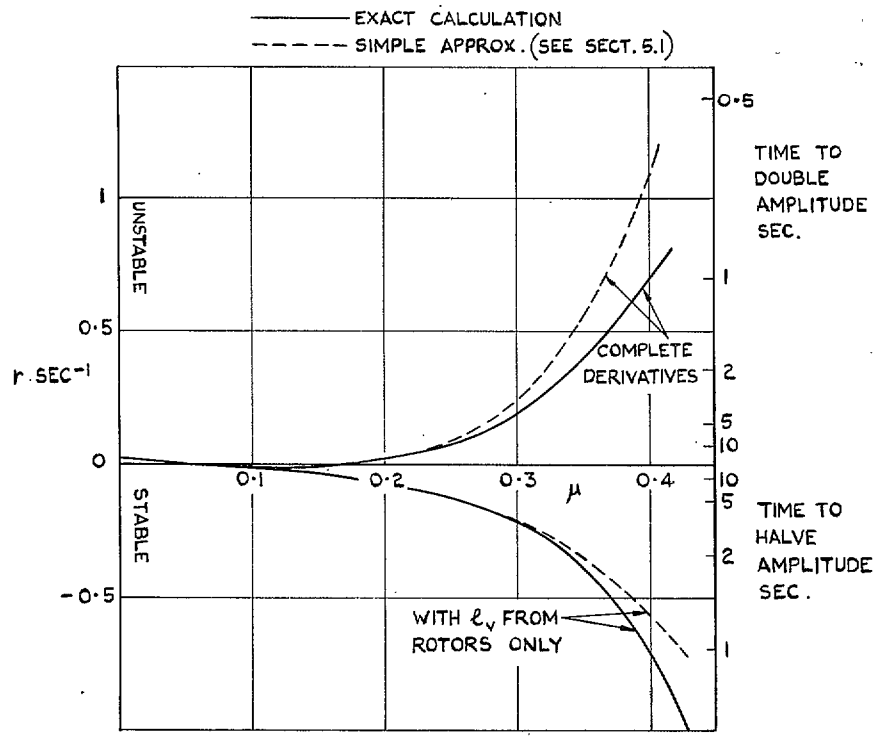

FIG. 6. Damping of lateral (Dutch roll) oscillation.

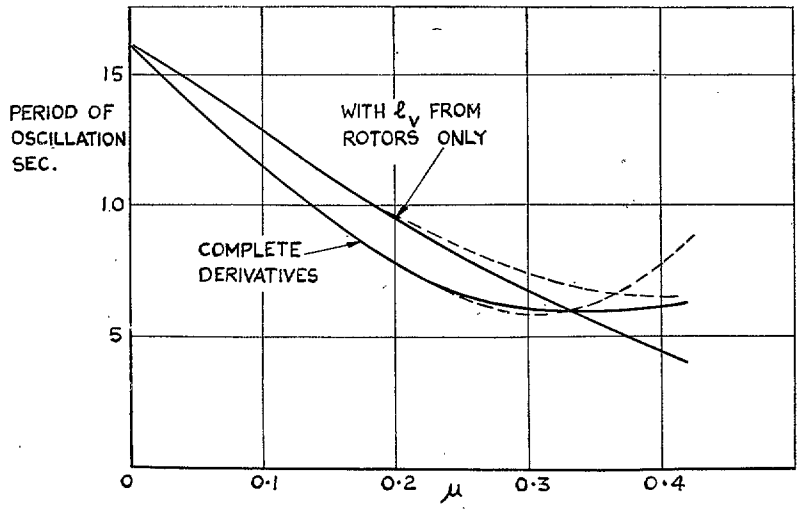

FIG. 7. Period of lateral (Dutch roll) oscillation.

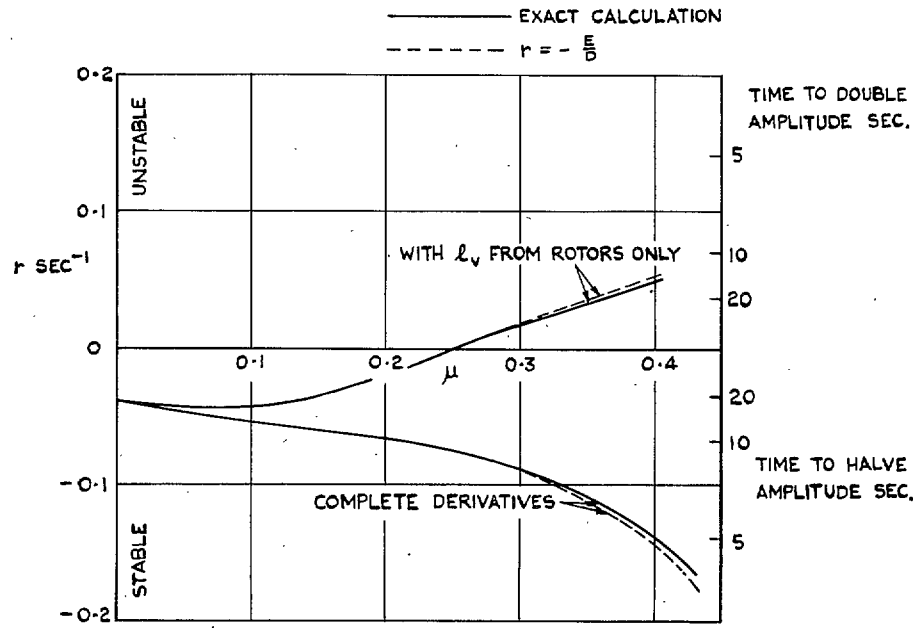

FIG. 8. Damping of spiral mode.

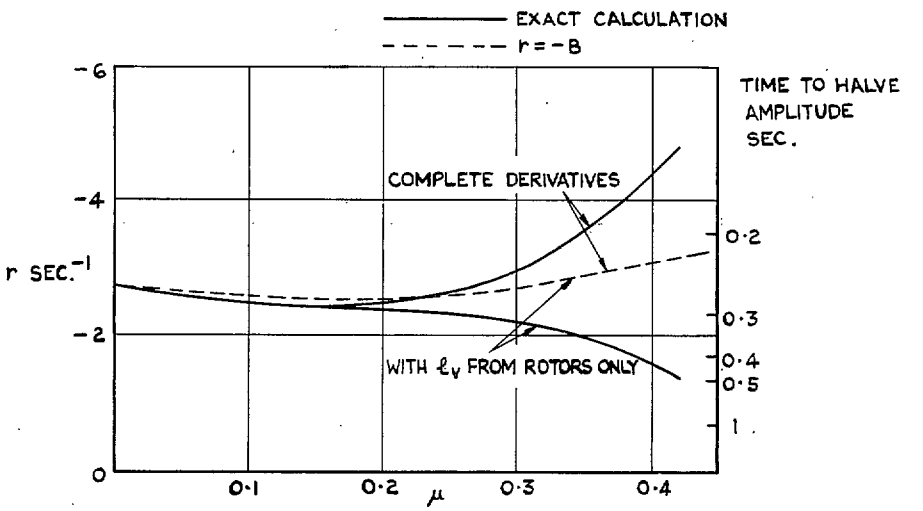

FIG. 9. Damping of rolling mode.

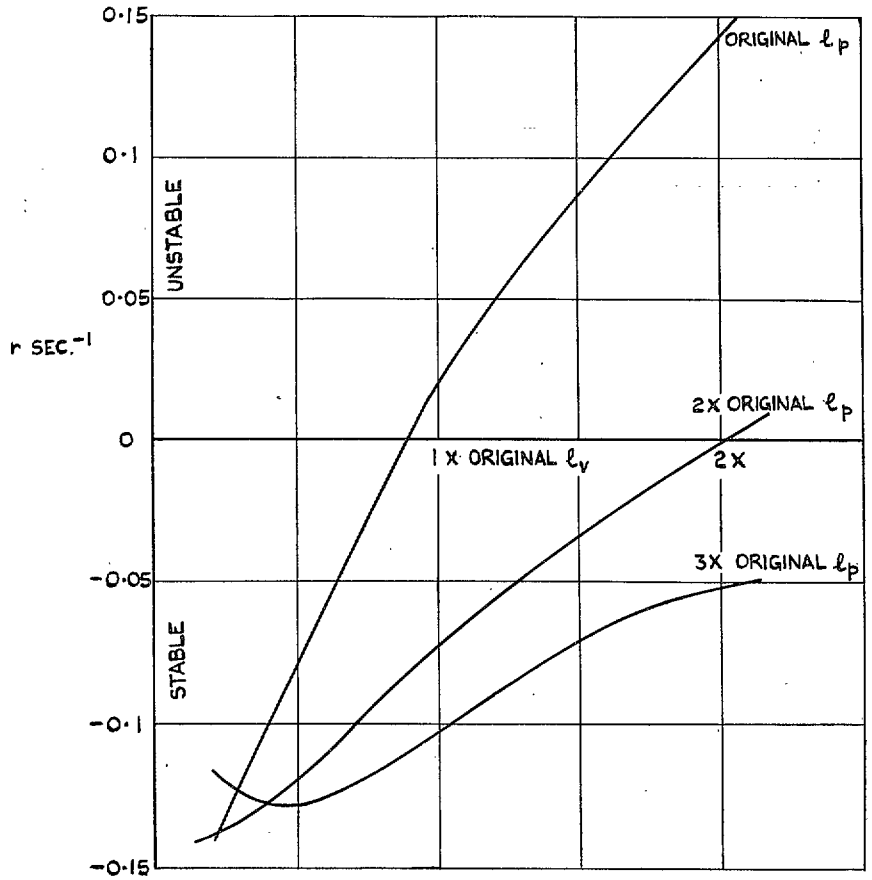

FIG. 10. Effect of l_v and l_p on damping of lateral (Dutch roll) oscillation ($\mu = 0{\cdot}2$).

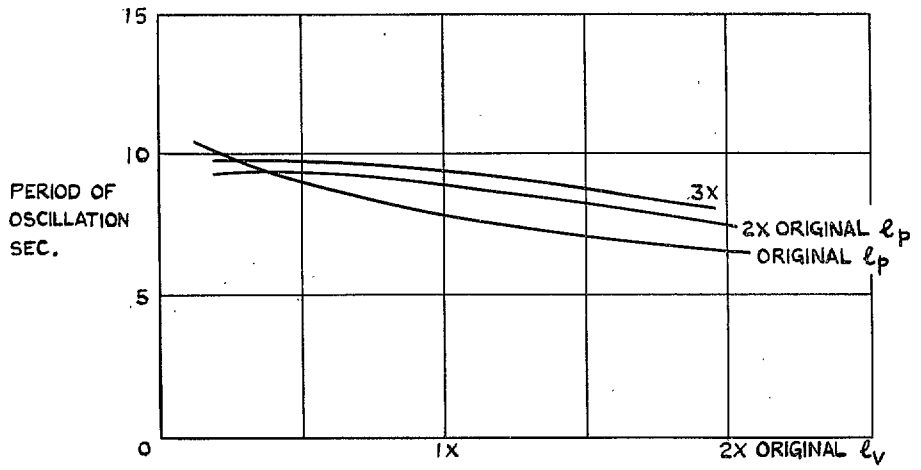

FIG. 11. Effect of l_v and l_p on period of lateral (Dutch roll) oscillation ($\mu = 0{\cdot}2$).

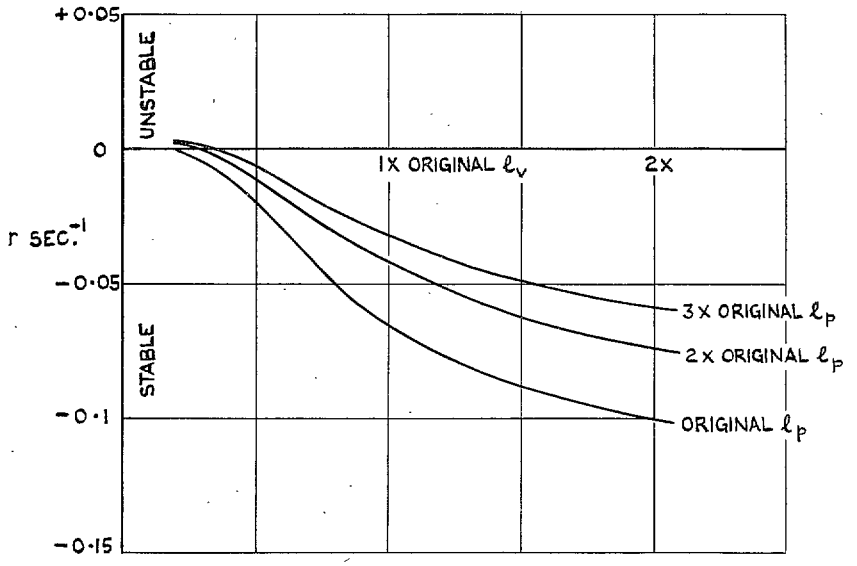

FIG. 12. Effect of l_v and l_p on spiral mode ($\mu = 0{\cdot}2$).

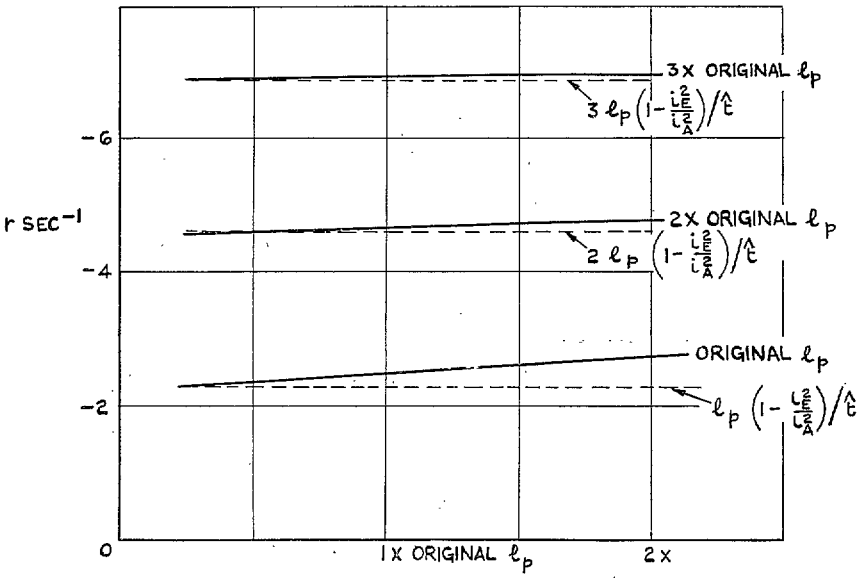

FIG. 13. Effect of l_v and l_p on damping in roll.

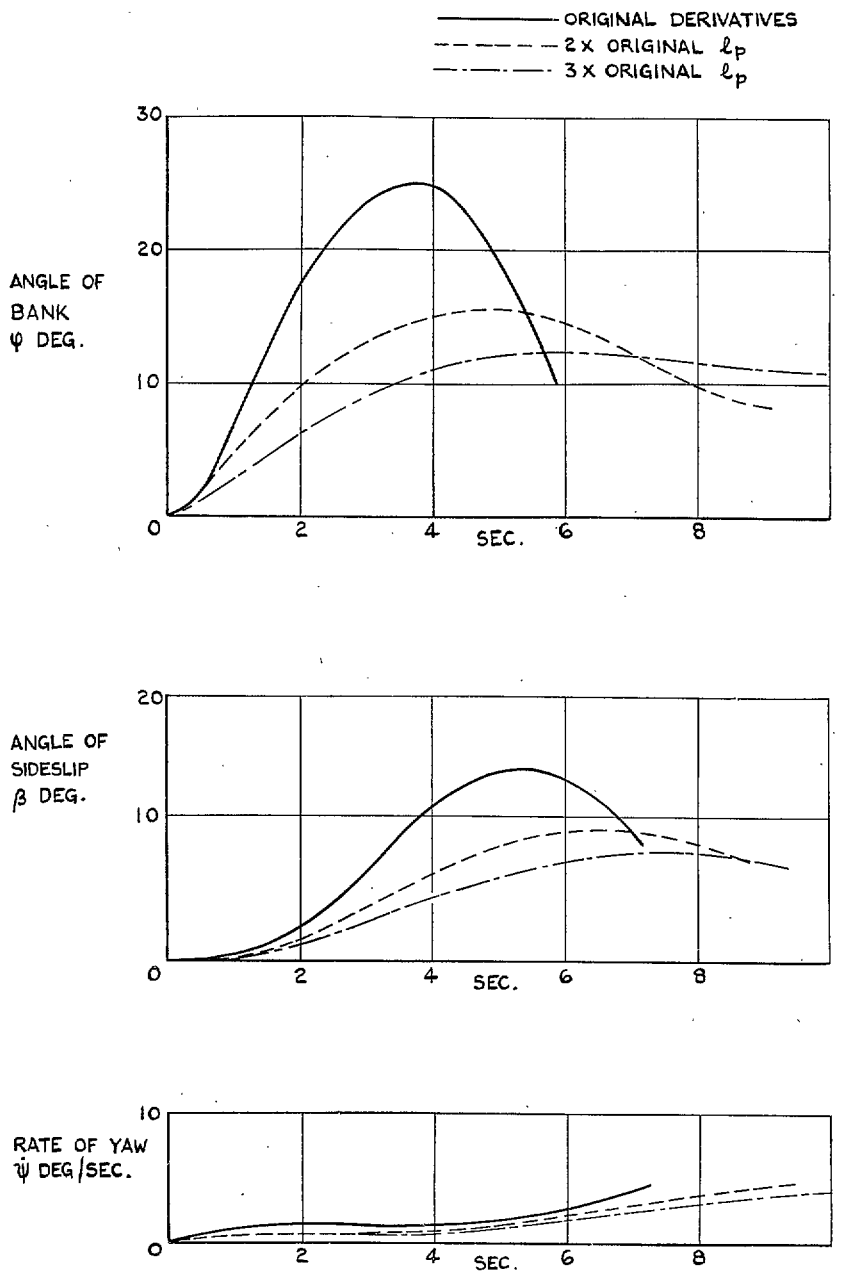

FIG. 14. Response to 1° lateral tilt of rotor discs. Effect of l_p ($\mu = 0{\cdot}2$).

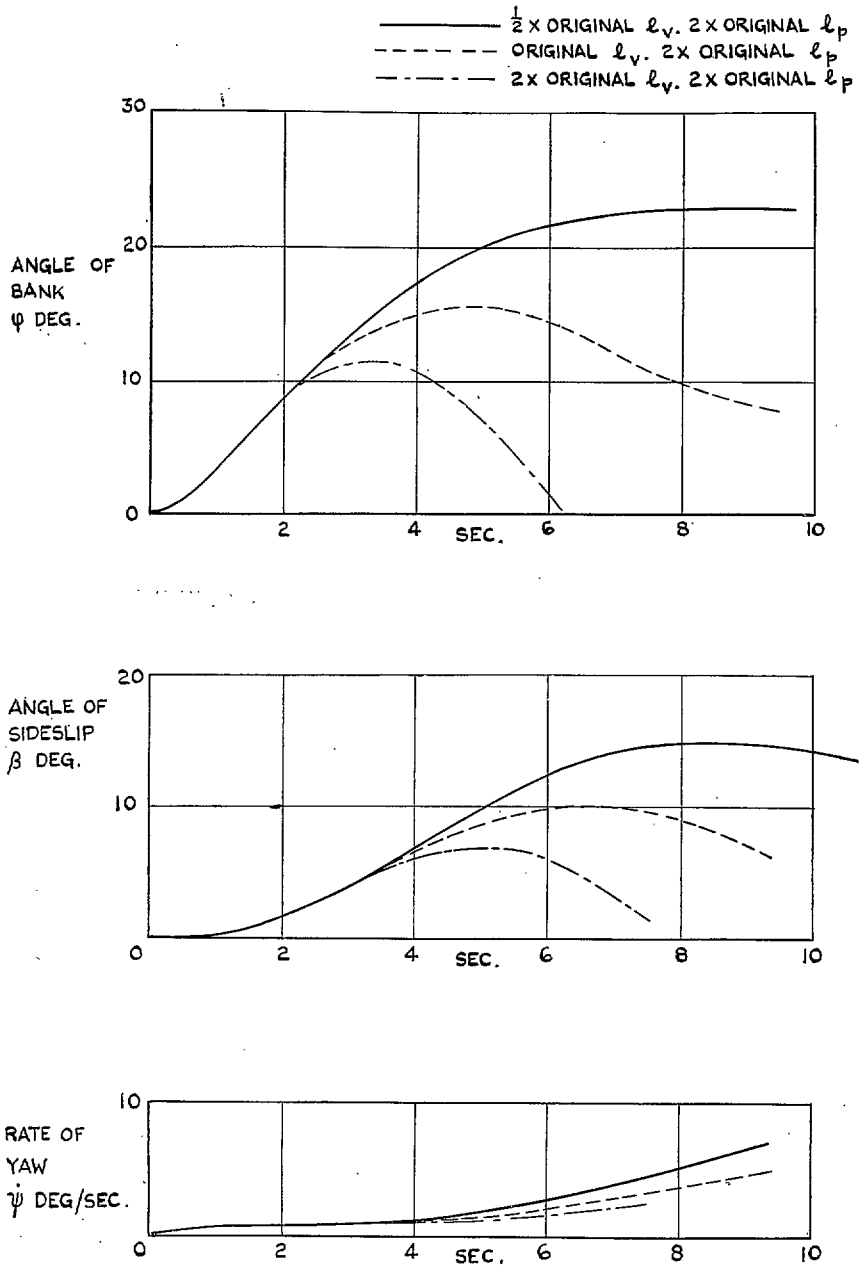

FIG. 15. Response to 1° lateral tilt of rotor discs. Effect of l_v ($\mu = 0{\cdot}2$).

(82028) Wt. 66/991 K 5 9/61 Hw.

Publications of the Aeronautical Research Council

ANNUAL TECHNICAL REPORTS OF THE AERONAUTICAL RESEARCH COUNCIL (BOUND VOLUMES)

1941 Aero and Hydrodynamics, Aerofoils, Airscrews, Engines, Flutter, Stability and Control, Structures. 63*s.* (post 2*s.* 3*d.*)

1942 Vol. I. Aero and Hydrodynamics, Aerofoils, Airscrews, Engines. 75*s.* (post 2*s.* 3*d.*)
Vol. II. Noise, Parachutes, Stability and Control, Structures, Vibration, Wind Tunnels. 47*s.* 6*d.* (post 1*s.* 9*d.*)

1943 Vol. I. Aerodynamics, Aerofoils, Airscrews. 80*s.* (post 2*s.*)
Vol. II. Engines, Flutter, Materials, Parachutes, Performance, Stability and Control, Structures. 90*s.* (post 2*s.* 3*d.*)

1944 Vol. I. Aero and Hydrodynamics, Aerofoils, Aircraft, Airscrews, Controls. 84*s.* (post 2*s.* 6*d.*)
Vol. II. Flutter and Vibration, Materials, Miscellaneous, Navigation, Parachutes, Performance, Plates and Panels, Stability, Structures, Test Equipment, Wind Tunnels. 84*s.* (post 2*s.* 6*d.*)

1945 Vol. I. Aero and Hydrodynamics, Aerofoils. 130*s.* (post 3*s.*)
Vol. II. Aircraft, Airscrews, Controls. 130*s.* (post 3*s.*)
Vol. III. Flutter and Vibration, Instruments, Miscellaneous, Parachutes, Plates and Panels, Propulsion. 130*s.* (post 2*s.* 9*d.*)
Vol. IV. Stability, Structures, Wind Tunnels, Wind Tunnel Technique. 130*s.* (post 2*s.* 9*d.*)

1946 Vol. I. Accidents, Aerodynamics, Aerofoils and Hydrofoils. 168*s.* (post 3*s.* 3*d.*)
Vol. II. Airscrews, Cabin Cooling, Chemical Hazards, Controls, Flames, Flutter, Helicopters, Instruments and Instrumentation, Interference, Jets, Miscellaneous, Parachutes. 168*s.* (post 2*s.* 9*d.*)
Vol. III. Performance, Propulsion, Seaplanes, Stability, Structures, Wind Tunnels. 168*s.* (post 3*s.*)

1947 Vol. I. Aerodynamics, Aerofoils, Aircraft. 168*s.* (post 3*s.* 3*d.*)
Vol. II. Airscrews and Rotors, Controls, Flutter, Materials, Miscellaneous, Parachutes, Propulsion, Seaplanes, Stability, Structures, Take-off and Landing. 168*s.* (post 3*s.* 3*d.*)

Special Volumes

Vol. I. Aero and Hydrodynamics, Aerofoils, Controls, Flutter, Kites, Parachutes, Performance, Propulsion, Stability. 126*s.* (post 2*s.* 6*d.*)
Vol. II. Aero and Hydrodynamics, Aerofoils, Airscrews, Controls, Flutter, Materials, Miscellaneous, Parachutes, Propulsion, Stability, Structures. 147*s.* (post 2*s.* 6*d.*)
Vol. III. Aero and Hydrodynamics, Aerofoils, Airscrews, Controls, Flutter, Kites, Miscellaneous, Parachutes, Propulsion, Seaplanes, Stability, Structures, Test Equipment. 189*s.* (post 3*s.* 3*d.*)

Reviews of the Aeronautical Research Council

1939–48 3*s.* (post 5*d.*) 1949–54 5*s.* (post 5*d.*)

Index to all Reports and Memoranda published in the Annual Technical Reports

1909–1947 R. & M. 2600 6*s.* (post 2*d.*)

Indexes to the Reports and Memoranda of the Aeronautical Research Council

Between Nos. 2351–2449	R. & M. No. 2450 2*s.* (post 2*d.*)
Between Nos. 2451–2549	R. & M. No. 2550 2*s.* 6*d.* (post 2*d.*)
Between Nos. 2551–2649	R. & M. No. 2650 2*s.* 6*d.* (post 2*d.*)
Between Nos. 2651–2749	R. & M. No. 2750 2*s.* 6*d.* (post 2*d.*)
Between Nos. 2751–2849	R. & M. No. 2850 2*s.* 6*d.* (post 2*d.*)
Between Nos. 2851–2949	R. & M. No. 2950 3*s.* (post 2*d.*)
Between Nos. 2951–3049	R. & M. No. 3050 3*s.* 6*d.* (post 2*d.*)

HER MAJESTY'S STATIONERY OFFICE

from the addresses overleaf

Printed and published by
HER MAJESTY'S STATIONERY OFFICE

To be purchased from
York House, Kingsway, London W.C.2
423 Oxford Street, London W.1
13A Castle Street, Edinburgh 2
109 St. Mary Street, Cardiff
39 King Street, Manchester 2
50 Fairfax Street, Bristol 1
2 Edmund Street, Birmingham 3
80 Chichester Street, Belfast 1
or through any bookseller

Printed in England

S.O. Code No. 23-3223